Commission of the European Community

JOINT
RESEARCH
CENTRE

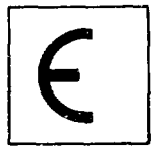

NEANDC (E) 252 "U" Vol. III Euratom
INDC (EUR) 018/G

ANNUAL PROGRESS REPORT ON NUCLEAR DATA

1983

CENTRAL BUREAU FOR NUCLEAR MEASUREMENTS

GEEL (BELGIUM)

May 1984

Commission of the European Community

JOINT
RESEARCH
CENTRE

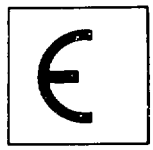

NEANDC (E) 252 "U" Vol. III Euratom
INDC (EUR) 018/G

ANNUAL PROGRESS REPORT ON NUCLEAR DATA

1983

CENTRAL BUREAU FOR NUCLEAR MEASUREMENTS

GEEL (BELGIUM)

May 1984

TABLE OF CONTENTS

N U C L E A R D A T A

1. N E U T R O N D A T A

1.1 CROSS SECTIONS OF ACTINIDES

Evaluation of the thermal neutron constants of ^{233}U, ^{235}U, ^{239}Pu and ^{241}Pu and the fission neutron yield of ^{252}Cf

E.J. Axton*

The above evaluation will be published as a European Applied Research Report. The abstract reads as follows:

"The thermal neutron constants comprise the thermal neutron (2200 $m.s^{-1}$) absorption and fission cross sections, $\bar{\nu}$ (total number of neutrons emitted per fission), and η (total number of neutrons emitted per neutron captured) for the nuclides ^{233}U, ^{235}U, ^{239}Pu, and ^{241}Pu. $\bar{\nu}$ for ^{252}Cf is included because it is widely used as a standard for the measurement of $\bar{\nu}$ for neutron-induced fission of the other nuclides. The importance of these data stems from the role they play in the prediction of the neutron economy in nuclear power reactors. The continued appearance of new data has prompted a continuous re-evaluation of the data over the years. Owing to the correlated nature of the measurements these evaluations necessarily take the form of simultaneous least-squares fits to all the data together with updating older data in terms of newer values for standard cross sections, half-lives, etc. In the past, the more important correlated errors have been dealt with by treating them as independent variables to be fitted in the evaluation. The purpose of the present exercise is to investigate the effect of treating all correlated errors by the introduction of a full covariance matrix. Results for various subsets of data, and comparisons with previous evaluation are presented.
The results of the calculation are shown below.

			Uncertainty
$\bar{\nu}_T$	^{233}U	2.488	.006
	^{235}U	2.427	.005
	^{239}Pu	2.876	.007
	^{241}Pu	2.937	.007
	^{252}Cf	3.766	.005
σ_a	^{233}U	574.1 b	1.8 b
	^{235}U	681.5 b	1.7 b
	^{239}Pu	1017.7 b	3.8 b
	^{241}Pu	1378.9 b	12.7 b

* Visiting Scientist from NPL, UK

σ_f	^{233}U	531.9 b	2.4 b
	^{235}U	584.7 b	1.7 b
	^{239}Pu	748.3 b	2.4 b
	^{241}Pu	1018.0 b	10.0 b
σ_γ	^{233}U	42.2 b	1.8 b
	^{235}U	96.8 b	1.8 b
	^{239}Pu	269.4 b	3.4 b
	^{241}Pu	360.9 b	5.6 b
$\bar{\nu}_T$ ratios	$^{233}U/^{252}Cf$	.6607	.0015
	$^{235}U/^{252}Cf$	.6445	.0012
	$^{239}Pu/^{252}Cf$	.7637	.0016
	$^{241}Pu/^{252}Cf$	.7800	.0017
η	^{233}U	2.305	.0063
	^{235}U	2.083	.0055
	^{239}Pu	2.115	.0069
	^{241}Pu	2.169	.0083
$1 + \alpha$	^{233}U	1.079	.004
	^{235}U	1.166	.003
	^{239}Pu	1.360	.005
	^{241}Pu	1.355	.006
σ_a	SULPHUR	.525 b	.129 b

When propagated into reactor calculations this data should always be accompanied by the associated correlation matrix."

Fission cross-section of ^{233}U and ^{235}U

C. Wagemans*, A. Deruytter, R. Barthélémy, J. Van Gils*

The $^{233}U(n,f)$ measurements have been analysed. For the $^{235}U(n,f)$ reaction, a new series of measurements has been started, in which the neutron energy region from thermal up to 30 keV is covered under different experimental conditions. One of the goals of these measurements is the accurate determination of the secondary normalization integrals

$$\int_{7.8eV}^{11eV} \sigma_f(E)dE \quad \text{and} \quad \int_{100eV}^{1000eV} \sigma_f(E)dE.$$

Preliminary results of these measurements have been presented at the IAEA Consultants Meeting on the ^{235}U Fast Neutron Fission Cross Section (Smolenice, CSSR, 28 March - 1 April 1983). These measurements will be continued.

---

* SCK/CEN Mol, Belgium

At the same conference, a review has also been given of fission cross-section normalization problems.

Analysis of intermediate structure in the fission cross section of ^{235}U+n

F. Corvi, H. Weigmann, L. Calabretta★, M.S. Moore★★

High resolution measurements of fission and capture cross sections of ^{235}U+n were performed by Corvi et al [1] in the energy range from 2 to 85 keV. A plot of the measured fission-to-capture ratio σ_f/σ_γ from 6 to 33 keV is given in fig. 1.

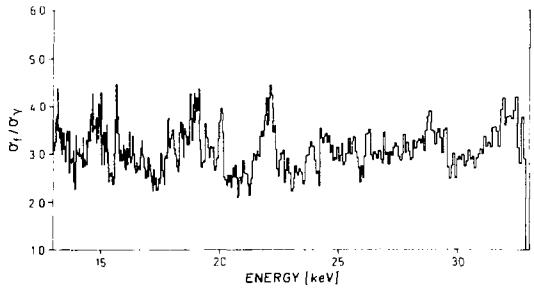

Fig. 1. The fission-to-capture cross-section ratio for ^{235}U+n vs neutron energy from 6 to 33 keV

These data were recently analysed in order to extract the energy dependence of the average s-wave fission width $\bar{\Gamma}_f$ and neutron strength function S_o. A correlation analysis of the various measured quantities σ_f, σ_γ, $\sigma_a = \sigma_f + \sigma_\gamma$, $\alpha = \sigma_\gamma/\sigma_f$ and the derived parameters $\bar{\Gamma}_f$ and S_o indicated that the large fluctuations in α can only be due to fluctuations in $\bar{\Gamma}_f$. These are much larger than those expected from a statistical model which assumes fission widths distributed according to a chi-squared law with a few degrees of freedom. The structure found was then simulated by using a double humped

---

(1) F. Corvi et al., Proc. NEANDC/NEACRP Specialists' Meeting on Fast-Neutron Capture Cross-Sections, Argonne, 1982, Rep. ANL-33-4, p. 347

★ Bursary of the Commission of the European Communities, now at Catania University, Italy

★★ Los Alamos National Laboratory, USA

barrier model that takes into account coupling of Class I and Class II states in exactly the same way as was used successfully to describe structure in sub-threshold fission. Simulated and experimental data were then compared by applying both the Wald-Wolfowitz runs-distribution test and the Levene-Wolfowitz runs-up-and-down test. Best agreement with the observed structure was found using an average spacing for Class II levels D_{II} = 210 ± 70 eV. Under the assumption that the symmetries in nuclear shape are the same for the first and second wells, this leads to a difference of 2.74 ± 0.14 MeV for the Class I and Class II minimum, in reasonable agreement with the fission systematics of Bjørnholm and Lynn [1].
A paper on this subject has been submitted to Phys. Rev. C.

Fission fragment mass- and energy distribution for the spontaneous fission of ^{238}Pu

C. Wagemans*, P. Schillebeeck*, A. Deruytter, R. Barthélémy

For the spontaneous fission of ^{238}Pu, no information is available on the characteristics of the energy- and mass-distributions of the fission fragments. In the frame of a systematic study of these characteristics for the Pu-isotopes, measurements have been performed at the BR1 reactor. A mixed ^{238}Pu-^{239}Pu sample is used, allowing a direct comparison of the ^{238}Pu(s.f.) with the $^{239}Pu(n_{th},f)$ characteristics. A partial analysis of the data reveals the presence of very prominent fine structures in the mass distribution. The analysis will be continued and the results will be interpreted and compared with our corresponding data for $^{240,242,244}Pu$(s.f.).

Fission fragment mass- and energy distribution for the thermal neutron induced fission of ^{239}Pu and the spontaneous fission of ^{240}Pu

E. Allaert*, C. Wagemans*, A. Deruytter, P. Schillebeeckx*, R. Barthélémy

In addition to the experiments performed at the linear accelerator, two further measurements were performed at the BR1 reactor. In the first one a 19 $\mu g/cm^2$ mixed $^{239}PuF_3$-$^{240}PuF_3$ layer (24 % $^{239}PuF_3$ - 76 % $^{240}PuF_3$),

(1) S. Bjørnholm and J.E. Lynn, Revs. Mod. Phys. 52, 725

* SCK/CEN Mol, Belgium

Table 1. Main characteristics of the $^{240}Pu(s.f.)$ and the $^{239}Pu(n_{th},f)$ fragment mass and energy distributions. The errors are only statistical

	Low geometry measurement		"4π" geometry measurement		
	$^{239}Pu(n_{th},f)$	$^{240}Pu(s.f.)$	$^{239}Pu(n_{th},f)$	$^{240}Pu(s.f.)$	$^{240}Pu(s.f.)$ total
$\bar{E}_K$ (MeV)	175.38 ± 0.01	177.04 ± 0.12	175.40 ± 0.01	177.40 ± 0.10	177.28 ± 0.08
$\bar{E}_K^*$ (MeV)	177.65 ± 0.01	178.76 ± 0.12	177.67 ± 0.01	179.16 ± 0.10	179.00 ± 0.08
σ_{E_K} (MeV)	12.15	12.15	12.50	12.51	12.37
$\bar{E}_L^*$ (MeV)	103.29 ± 0.01	103.18 ± 0.09	103.32 ± 0.01	103.43 ± 0.07	103.33 ± 0.06
$\bar{E}_M^*$ (MeV)	74.36 ± 0.01	75.56 ± 0.09	74.35 ± 0.01	75.73 ± 0.07	75.67 ± 0.06
$\bar{m}_L^*$ (amu)	100.30 ± 0.01	101.32 ± 0.06	100.27 ± 0.01	101.31 ± 0.05	101.31 ± 0.04
$\sigma_{m_L}^* = \sigma_{m_H}^*$	6.64	5.74	6.63	5.74	5.74
$\bar{m}_H^*$ (amu)	139.70 ± 0.01	138.68 ± 0.06	139.73 ± 0.01	138.69 ± 0.05	138.69 ± 0.04
Peak yield( )	6.08	7.57	6.01	7.49	7.52
P/V (5 pts)	114	577	119	559	566
N	4.2 x 10^6	10^4	1.9 x 10^6	1.5 x 10^4	2.5 x 10^4

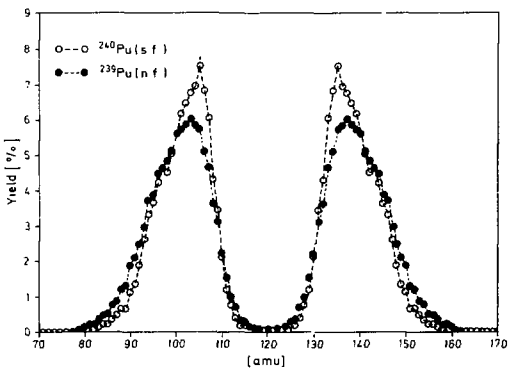

Fig. 2. Preneutron fragment mass for $^{240}Pu(s.f.)$ and $^{239}Pu(n,f)$

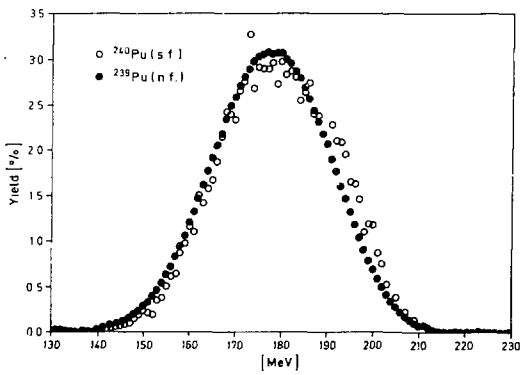

Fig. 3. Total kinetic energy for $^{240}Pu(s.f.)$ and $^{239}Pu(n,f)$

evaporated onto a 29 $\mu g/cm^2$ polyimide foil, was sandwiched between two 6 cm^2 surface barrier detectors, resulting in an almost 4π detection geometry. This "sandwich" was mounted straight in the collimated neutron beam. In the second measurement a more classical low geometry configuration was used, in which a 57 $\mu g/cm^2$ target was viewed by two collinear 20 cm^2 surface barrier detectors placed outside the neutron beam.

Since the BR1 reactor was only operational during the day, a good alternation of $^{239}Pu(n_{th},f)$ and $^{240}Pu(s.f.)$ measurements was possible, allowing a careful detector calibration via the $^{239}Pu(n_{th},f)$ reaction. So a sequence of separate $^{240}Pu(s.f.)$-$^{239}Pu(n_{th},f)$ measurements was performed (in both geometries) which were analysed individually and summed afterwards.

The main results of both measurements are summarized in Table 1., which clearly shows that the low and the "4π" geometry measurements are in good agreement. A graphical comparison of the $^{239}Pu(n_{th},f)$ and the $^{240}Pu(s.f.)$ fragments mass- and energy-distributions is given in Fig. 2 resp. Fig. 3. From these measurements it is clear that the fissioning system ^{240}Pu behaves in a very similar way as ^{242}Pu, i.e. a higher average total kinetic energy for $^{240}Pu(s.f.)$ than for $^{239}Pu(n_{th},f)$, a much higher peak yield, more pronounced fine structure and a narrower mass-distribution for the spontaneous fission than for the neutron induced fission. These differences can be explained in terms of the static scission point model of Wilkins et al. (1). A final report on these measurements was written and submitted to Physical Review.

Fission cross section of ^{242}Pu

J.A. Wartena, H. Weigmann, C. Bürkholz, R. Pijpstra

The measured fission cross section of ^{242}Pu in the threshold region is shown in fig. 4 together with a cross section calculated from the statistical model. The model assumes two fission channels for each $K^\pi \leqslant 5/2^\pm$ and one channel for $K^\pi = 7/2^\pm$ within the first 400 keV above the lowest barrier, together with the associated rotational bands.

The parameters of the lowest barrier (assumed $K = 3/2^\pm$) are:

E_A	= 5.87 MeV	E_B	= 5.2 MeV
$\hbar\omega_A$	= 0.8 MeV	$\hbar\omega_B$	= 0.52 MeV

(1) B.D. Wilkins, E.P. Steinberg, R.R. Chasman, Phys. Rec. C14 (1976) 1832

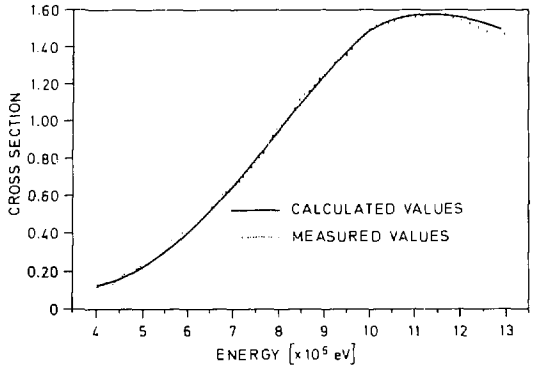

Fig. 4. Fission cross section of ^{242}Pu

Below threshold, the fission cross section of ^{242}Pu shows a large amount of structure. This is illustrated in fig. 5 which shows the measured fission cross section between 200 keV and 500 keV neutron energy.

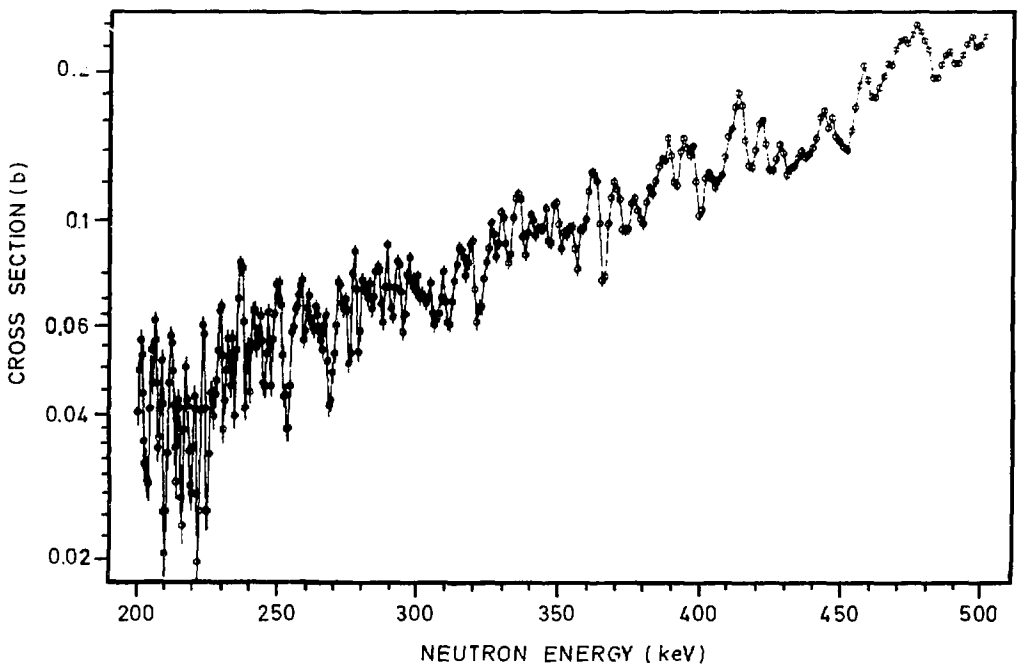

Fig. 5. The measured fission cross section of ^{242}Pu between 200 and 500 keV neutron energy

Below 70 keV neutron energy individual peaks are observed, most of which are interpreted as intermediate structure resonances due to Class II states in the second wall of the deformation potential. A total of 98 Class II states has been observed.

A statistical analysis has been started which attempts to reproduce the characteristic features of this structure. Sequences of Class I and Class II levels with spin $J \leq 5/2$ are generated from the relevant distribution laws: Fission and coupling widths of Class II levels for each fission channel are sampled from Porter-Thomas distributions with expectation values calculated from the relevant fission barrier parameters. The same sequence of transition states is assumed as was used for the statistical model calculation in the threshold region. The Class I levels with spacing $D(J=1/2) = 17.5$ eV are given neutron widths also sampled from Porter-Thomas distributions with energy dependent expectation values corresponding to strength functions $S_0 = 0.9 \cdot 10^{-4}$, $S_1 = 2.6 \cdot 10^{-4}$, $S_2 = 1.4 \cdot 10^{-4}$. The coupling between Class I and Class II levels is introduced in the usual way, again allowing for Porter-Thomas fluctuations of the individual fine structure fission widths. From the sequence of resonances constructed this way, the contribution of each Class II level to the fission cross section is calculated, and the results compared to the experimental observation.

In the region of resolved Class II states, i.e. below 70 keV neutron energy, the quantities compared between the statistical calculation and the experiment are the number of peaks with a fission area above the energy dependent experimental detection limit and their average fission area.

In the range 200 keV $\leq E \leq$ 500 keV, the quantities adopted as a measure of the amount of fluctuation in the cross section are:

- the relative variance $v = \frac{1}{n-1} \Sigma(1 - \sigma/\sigma_s)^2$, where the sum is over the n data points representing the cross section σ, and σ_s in a smooth cross section of the form $\sigma_s = \exp(a E_n - b)$, where a and b are adjusted such as to minimize v.
- the number of runs, r, for σ being above (h) and below (ℓ) σ_s.

Again the quantities v and r as obtained from the statistical calculation, are compared to their experimental counterparts.

The conclusion from the comparison of the statistical calculations with experiment in both energy ranges, $E \leq 70$ keV and 200 keV $\leq E \leq$ 500 keV, are as follows:

- the spacing of Class II levels must be of the order of $D_{II}(J=1/2)= 1$ keV; this implies that about half of the groups of fission resonances observed below 4 keV neutron energy must be due to p-wave neutron interaction.
- the lower energy data require a higher outer barrier (E_B = 5.6 MeV) than was obtained from the statistical model calculation in the threshold region. The value obtained in the latter calculation is, however, very sensitive to assumptions made about strength functions and competition from inelastic channels; thus we regard the value of E_B = 5.6 MeV obtained from the low energy data as more reliable.
- the amount of fluctuations observed in the energy range 200 keV $\leq$ E $\leq$ 500 keV, expressed by means of the quantities v and r is approximately reproduced by the statistical calculation, indicating that the assumption made with respect to the number of fission channels, and the assumption of complete damping of vibrational resonances are approximately correct.

Neutron capture measurements on ^{241}Am

E. Cornelis*, G. Rohr, T. van der Veen, G. Vanpraet*, S. Raman**

A series of neutron capture measurements have been performed at GELINA with a 1.74 g metallic ^{241}Am sample (2 x 2 cm^2 disk), canned in a stainless-steel cylinder. These test measurements were made at a flight path of 10 m. in the neutron energy range from 0.5 keV up to 300 keV. The gamma-ray detectors were two C_6D_6 liquid scintillators, shielded by a 5 mm lead cap. To suppress the gamma-flash, a 5 mm thick lead stop was kept permanently in the 50 cm long, supplementary beam collimator tapered to a 2 cm hole-diameter. Neutron scattering by the stainless-steel container was found to be negligible. For the flux measurements with the boron sample, the 0.6 mm thick ^{10}B disk was placed in the same position as the ^{241}Am sample.
The background was obtained by means of the black resonance technique using S, Na, Co and Ag filters. With these experimental conditions and a linac repetition rate of 800 Hz, we checked the feasibility of performing first a relative measurement for the average capture cross section. Our results have been normalized at 10 keV to those of Harwell (Gayther et al.).

---

* University of Antwerp, RUCA, Belgium
** ORNL, U.S.A.

As shown in Fig. 6 a comparison is made of our results with measurements of Harwell and ORNL (Weston et al.) obtained with an oxide sample. These results for the total absorption cross section which is practically equal to the capture cross section between 10 and 250 keV, are given with an accuracy of 10 and 12 % respectively, but the two results normalized between 1 and 2 keV to ORNL are discrepant by up to 20 % between 10 and 100 keV.

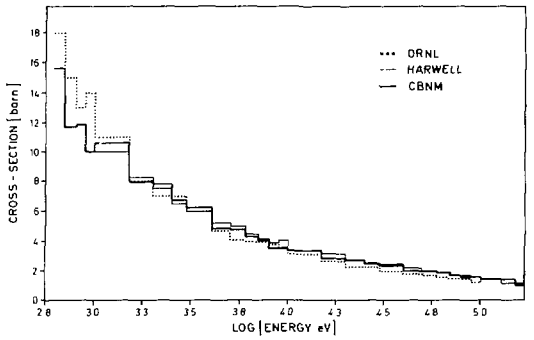

Fig. 6. Capture cross section of ^{241}Am

More recent results of KfK (Wisshak et al.) give absolute data points (not shown here in Fig. 6), using the ENDF/B-IV cross section for gold, with a total uncertainty of 4 to 6 % for energies between 20 and 160 keV. The KfK data agree very well with the data of Harwell and meet even the required accuracies for cross section data. Our data fit in shape and slope consistently with Harwell and consequently with KfK. However we still have to normalize to absolute values obtained via a few well known low energy resonances in ^{241}Am. When flightpath 2 becomes available these measurements will be done with other, suitable neutron beam parameters using Cd instead of B as overlap filter. The emphasis will be on an optimal signal-to-background ratio to achieve a high statistical accuracy by improving our experimental set-up, using a large shielding facility, made available to us by SCK-CEN Mol.

Fission cross section measurements of ^{243}Am

H.-H. Knitter, C. Budtz-Jørgensen, H. Bax, R. Vogt

There are three priority 1 requests from countries of the European Community to measure this cross section in a neutron energy range from thermal to 15 MeV. These requests and the large difference of 30 % between the neutron induced fission cross section inferred from charged particle induced fission and the, at present available, experimental neutron induced fission cross sections in the MeV region prompted us to start a measurement of this quantity. Two samples of 0.2 mg and 1.1 mg ^{243}Am prepared by spraying of a suspension of Am-oxide on stainless steel backings with active circular areas of 28 mm diameter were tested in an ionization detector. It was shown that neither of the targets was homogeneous enough to obtain a clear discrimination between alpha particle and fission fragment signals, and thus to measure absolutely the fission cross section.

The thinnest of the two available samples, however, allows to measure the relative fission cross section ratio between ^{243}Am and ^{235}U. This quantity was measured at the Van de Graaff in the neutron energy range between 0.2 and 4 MeV. Since in the neutron energy range between 50 eV and 10 keV there exist only data from one bomb shot experiment, the same fission fragment detector which was used at the Van de Graaff was then installed at an eight meter flight path at GELINA. Fission cross section ratio data were accumulated over a period of several weeks, covering an energy interval from about 0.8 eV up to the MeV-region. Fig. 7 shows a plot of the time-of-flight spectrum obtained with the americium fission fragment detector. In the region below 50 eV, where until now no fission cross section measurements exist, the time-of-flight spectrum shows some thirty statistically relevant resonances. No attempt has yet been made to come to a quantitative

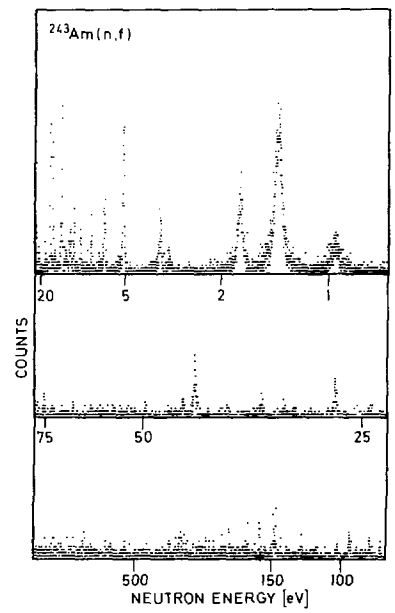

Fig. 7. The relative ^{243}Am(n,f)/^{235}U(n,f) cross section data as accumulated over a period of several weeks

analysis of the data, since no absolute normalization is possible at present. For this normalization a thin and homogeneous americium sample prepared by electroplating is needed, which was demanded from CBNM's sample preparation group.

Low energy neutron measurements

The observed discrepancy between measured and calculated values of the temperature coefficient of criticality for thermal reactors has shed doubt on the validity of the shapes of the existing ^{235}U η measurements and $^{238}U(n,\gamma)$ data, at the low energy side of the thermal neutron spectrum [1]. An ad hoc Working Group has been set-up to study the feasibility of such measurements at the linear accelerator of CBNM and - since the response was positive - to tackle the problems.

Fission cross-section measurements of ^{235}U at low neutron energies

C. Wagemans*, A. Deruytter, R. Barthélémy, J. Van Gils*

After a series of test measurements, a pilot experiment to determine the $^{235}U(n,f)$ low-energy cross-section was performed under the following experimental conditions:

- moderator thickness: 12 cm (polyethylene, not cooled)
- linac repetition frequency: 25 Hz; pulse width: 2 μs
- 25 $\mu g/cm^2$ ^6LiF foil back-to-back with a 100 $\mu g/cm^2$ $^{235}UF_4$ foil
- $^6Li(n,\alpha)$-particles and $^{235}U(n,f)$-fragments detected with surface barrier detectors.

From these measurements the $\sigma_f(E)\sqrt{E}$ curve from 5 to 500 meV (Fig. 8) was calculated, which was normalized to earlier results [2] in the energy region from 20 to 60 meV. In Fig. 9 the present results from 5 to 150 meV are compared with the data of Deruytter et al., showing an excellent agreement

(1) J. Bouchard et al., Nuclear Data for Science and Technology, Proceedings of the Int. Conf., Antwerp, Sept. 1982, p. 21-27

(2) A.J. Deruytter, J. Spaepen, and P. Pelfer, Journ. Nucl. En. 27 (1973) 645

* SCK/CEN Mol, Belgium

above 10 meV. Below this energy, the data of Deruytter et al. are slightly lower. Their experimental conditions, however, were optimized for the determination of an absolute σ_f(0.0253 eV)-value, and not for measurements at extreme low energies.

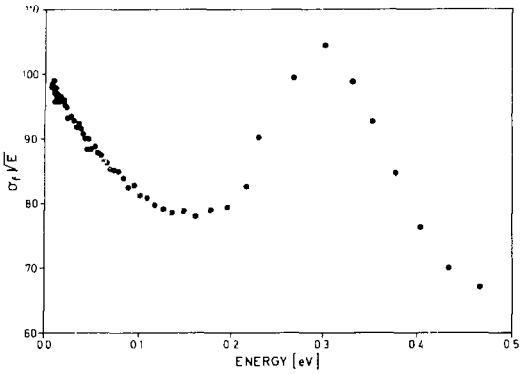

Fig. 8. Fission cross section of ^{235}U

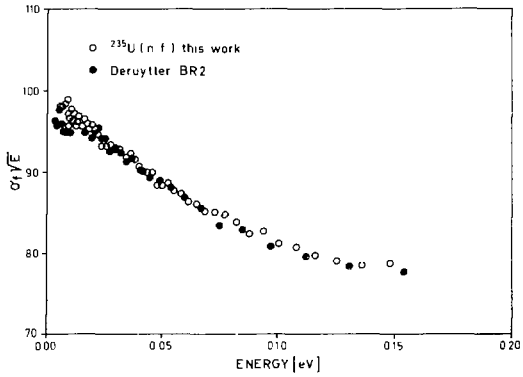

Fig. 9. Fission cross section of ^{235}U

Accurate measurements below 5 meV require the installation of a cooled moderator, which will strongly increase the neutron flux below 10 meV. In this respect, several tests have already been performed.

Capture cross section measurements of ^{238}U at low neutron energies

F. Corvi, R. Buyl, M. Riemenschneider, T. van der Veen

A key role in the accurate measurement of the shape of a cross section vs neutron energy is played by the neutron flux detector. This detector should be thin in order to be used in transmission even at sub-thermal energies and should have a cross section strictly 1/v over the range of interest. Our choice has been a gridded ionization chamber of the continuous gas flow type, having back-to-back coatings of ^{10}B of 5 $\mu g/cm^2$ thickness. A gas mixture of 95 % Ar and 5 % CO_2 at atmospheric pressure could be used. Due to the very thin deposits, it is expected an almost 100 % detection efficiency for both α and ^7Li particles.

The chamber was built and successfully tested with a Linac neutron beam at a 10 m long flight path. Both ^{4}He and ^{7}Li peaks are well resolved and the ^{7}Li peak-to-valley ratio is of the order of 90 to 1.

Resonance Data of ^{238}U (International Task Force)

F. Poortmans (local task force member) - SCK/CEN Mol, K.H. Böckhoff

One of the concerted actions organized by NEANDC concerns the resonance parameters of ^{238}U above 1.5 keV (for the other task force see Chapter 1.2). ORNL, Harwell, JAERI and CBNM have agreed to join this action.
In the frame of this task force the data obtained from the extensive measurement campaign on ^{238}U at GELINA which was finished in 1975, were critically reviewed and data reduction was repeated. The results were sent to the NEA Data Bank from where they were disseminated to the other involved labs for an independent analysis.

1.2 CROSS SECTIONS OF STRUCTURAL MATERIALS

Neutron scattering width of the 1.6 keV resonance in ^{52}Cr

A. Brusegan, C. Van der Vorst

Within the framework of the structural materials programme at CBNM Geel, high resolution neutron transmission measurements have been performed in the energy range from 500 eV to 100 keV on natural Cr (metallic) and enriched ^{52}Cr (oxide) samples.
The same samples were measured under different running conditions of the 150 MeV Linac (GELINA):

a) 4.5 ns burst width and 4 kW
b) 14 ns burst width and 9 kW (rotary target).

Two 4" x 3" NaI(Tl) detectors, placed at 48.9 m flight distance, were viewing a 0.5 cm thick $^{10}B_4C$ slab.
The background was determined with the black resonance technique (Bi, Na, S) and a $^{10}B_4C$ filter, $1.93 \cdot 10^{-2}$ atoms/b thick in ^{10}B, was set in the beam as anti-overlap filter. The purity of the oxide sample was 99.74 % ($\pm$ 0.02 %), giving a thickness in ^{52}Cr of $1.133 \cdot 10^{-2}$ atoms/b.

The two natural metallic samples, respectively (0.117 ± 0.003) cm and (0.187 ± 0.004) cm thick showed a relatively important irregularity in the thickness. The density of the sample has been taken as 7.014 ± 0.182 g/cm^3. After reduction to transmission spectra, the data have been analysed with a modified version of the shape analysis code SIOB [1] in order to deduce the resonance parameters of the 1.6 keV resonance in ^{52}Cr.

For the metallic sample, the characteristic (Debye) temperature at room temperature is 450 K, which gives a Doppler width much larger than the resolution width which was calculated by Bignami et al. [2].

For the oxide compound the Debye temperature is unknown and a value of 353 K has been assumed for the effective temperature: in Table 2 the results of the oxide sample spectra are given for completeness.

Table 2. Shape analysis results for the 1626 eV resonance in ^{52}Cr, assuming Γ_γ = 0.5 eV

Nr.	Sample	T_{eff} (°K)	Γ_n (meV)	Black resonance Filters
1	0.117 cm thick natural metallic	324	29.9 ± 1.1	S, Na, Bi
2		324	29.2 ± 1.5	Na, Bi
3	0.18 cm thick natural metallic	316	26.7 ± 0.7	Na, Bi
4		316	28.2 ± 0.5	Na, Bi, Al
5		316	30.3 ± 0.7	S, Na, Bi
6	Cr_2O_3	353	30.3 ± 0.8	Na, Bi
7		353	30.4 ± 0.8	S, Na, Bi

As published by Kopecky et al. [3], the spin and parity of the 1.6 keV resonance in ^{52}Cr is $J^\pi = (3/2)^-$.

---

(1) G. de Saussure, D.K. Olsen, and R.B. Perez, Rep. ORNL/TM-6286

(2) A. Bignami, C. Coceva, and R. Simonini, Rep. EUR 5157e (1974)

(3) J. Kopecky, R.E. Chrien, and H.I. Liou, Nuclear Physics A334 (1980) 35-44

The simultaneous calculation of the capture and neutron widths results in a large dispersion of the Γ_γ values suggesting a low sensitivity of the experiment to the capture widths.

In Table 2 the results of the shape analysis are quoted only for the fixed value Γ_γ = 0.5 eV: the neutron widths are given with their statistical uncertainties.

Taking a weighted average of the first 5 determinations of Γ_n deduced from the metallic samples spectra, yields $\overline{\Gamma}_n$ = (28.5 $\pm$ 0.3) meV (statistical error only). The assumption of broad limits ($\pm$ 50 %) on the quoted Γ_γ value, introduces a supplementary uncertainty of 1.4 meV on $\overline{\Gamma}_n$. A 3 % systematic uncertainty is deduced from the uncertainty of the sample thicknesses and densities: the resulting final value of the error on $\overline{\Gamma}_n$ is 2.6 meV.

The calculated value of $g \frac{\Gamma_n \Gamma_\gamma}{\Gamma}$ becomes $(53.9 \begin{smallmatrix} + 3.6 \\ - 5.0 \end{smallmatrix})$ meV. It must be said that a reduction of 10 % in T_{eff} for the oxide measurement implies a change of Γ_n of 1.6 %.

In Fig. 10 the continuous line reproduces the SIOB fit to the experimental transmission data measured with the 0.187 cm thick metallic sample. The quoted results for $\overline{\Gamma}_n$ and $g \frac{\Gamma_n \Gamma_\gamma}{\Gamma}$ should be considered as preliminary.

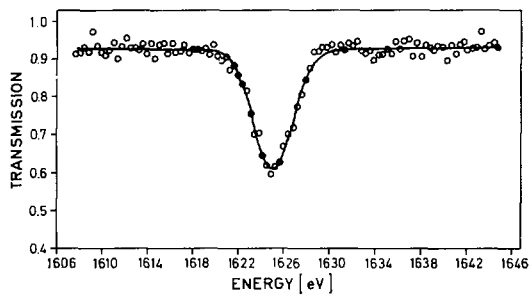

Fig. 10. Shape analysis fit to the 1.6 keV resonance transmission data

The capture area of the 1.6 keV resonance of ^{52}Cr

G. Rohr, R. Shelley, A. Brusegan, F. Corvi, T. van der Veen

Precise resonance data of the 1.6 keV resonance are interesting for the following reasons:

- ^{52}Cr is included as contamination in all samples of separated chromium isotopes used in the capture measurements performed at Geel and the 1.6 keV resonance can be applied to normalize the capture data. This resonance is a pure capture resonance ($\Gamma_n \ll \Gamma_\gamma$) and hence the capture area can be measured very accurately in a neutron transmission experiment. Normalization with this resonance has the advantages that there is need neither for a special normalization run nor for extrapolation of the neutron flux from the eV range to the keV-range as would be the case for Au- and Ag-resonances generally used for this purpose. Furthermore the hardness of the γ-ray spectrum of the normalization resonance is similar to that of the resonances which have to be measured.
- To see whether or not a similar discrepancy exists between the transmission and capture measurement results as that observed for the 1.15 keV resonance of ^{56}Fe, measured by liquid scintillation and by the weighting technique. This discrepancy has led to the ^{56}Fe-task-force and is still not explained.

The main neutron capture measurements for the Cr-isotopes have been performed at a 60 m flight path. However, before analysing the data and especially in view of the points mentioned, a special 30 m flight path normalization measurement has been performed and analysed and the results for the 1.6 keV resonance compared with those obtained from the transmission measurement reported above.

This 30 m capture measurement was performed using two C_6D_6 liquid scintillators viewing a natural Cr sample containing 8.592×10^{21} atoms.cm^{-2}. The detector events were weighted according to the energy of the detected photons resulting in a detector response proportional to the total energy released in the capture process. Recording of the events, amplitude and time, was done with a Nuclear Data ND 6600 data acquisition system. The neutron flux was measured using a 0.5 mm lithium glass scintillator.

For normalization purposes 1 mm Ag and Fe samples have been used. Additionally the Fe normalization has been repeated with both Fe and Cr samples in the neutron beam. The capture area (A) of the 1.6 keV resonance in ^{52}Cr determined for the different normalizations is:

- using 5 Ag-resonances between 16-71 eV: A = 58.0 $\pm$ 3.0 meV
- using the 1.15 keV resonance in ^{56}Fe: A = 48.75 $\pm$ 2.5 meV

The capture area obtained when normalized to Ag is in very good agreement with the transmission result obtained with an oxide sample of ^{52}Cr; i.e. A = 57.2 $\pm$ 4.0 meV. However the capture area normalized to the resonance parameters of ^{56}Fe obtained in transmission yield a 19 % smaller value. We conclude that there is a discrepancy between the capture areas obtained from transmission and from capture measurements for the 1.15 keV resonance in ^{56}Fe, but not for the 1.6 keV ^{52}Cr and also not for the 1.6 keV ^{57}Fe resonance [1].
One possible explanation of this discrepancy is the known hardness of the γ-ray spectrum of the 1.15 keV ^{56}Fe resonance [2]. However the γ-ray spectrum of the 1.6 keV ^{52}Cr resonance is very soft and in fact comparable to those of Ag and An resonances.

Analysis of capture data of the other measured resonances

G. Rohr, R. Shelley, A. Brusegan, F. Corvi, T. van der Veen

The analysis has been finished for resonances up to 300 keV using literature values for Γ_n. It will be repeated as soon as the Γ_n values from transmission measurements performed at GELINA become available.

Resonance parameters of ^{53}Cr
High resolution neutron capture cross section measurements

A. Brusegan, F. Corvi, G. Rohr, R. Shelley, T. van der Veen, G. Van der Vorst

The ^{53}Cr capture yield has been normalized to the area of the 1.6 keV resonance of the ^{52}Cr isotope, present as a 3.44 % impurity in the sample. The

(1) G. Rohr, A. Brusegan, F. Corvi, R. Shelley, T. van der Veen, and C. Van de Vorst, Proc. of Int. Conf. Nuclear Data for Science and Technology, Antwerp 1982, p. 139

(2) G. Rohr, Proc. Spec. Meeting on Fast Neutron Capture Cross Sections, Argonne, 1982, NEANDC(US)-214/L, p. 394

analysis of the capture data is in progress. It will be completed as soon as the resonance data from transmission measurements at GELINA become available. In fig. 11, the measured capture yield of ^{53}Cr, reduced to capture cross section, is plotted versus the neutron energy for the four s-wave resonances at 4.2, 5.7, 6.7 and 8.2 keV. The shape of the resonances is strongly influenced by multiple scattering and prompt background contributions which make the analysis very difficult.
Similar problems appear at higher energy, where several resonances have large neutron widths.

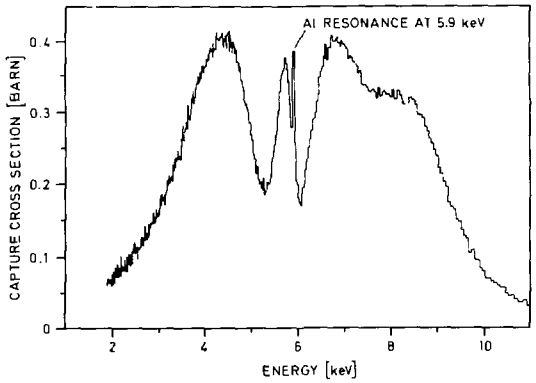

Fig. 11. ^{53}Cr neutron capture cross section in the energy range 2 - 11 keV

Resonance parameters of ^{54}Fe

A. Brusegan, F. Corvi, G. Rohr, R. Shelley, T. van der Veen, G. Van der Vorst

A detailed description of the present ^{54}Fe neutron capture measurements has been published previously in the Proceedings of the International Conference [1] held in Antwerp in 1982 and reported in the second Programme Progress Report of Nuclear Measurements of the same year. Resonance parameters and capture areas were given up to 200 keV and compared with the results of B.J. Allen et al. [2].

---

(1) A. Brusegan, F. Corvi, G. Rohr, R. Shelley, T. van der Veen and G. Van der Vorst, Proc. Int. Conf. on Nuclear Data for Science and Technology, Antwerp, 1982, p. 127

(2) B.J. Allen, A.R. de L. Musgrove, J.W. Boldeman and R.L. Mäcklin, AAEC/EU03, (1977) and Proc. Spec. Meeting, CBNM, Geel, 1977, p. 447

Actually, the analysis has been extended up to 300 keV, but using a modified version of the shape analysis programme FANAC extended by the following features:

- the number of mesh points in the cross section tables has been increased up to 4100
- the resolution can now be described either by a Gaussian or by a χ^2-function. The latter, already defined in the original version of the programme for $\nu = 4$ degrees of freedom, has been modified to accept any value of ν. In the present analysis the empirical value $\nu = 24$ has been adopted, which has to be compared with $\nu = 17$ given in the calculations of Bignami et al. (1).

Above 244 keV, the resonance neutron widths have been taken from a recent analysis of a new high resolution measurement of the ^{54}Fe total cross section performed by Cornelis et al. (2). These results are still considered as preliminary.
In the high energy capture cross section of ^{54}Fe, background and multiple scattering contributions can hardly be distinguished and, in particular, separated from the yield of the very large s-wave resonances. In those cases, where the neutron widths are of the order of 20 keV, important corrections related to prompt background contributions must be introduced. Data below 200 keV will be analysed once more in order to take into account the effects of the asymmetric resolution function.

Resonance parameters of ^{56}Fe

F. Corvi, A. Brusegan, R. Buyl, G. Rohr, R. Shelley, T. van der Veen

Resonance analysis

The following improvements were introduced in the shape programme FANAC in order to better describe the resonance structure at high neutron energy and in conditions of high resolution:

- the number of mesh points describing the energy zone under investigation was increased from 3060 to 4100;

---

(1) A. Bignami, C. Coceva and R. Signorini, Rep. EUR 5157e (1974)
(2) E. Cornelis, F. Poortmans and L. Mewissen: private communication

- the Gaussian resolution function used up to now was replaced by a χ^2-function with ν = 24 degrees of freedom. Such an option, which was already present in the original FANAC programme was implemented in order to correctly take into account the asymmetry of the moderation time jitter. The value of ν = 24, which was derived from best fitting the data, has to be compared with the value ν = 17 calculated by Bignami et al. [1] for the region above 30 keV.

An example of fit with such an asymmetric profile is shown in Fig. 12 for the ^{56}Fe doublet at E_0 = 102.8 - 103.2 keV.

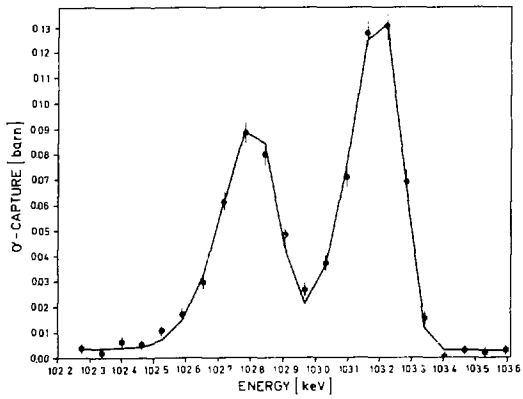

Fig. 12. Fit of the ^{56}Fe capture doublet at 102.8 - 103.2 keV with an asymmetric resolution function (programme FANAC)

Since a systematic discrepancy was noted between the resonance parameters obtained from FANAC and those obtained from the area programme TACASI for the same isolated resonances, this last programme was also carefully re-examined. Several improvements were introduced, the most important of which is also an increase in the number of mesh points up to 3000 in order to more completely cover the energy region reached by a neutron after a single scattering in the sample. The ^{56}Fe capture data were re-analysed with such improved programmes; moreover the energy region under investigation was

(1) A. Bignami, C. Coceva, and R. Simonini, Rep. EUR 5157e (1974)

extended up to 350 keV and parameters for a total of 115 resonances were deduced. As a consequence of the improvements done, the discrepancy between the results of FANAC and TACASI has practically disappeared.

Measurement of the scattered neutron sensitivity

In order to precisely determine the capture widths of s-wave resonances one must know the contribution to their capture areas due to prompt detection of scattered neutrons. To meet this goal, a measurement of the scattered neutron sensitivity as a function of energy was recently carried out in the following way. The counting rate of a 7 mm thick graphite sample, which scatters about 27 % of the neutrons, was compared to that of a 0.5 mm thick gold sample. "Black resonance" filters of S and Na were continuously kept in the beam in order to monitor the background around 102 keV and 2.85 keV. In the graphite sample run, a sizeable dip was apparent at about 102 keV, corresponding to a signal-to-background ratio of 1:1, while practically no dip was visible at 2.85 keV. Additionally, an "open beam" run was performed, always with the same filters in place: the TOF spectrum from such a run was then taken as a background for the other runs after normalization to the same counting rate at 102 keV. The results are compared to those of other detector set-ups in fig. 13.

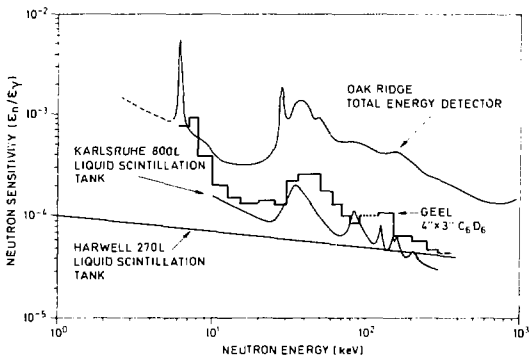

Fig. 13. Scattered neutron sensitivity of the Geel scintillators compared to that of other detector systems

Our neutron sensitivity follows the same trend as the Oak Ri ge detectors but is a factor 2 to 5 lower. This is probably due to the absence of fluorine in the scintillators and of any massive material in the vicinity except for a light aluminium support. After correction of the Γ_γ of s-waves for the above effect, the final data including parameters for 115 resonances have been presented at the Consultants' Meeting on Nuclear Data for Structural Materials, IAEA, Vienna, 2-4 November 1983, under the title "The Neutron Capture Cross Section of ^{56}Fe from 1 to 350 keV".

1.15 keV resonance of ^{56}Fe (International Task Force)

G. Rohr, A. Brusegan, F. Corvi, K.H. Böckhoff

The large difference in Γ_n values (about 30 %) of the important 1.15 keV resonance as they were obtained on one hand from neutron transmission and on the other hand from neutron capture measurements is the matter of concern of this task force. The discrepancy was first observed by G. Rohr. On request by the task force leader F. Perey (ORNL) the data from two different capture measurements on ^{56}Fe performed at CBNM (run I and run II) were re-examined in each detail, because the resulting capture areas of the 1.15 keV resonance differed on the average by 10 %. A partial explanation for this deviation has been found but no hint could be discovered leading to an explanation of the Γ_n discrepancy between capture and transmission results.
CBNM transmission data obtained in 1982 were sent to ORNL for analysis.

High resolution neutron transmission measurements in ^{56}Fe

E. Cornelis[★], L. Mewissen[★★], F. Poortmans[★★], H. Weigmann

The analysis of the high-resolution (0.01 ns/m) total cross section experiments on ^{56}Fe is completed.
The neutron widths were determined from a shape analysis of the data using the Reich-Moore multilevel routine MULTI up to the threshold for inelastic scattering at 850 keV. The assignment of spin and parity of sufficiently broad

---

★ Rijksuniversitair Centrum Antwerpen, Belgium

★★ SCK/CEN Mol, Belgium

resonances (resonance width not much smaller than resolution width) could be done on the basis of the resonance shape and peak total cross section. The best overall fit of the data was obtained with a channel radius R = 5.0 fm. In total 188 resonances were analysed in the energy range from 240 keV up to 850 keV. For 80 among them, the spin and parity was determined. This has yielded the following results for the strength functions in the energy range from 240 keV up to 850 keV:

$$S_0 = 2.6 \,^{+\ 0.9}_{-\ 0.6} \times 10^{-4} \qquad \text{(24 resonances)}$$

$$S_1 = 5.0 \,^{+\ 1.5}_{-\ 1.1} \times 10^{-4} \qquad \text{(30 assigned p-wave resonances)}$$

$$S_2 = 2.8 \,^{+\ 0.9}_{-\ 0.7} \times 10^{-4} \qquad \text{(26 assigned d-wave resonances)}$$

By comparing our results with the ENDF/B-V evaluation, good agreement for the s-wave structure but quite important discrepancies for the p-wave and d-wave structures are noted.

Resonance parameters of ^{57}Fe

G. Rohr, A. Brusegan, F. Corvi, R. Shelley, T. van der Veen, C. Van der Vorst

High resolution neutron transmission and capture measurements have been performed at GELINA with a 4 ns pulse width. An enriched ^{57}Fe-oxide sample has been employed at 50 m and 60 m, covering energy ranges up to 100 keV and 600 keV for transmission and capture measurements respectively. The detecting system consisted of a pair of 4" x 3" NaI(Tl) detectors together with a 5 mm $^{10}B_4C$ slab for transmission and a pair of 4" x 3" C_6D_6 liquid scintillators for the capture measurement.

The neutron resonance parameter results obtained from the transmission measurement for the 1.6 keV resonance have been used to normalize the capture measurement. For the capture yield the so-called weighting technique has been applied whereby the capture events were weighted according to their amplitude information in order to achieve a detector efficiency proportional to the total gamma ray energy released in the capture process. The relative neutron flux was measured with a 3 mm thick $^{10}B_4C$ slab using the capture detectors to view the 478 keV photons associated with the neutron absorption $^{10}B(n,\alpha\gamma)^7Li$ reaction.

Comparison was also made with the flux measured by a ^{6}Li glass detector below 100 keV and with that measured by a multiplate ^{235}U fission chamber above 100 keV, giving an agreement within 3 % up to 400 keV.

The data sets have been analysed by means of modified versions of the multi-level FANAL and FANAC programmes and the single level TACASI programme. The low inelastic scattering threshold (14.4 keV) for spin J = 1 resonances analysed with the multi-level Reich-Moore formalism, including the elastic and one inelastic channel, enabled the determination of the inelastic scattering cross section by means of the transmission measurement [1]. A typical neutron capture cross section for ^{57}Fe fitted by the FANAC programme is shown in Fig. 14.

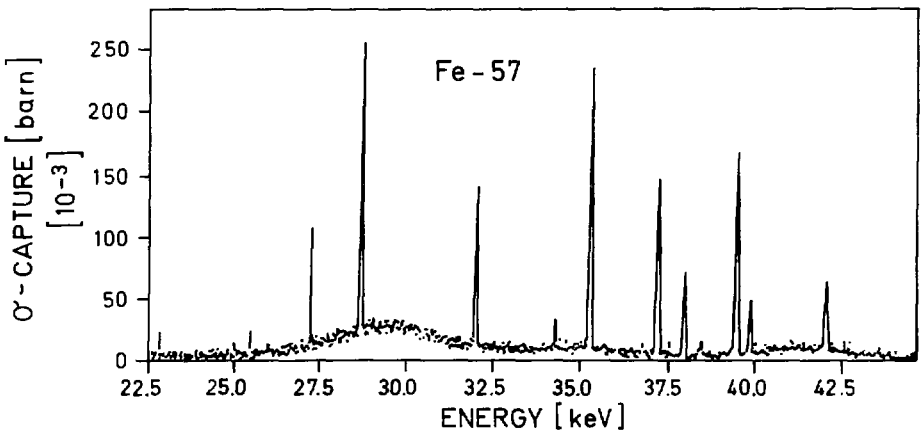

Fig. 14. Neutron capture cross section fitted by the R-matrix shape code FANAC over the energy range 23 to 44 keV

Neutron resonance parameter results for 120 resonances up to 200 keV were presented at the Antwerp conference [2] and tabulated along with earlier capture data published by ORNL. A comparison of the two capture area data sets, for well resolved p-wave resonances where our statistics are good, is best done in three energy ranges. Firstly below 20 keV, where two large

---

(1) G. Rohr and K.N. Müller, Z. Physik 227 (1969) 1

(2) G. Rohr et al., Int. Conf. on Nuclear Data for Science and Technology, Antwerp 1982, p. 139

s-wave structures are predominant and ten resonances are compared, our results are on average 15 % higher than those of ORNL. Between 20 keV and 50 keV agreement within 2 % is achieved, while over the rest of the energy range analysed, where as mentioned earlier broad s-wave resonances, poorer statistics and also a higher level density have made the analysis rather difficult, our results average 7 % higher. The agreement between ORNL and CBNM averaged over the whole energy range is within 8 % although this figure would be somewhat improved were it not for the large low energy discrepancy which may be caused by an incorrectly determined neutron flux. It should also be noted that the ORNL data have since been increased by 3.6 %, thus bringing both data sets to within 5 % of each other. Our uncertainties include statistical and systematic errors due to the background, neutron sensitivity, relative flux and inconsistency of our two analysis programmes as discussed earlier, but not for the difference in spectrum shape because of the unsettled situation of this problem.

1.3 CROSS SECTIONS OF FISSION PRODUCTS

Average capture measurements of ^{149}Sm

F. Corvi, A. Brusegan, T. van der Veen

At a 30 m flight path the capture measurements which extend up to 300 keV have been finished. A run extending up to 1 MeV is planned for beginning 1984 on a 60 m long flightpath.

1.4 GAS PRODUCING REACTIONS

Measurement of (n,α) cross sections from threshold to 14 MeV neutron energy

E. Wattecamps, F. Arnotte

A multi-telescope system has been used for the determination of (n,α) cross-sections of Cr, Fe and Ni from 5 to 10 MeV [1] and at 14 MeV [2]. Measurements

(1) A. Paulsen, H. Liskien, F. Arnotte, and R. Widera, Nuclear Science and Engineering, 78, 377-385 (1981)

(2) E. Wattecamps, H. Liskien, and F. Arnotte, Proc. of the Int. Conf. on Nuclear Data for Science and Technology, Antwerp, Sept. 1982, p. 156

of other elements with even smaller cross-sections are envisaged. To understand and possibly reduce the background a detailed investigation of energy "E", energy loss "ΔE" and time spread "τ" between E and ΔE was performed by simultaneous acquisition of these three parameters. The three-dimensional distributions in E, ΔE and τ were investigated by the analysis of two-dimensional spectra in (ΔE,E), (E,τ) and (ΔE,τ). It turns out that τ is energy- and energy loss-dependent. Areas in the (E,τ)- or (ΔE,τ)-distribution that are typical for α-particles are easy to define but coincide entirely and solely with all events of the alpha area in the (ΔE,E) distribution used up to now. It is therefore concluded that smaller resolving times of triple coincidences or even an energy dependent time window do not reduce the background significantly.

The Van de Graaff accelerator provides neutrons from 5 to 10 MeV by the $D(d,n)^3He$ reaction with a strong forward directed neutron yield. The below described test measurements were performed to see if this source property could be better exploited than in the hitherto used multitelescope.

The source-to-sample distance was chosen to be 5 cm (instead of the earlier 20 cm) and the sample-to-energy detector distance was fixed at 9 cm (instead of the earlier 4.5 cm). No neutron shield was used. Test runs at 8 MeV neutron energy for α-particle emission at 0°, 22° and 45° from a thin Ni-sample were performed using a single telescope made of two A-filled ΔE-proportional counters in front of a 9 cm^2 x 100 μm surface barrier semi-conductor acting as E counter. As expected from the angular distributions of the source neutrons the background (Fig. 15b) is much larger at 0° than at 45°. The net signal (Fig. 15c) amounts to about 7500 counts and illustrates that the α-particle spectrum below channel 20 (corresponding to approximately 3 MeV) is practically zero, as to be expected from the coulomb barrier repulsion and as observed in previous measurements. Thus the background determination at least for 45° and 22° is performed properly down to 1 MeV alpha particle energy, even though large numbers must be subtracted from each other.

A second sequence of runs was performed with the single telescope at 22° but with samples of Ni, Cu and Nb. The alpha particle energy spectra for these three elements, as observed in runs of approximately 4 hours each, are given in Fig. 16. The (n,α) yield of Cu is much lower than that of Ni, but measurable. The Nb run yielded only 125 net counts above 5 MeV α-particle energy, but the corresponding background run resulted in only 5 counts for the same energy threshold.

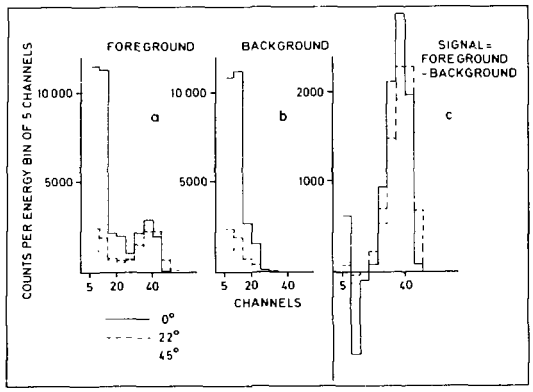

Fig. 15. (a) Foreground-, (b) background- and (c) signal of alpha particle spectra of Ni measured at 0° (—), 22° (—.—) and 45° (···) in counts per energy bin of 5 channels as obtained in 4 hours

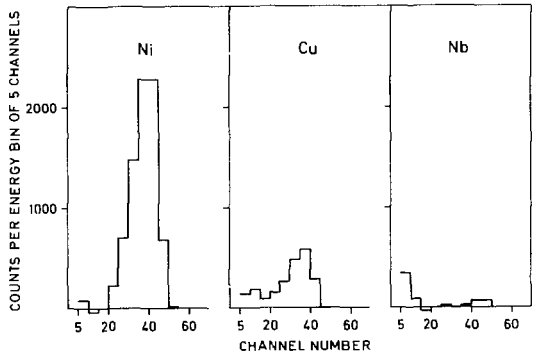

Fig. 16. Alpha particle energy spectra of Ni, Cu and Nb in counts per energy bin of 5 channels as obtained in 4 hours

We conclude from the above described runs, that an extension of these tests to backward angles, is justified.

1.5 VARIOUS MEASUREMENTS AND DEVELOPMENTS

Determination of double-differential neutron emission cross-section for ^{7}Li

E. Dekempeneer*, H. Liskien, F. Poortmans*

This cross section will be determined in view of its importance for the neutron spectrum in blankets of fusion reactors. Pulsed neutrons at 40 m from a bare U-target at GELINA will serve as primary neutrons up to 16 MeV. Detection of scattered neutrons occurs in six 5 x 5 cm NE 213 - scintillators coupled to RCA 8850 photomultipliers. These detectors serve as double spectrometers. The primary neutron energy is determined by TOF, the energy of scattered neutrons by pulse-height unfolding.
The calibration of these detectors has been obtained with mono-energetic neutrons from the reaction $T(p,n)^{3}He$, $D(d,n)^{3}He$ and $T(d,n)^{4}He$ using the Van de Graaff accelerator. The absolute scale is based on proton recoil counting employing a telescope counter.
Fig. 17 shows the results of the efficiency determination for a bias setting of 171 keV electron energy. The dotted line represents the results from Monte-Carlo calculations using the code NEFF4 (1) of PTB.

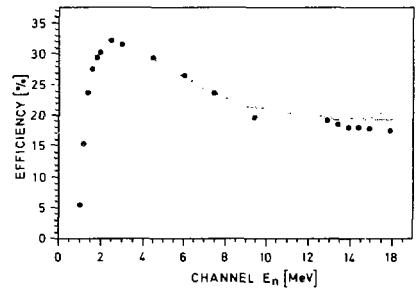

Fig. 17. Efficiency of a 5 cm Ø x 5 cm NE213 scintillator with a bias setting at 171 keV electron energy. The dotted line is the result of Monte Carlo calculations

(1) G. Dietze and H. Klein, PTB-Bericht ND-22 (1982)

* SCK/CEN Mol, Belgium

Figures 18 and 19 show selected response functions at 3.0 and 9.5 MeV neutron energy, respectively. The spectrum shape at lower pulse-heights is determined by neutron interactions with the carbon nuclei of the scintillator. Again, the dotted lines are the results from the PTB code NRESP4E [1].

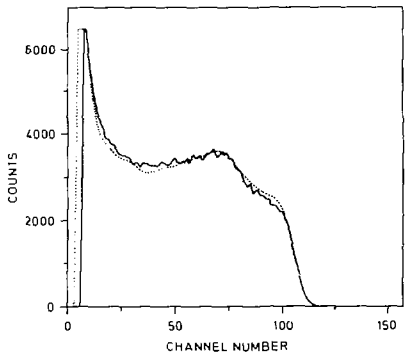

Fig. 18. Response function for 3 MeV neutrons. The dotted line is obtained by Monte Carlo calculation

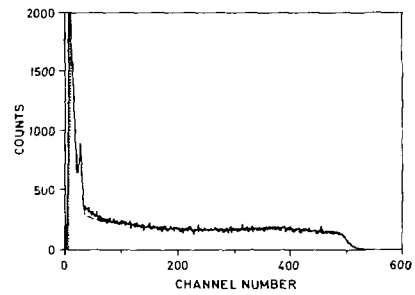

Fig. 19. Response function for 9.5 MeV neutrons. The dotted line is obtained by Monte Carlo calculation

It is planned to check these response functions on a relative base with non-monoenergetic neutrons from GELINA in the final experimental set-up.

On-line neutron time of flight to energy conversion

C. Bastian, P. ter Meer

In conventional time of flight spectroscopy, the digital output of a time coder is used as the address where to increment the memory of a multichannel analyser. Nuclear events are thus sorted by neutron time of flight, a neutron energy spectrum may only be obtained by an off line conversion involving the flightpath distance and the time lag of the detection chain. In particular, this means that simultaneous measurements with e.g. two detectors at different distances cannot be brought in direct channel-to-channel correspondence on an energy scale.

---

(1) G. Dietze and H. Klein, PTB-Bericht ND-22 (1982)

Using an Intel 8086 microprocessor board * connected between a 4 ns CBNM time coder at the input, and a ND 6660 multichannel analyser at the output, we designed and tested a PASCAL software package for on-line TOF-to-energy conversion. This package essentially converts the time of flight address directly to an energy address on a linear or (optionally) logarithmic scale. It may handle simultaneously the input of up to 16 different detectors, provided that they are identified by corresponding tag bits in the time coder output.

As a test run, we recorded the output of a flux detector through a ^{238}U filter. The energy of the resonances can be directly determined on the raw spectrum of fig. 20 (upper trace) or on the spectrum in which the count rate fluctuations have been eliminated (lower trace). The recording energy scale is linear, from 1 eV to 50 keV.

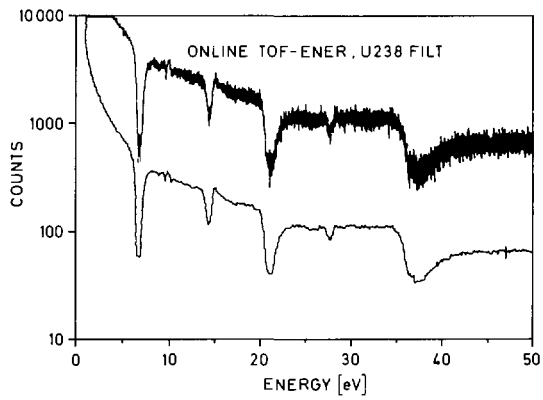

Fig. 20. On-line time-of-flight to energy conversion

* this board is a part of an INtellec Development System (Series III)

1.6 STANDARD NEUTRON DATA

Intercomparison of neutron flux detectors

K.H. Böckhoff, C. Bastian, A. Brusegan, C. Budtz-Jørgensen, F. Corvi, H.-H. Knitter, J. Wartena, H. Bax, C. Bürkholz, R. Buyl, C. Van der Vorst

Neutron flux detectors play a crucial role in partial neutron cross section determination. The uncertainty of the neutron flux data obtained with them has a large impact on the quality of the partial cross section data, in particular when high accuracies are requested.
Over the years a variety of different neutron flux detectors has been developed and used at GELINA, all employing the conventional neutron standard reactions.
A campaign of intercomparing the shapes of the response functions of these detectors in a given neutron energy spectrum has been launched at GELINA. The goals of this exercise are:

- to improve our knowledge about the relative merits of these detectors
- to prepare for an international intercomparison of neutron flux detectors
- to arrive at an improved knowledge of the neutron fluxes available at GELINA, in particular at higher energies (MeV range).

The first part of this campaign deals with neutron flux detection in the lower part of the neutron energy spectrum of the Linac neutron source which is enhanced by means of moderators. The detectors to be intercompared are grouped into two classes:

- high efficiency (count rate) detectors
- low efficiency (count rate) detectors.

The response functions of the detectors of each group will be compared. The information obtained for each group will be linked by means of one detector which is common to both groups.

Intercomparison of high efficiency neutron flux detectors

The energy range of interest extends from a few eV to about 1 MeV. The types of flux detectors, their size, the reaction involved, the thickness in at/b of the target isotope, the flight path station and the linac parameters are listed in Table 3. The detectors 1 to 5 were used one at a time on the same

Table 3. Main parameters of the intercomparison of high efficiency neutron flux detectors

Detector				Flight path		Linac Parameters		
	Type	Size (cm)	Reaction	Thickness (at/b)	Number	Length (m)	f (Hertz)	Δt (ns)	P (kW)
1	Multi-plate fission chamber	ø = 9.0	$^{235}U(n,f)$	0.10×10^{-3}	14	28	400	12	4
2	Au t = 0.6 mm two C_6D_6 scint.	ø = 9.0	$Au(n,\gamma)$	3.58×10^{-3}	14	28	400	12	4
3	^{10}B slab t = 0.6 mm + two C_6D_6 scint.	ø = 8.0	$^{10}B(n,a\gamma)$	6×10^{-3}	14	28	400	12	4
4	^{10}B slab t = 3 mm + two C_6D_6 scint.	9.0 x 9.0	$^{10}B(n,a\gamma)$	0.03	14	58	100	12	1
5	^{6}Li glass t = 0.5 mm	ø = 9.0	$^{6}Li(n,T)$	0.84×10^{-3}	14	58	100	12	1
6	^{6}Li glass t = 0.5 mm	ø = 10.0	$^{6}Li(n,T)$	0.84×10^{-3}	16	58	100 400	12 12	1 4

flight path 14. However, depending on their counting efficiency, the detectors 1 to 3 were placed at a distance of 28 m from the target, while the others were placed at 58 m. To avoid overlapping from previous cycles, the same ^{10}B filter of thickness 5.68×10^{-3} at/b was used throughout. Finally, detector 6, which was placed on a separate flight path, acted as a sort of reference detector: its data were recorded during the course of the whole exercise in order to check the stability of the neutron flux shape and possibly correcting for small deviations. Background was determined using "black" filters of S, Na, C, W, Ag. The analysis of the data is underway. Prior to the continuation of the analysis of the data an action was taken to improve the programme currently used for background and flux determination at the Linac. We kept to the idea of the modular programme ANGELA, originally written in FORTRAN to be executed in batch as a chain of standard spectrum to spectrum operations (e.g. additions, fits, normalizations, etc...). The newer tool is an APL workspace, also called ANGELA for ANalysis of GEel LAboratory results. This newer version is operated interactively. It does not put any intrinsic limit to the size of the spectra (4096 channels at most in the former version). It also ensures a complete parallel treatment of the error propagation, associating to every intermediate result a variance spectrum (uncorrelated) and a covariance matrix (correlated errors).

We attempt a comparison of some available experimental data. The result [1] is an estimate of the flux in the range 1 keV - 1 MeV relying on the older version for fit operations.
All options necessary for the intercomparison are now operational. A complete test run was done with data from Brusegan (B-slab at 30 and 60 m). The results at 30 m are shown in Fig. 21.

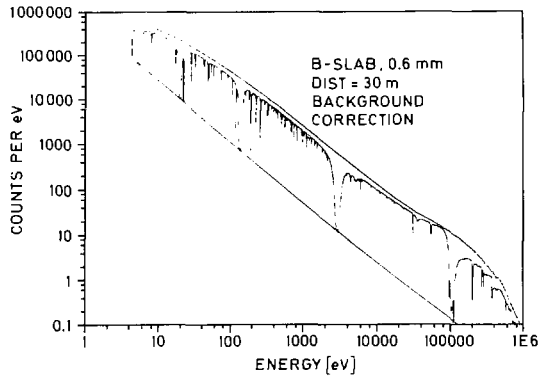

Fig. 21. Analysis of detector comparison

Intercomparison of low efficiency neutron flux detectors

The useful energy range extends here from 7 eV to 100 keV. In a first run the detectors quoted in Table 4 were investigated.
The intercomparison of the response revealed large deviations from results to be expected under ideal circumstances, in particular towards higher energies. The discrepancies are probably due to γ-flash effects which are strong at the short flight paths used. To overcome these effects, the detectors have been moved to a 30 m station and the measurements were started again, of course with strongly reduced neutron intensities and therewith long data accumulation times.

(1) GE/R/LI/105/83 (Internal Report)

Table 4. Main parameters of the intercomparison of low efficiency neutron flux detectors

	Detector					Flight path		Linac Parameters		
	Type	Size (cm)	Reaction	Sample N°	Thickness µg/cm²	N	Length (m)	f (Hertz)	Δt (ns)	P (kW)
1	Ion chamber	4.5	$^{6}Li(n,\alpha)$	2	245	2	7.536	800	1.6	7
2	Ion chamber	4.5	$^{10}B(n,\alpha)$	2	30	2	7.6505	800	1.6	7
3	2 ion chambers	4.5	$^{235}U(n,f)$	2	193.5	2	7.6105 7.6505	800 800	1.6 1.6	7 7
4	Parallel plate prop. counter	7.5	$^{10}B(n,\alpha)$	2	1.28	2	8.607	800	1.6	7
5	Gaseous scintillator	*)	$^{6}Li(n,\alpha)$		19 mg	2	10.40	800	1.6	7
6	Gaseous scintillator	*)	$^{10}B(n,\alpha)$		4 mg	2	10.40	800	1.6	7

*) Cylindrical samples with an effective area of 200 cm^2

Linac neutron spectrum measurements

H.-H. Knitter, C. Budtz-Jørgensen, H. Bax, E. Vogt

For neutron detection using the time-of-flight technique three ionization chambers detecting the reaction products of the nuclear reactions $^{235}U(n,f)$, $^{10}B(n,\alpha)^{7}Li$, $^{7}Li^{*}$ and $^{6}Li(n,t)^{4}He$ respectively were constructed and set up at a 8 m station of the CBNM Linac. The ^{10}B-detector is in use for the first time. It consists of two layers of ^{10}B, 30 $\mu g/cm^2$ thick and with a diameter of 4.5 cm, mounted back-to-back on a common cathode of two gridded ionization chambers, so that the reaction products are detected in the whole 4π-solid angle. Preliminary tests performed at an eight meter target distance have shown that the γ-flash of the linac induces a signal which is about two times larger in amplitude than the one detected for the particles. Therefore, a time interval of $\sim 1\ \mu s$ was gated out. The pulse height distributions obtained then from the cathode and from one of the anodes acquired during a few minutes are shown in Fig. 22. The ^{7}Li and alpha particle pulses are well separated from the electronic noise and from neutron-induced counter gas recoils. This good separation and the timing resolution of about 20 ns make also this detector able for neutron spectrum measurements at the CBNM linac.

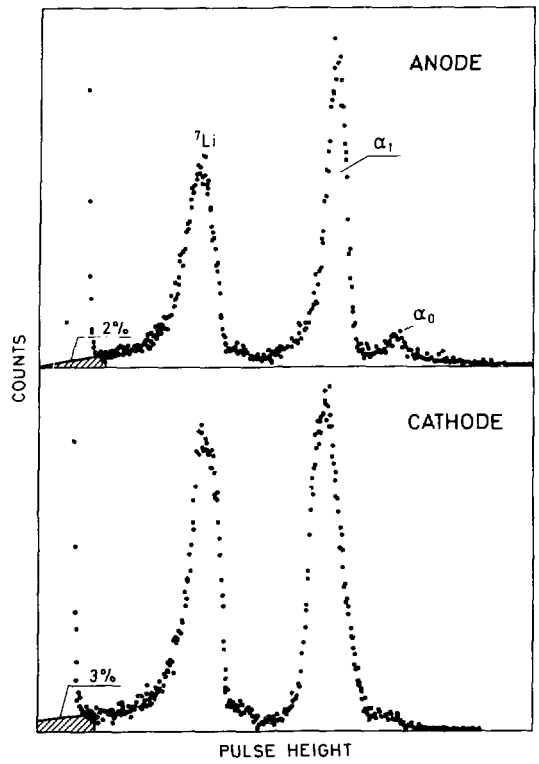

Fig. 22. The anode and cathode pulse height spectra obtained from a gridded ion chamber by the products of the $^{10}B(n,\alpha_{0,1})^7Li_{0,1}$ reactions are shown in the upper and lower part respectively

Calculation of neutron yields from heterogeneous uranium-beryllium targets

H. Weigmann

Approximate calculations of neutron yields from the bombardment of targets consisting of sequences of U- and Be-plates by 120 MeV electrons have been made. Monte Carlo techniques have been used for most of the calculations.

The four targets which will be discussed below are schematically shown in Fig. 23: Target A is a pure U-target of 10 cm length; target B consists of a 3 mm U converter followed by a 20 cm Be block; target C consists of 10 plates of U, each 2 mm thick, and 10 plates of Be, each of 2 cm, arranged in an alternating sequence; target D has the same Be-plates as C, but the U-plates have increasing thickness (from 1 to 4 mm) as shown in the figure.

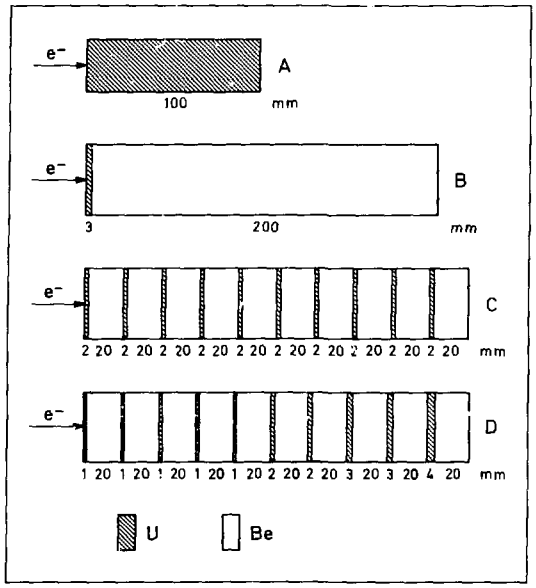

Fig. 23. Schematic drawing of the targets investigated; numbers are thicknesses of plates in mm

Several other similar geometries have been tried as well, with results differing only slightly from the ones discussed below. Since the production of bremsstrahlung as well as the creation of secondary electrons by photo- and compton-effect and pair-production at the energies of interest are strongly forward peaked, the angular distribution in these processes is ignored and the electron-gamma cascade is calculated in a one dimensional model. This represents the most important approximation in the present calculations. Also, the angular distribution of the emitted neutrons is

not investigated, but only the overall neutron production is calculated. However, within the accuracy which can be expected from a rough model calculation, the assumption of an isotropic emission of the neutrons produced will not be too crude. The main source of neutrons from U are (γ,n), $(\gamma,2n)$, and (γ,f) reactions through the giant resonance. The giant resonance parameters as determined by Caldwell et al. [1] have been used.

The fission neutron multiplicity $\bar{\nu}$ as a function of photon energy has been taken from Caldwell et al. [2]. The spectrum of fission neutrons is assumed to be a Maxwell spectrum with the temperature depending on $\bar{\nu}$ as given by Terrell [3]. Apart from the giant resonance part a pre-equilibrium contribution to the $^{238}U(\gamma,n)$ reaction is assumed. The experimental data of Kaushal et al. [4] on high energy neutron spectra from 55-85-MeV photon bombardment of U have been used to parametrize this contribution.

Since one of the purposes of the present investigation was to look for a possible improvement in the output of high energy neutrons by the use of Be as compared to the standard pure U-target, care has been taken not to underestimate the pre-equilibrium contribution from U but rather to use a high estimate for it. Nevertheless, this contribution provides the main source of uncertainty for the comparison below.

The neutron yield from the interaction of photons with Be is due to several reaction channels. At lower energies ($E_\gamma < 18$ MeV) essentially three channels compete: $^{9}Be(\gamma,n)^{8}Be$, $^{9}Be(\gamma,n)^{8}Be^{\star}$, and $^{9}Be(\gamma,\alpha)^{5}He$ with $^{5}He \rightarrow {}^{4}He+n$. At higher energies also $^{9}Be(\gamma,2n)$ and $^{9}Be(\gamma,pn)$ come into play. The cross sections and branching ratios have been expressed in simple parametrizations

---

(1) J.T. Caldwell, E.J. Dowdy, B.L. Berman, R.A. Alvarez, and P. Meyer, Phys. Rev. C21 (1980) 1215

(2) J.T. Caldwell, E.J. Dowdy, R.A. Alvarez, B.L. Berman, and P. Meyer, Nucl. Sci. Eng. 73 (1980) 153

(3) J. Terrell, Proc. of Symp. on Physics and Chemistry of Fission, Salzburg 1965, Vol. II, p. 3; IAEA Vienna 1965

(4) N.N. Kaushal, E.J. Winholds, P.F. Yergin, H.A. Medicus, and R.H. Augustson, Phys. Rev. 175 (1968) 1330

which reproduce experimental data given in ref. [1-4]. The energy distribution of the emitted neutrons for the lower energy region is obtained according to the branching ratios into the three competing reaction channels. For the higher neutron energies again the experimental data of Kaushal et al. [5] have been used for a parametrization.

The results of the calculations are given in Table 5 and in Figs. 24, 25, 26. Table 5 gives the overall number of neutrons produced in U, Be, and totally, for the four above targets, when bombarded with 120 MeV electrons at 10 kW average power.

Table 5. Numbers of neutrons produced (10^{13} neutrons/s)

Target	U	Be	Totally
A	4.08	---	4.08
B	0.22	0.47	0.69
C	2.03	0.36	2.39
D	1.77	0.35	2.12

Fig. 24 shows the neutron spectra obtained for the same conditions. Although the total neutron output from the heterogeneous U-Be-targets (C and D) is lower than the one from the pure U-target, the increased intensities at high neutron energies (above 7 MeV) makes them interesting e.g. for work in the field of nuclear data measurements for fusion reactor applications.

(1) F. Ajzenberg-Selove, Nucl. Phys. A320 (1979) 1

(2) R.J. Hughes, R.H. Sambell, E.G. Muirhead, and B.M. Spicer, Nucl. Phys. A238 (1975) 189

(3) U. Kneissl, G. Kuhl, K.-H. Leister, and A. Weller, Nucl. Phys. A247 (1975) 91

(4) J. Ahrens, H. Borchert, K.H. Czock, H.B. Eppler, H. Gimm, H. Gundrum, M. Kroening, P. Riehn, G. Sita Ram, A. Zieger, and B. Ziegler, Nucl. Phys. A251 (1975) 479

(5) N.N. Kaushal, E.J. Winhold, P.F. Yergin, H.A. Medicus, and R.H. Augustson, Phys. Rev. 175 (1968) 1330

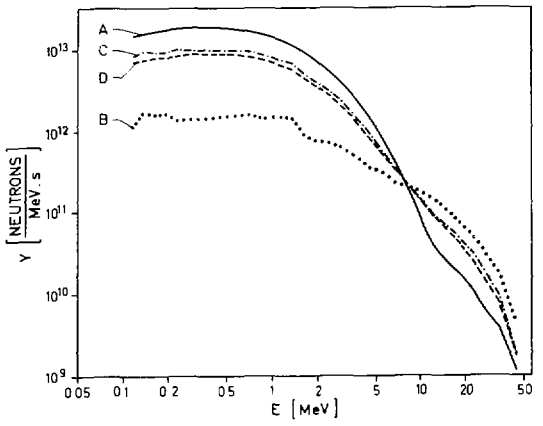

Fig. 24. Calculated neutron spectra

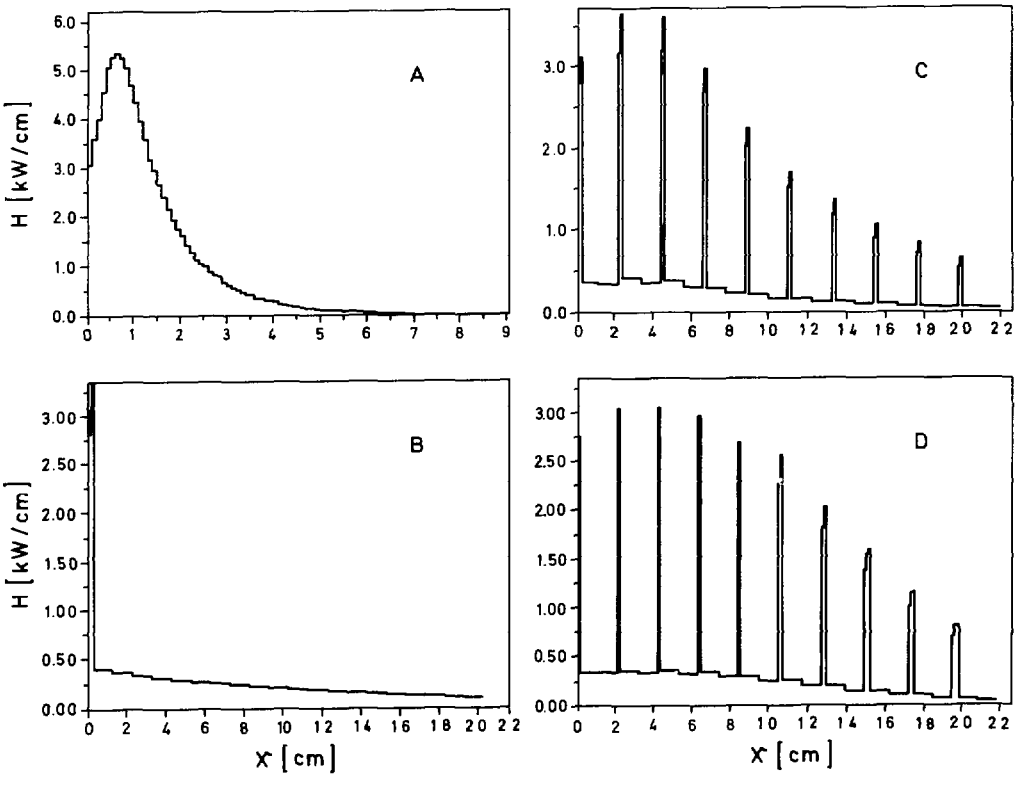

Fig. 25. Heat dissipation in the targets: note that the abscissa of A is different from the others

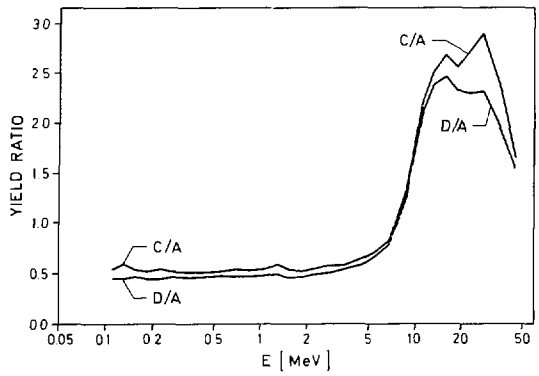

Fig. 26. Ratios of neutron yields from targets C and D, divided by yield from A

In Fig. 25 the heat dissipation within the targets is shown. One of the main advantages of the heterogeneous U-Be-targets lies in the fact that the heat dissipation is distributed over a larger volume, and therefore cooling of these targets will provide no essential problem.
In order to arrive at a still more uniform heat distribution than obtained with target C, target D has been included in the study. As seen from Fig. 24 the neutron output of these two targets differs only slightly. Finally, Fig. 26 gives the ratios of neutron yields from targets C and D, divided by the yield from the standard pure U-target A.

Absolute charged particle counting using a gridded ion chamber

C. Budtz-Jørgensen, H.-H. Knitter, H. Bax, R. Vogt

A method employing the combined energy and angle information from a gridded ion chamber was developed for precise charged particle counting. The method was tested both with spontaneous alpha particles and with neutron induced fission fragments.
As an illustration of the potential of the present technique the measured cos ϑ distributions of fission fragments emitted from a set of ^{235}U fission layers are given in Fig. 27.

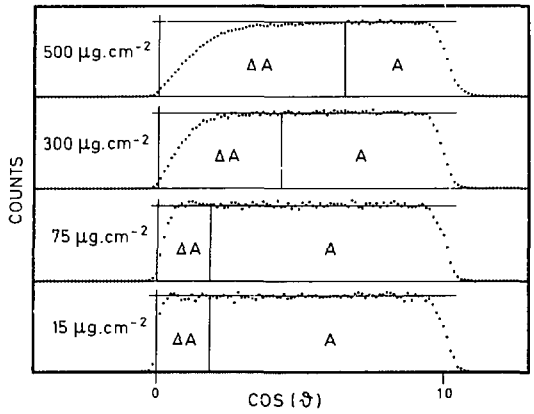

Fig. 27. The cos ϑ distributions of fission fragments from thermal neutron induced fission of ^{235}U for four samples of different thicknesses

From these distributions the absolute number of fission events induced in the layers can be determined to better than 0.5 % circumventing sample fragment absorption and scattering problems.

The experience and results obtained with the present technique were reported in two papers, "A precise method for charged particle counting employing energy and angle information from gridded ion chambers" and "Investigation of fission layers for precise fission cross section measurements with a gridded ionization chamber". The first paper was presented at the Seminar on Alpha Particle Spectrometry and Low Level Measurements (Harwell, May 1983). The second paper was presented at the IAEA $^{235}U/^{252}Cf$ Consultants' Meeting (Smolenice, April 1983) and is accepted for publication in Nuclear Science and Engineering. Its abstract reads as follows:

" An ionization chamber with Frisch-grid is used to determine both the energy (E) of the charged particles emitted from the source positioned coplanar with the cathode, and the cosine of the emission angle (ϑ) with respect to the normal of the cathode. In the plane determined by the variables cos ϑ and E it is possible to identify an area which is unaffected by backscattering and selfabsorption. Events belonging to this area show an isotropic angular distribution for alpha particles and also for fission fragments induced by thermal neutrons, which, extrapolated to 90°, yields the absolute number of events. The capabilities of this

technique are demonstrated by the investigation of four evaporated $^{235}UF_4$ layers and one suspension sprayed $^{235}U_3O_8$ layer. For the UF_4 layers the alpha particle source strengths were determined, and agreement was found within 0.3 % with values independently measured by low geometry alpha counting.
The same method was applied also to fission events induced by thermal neutrons. An accuracy for the determination of the total number of fission events of better than 0.5 % is reached. The longstanding doubts on the magnitudes of fragment absorption and scattering are in principle circumvented by the present method and therefore no assumptions on fragment ranges and scattering cross sections are needed. It is also emphasized that the present method, within reasonable limits, is insensitive to source shape and thickness homogeneity."

Neutron emission from the spontaneous fission of ^{252}Cf

C. Budtz-Jørgensen, H.-H. Knitter, R. Vogt, H. Bax

Several attempts have recently been made to give a theoretical description of the standard neutron spectrum of ^{252}Cf. However, these theoretical approaches suffer from a lack of knowledge about the mechanism of the fission emission i.e. the fraction of scission neutrons, emission during fragment acceleration, etc. There is therefore a strong need not only for precise neutron spectrum data, $N(E_n)$, but also for double- or multiple-differential measurements, $(N(E_n,\theta_n, A,TKE)$ which can help to clarify the nature of the fission neutrons.
The gridded ion chambers developed at CBNM provide a powerful tool for such measurements since fission fragment angle, kinetic energy and mass distributions can be determined simultaneously with an angular efficiency close to 4π. Preliminary tests have been made with a fission chamber loaded with a ^{252}Cf source of $\sim 4 \times 10^3$ fiss.s^{-1}. However, the source backing, 0.5 mm stainless steel, did only allow the detection of one fragment per fission event. Therefore, only a rough distinction between light and heavy fragments could be made based on the fission fragment energy spectrum. The fission neutrons were detected with a 4" x 2" plastic scintillator and conventional time-of-flight electronics. The coincidence resolution between the neutron detector and the fission chamber was < 2 ns. The neutron detector was placed 2.05 m from the ^{252}Cf source with a direction normal to the chamber electrodes. The cosines of the angles θ, between this direction and the path of the light fission fragments were determined using the chamber anode and cathode pulses. Figure 28 displays a biparametric plot of the number of neutrons versus cos θ and versus the neutron time-of-flight. At higher

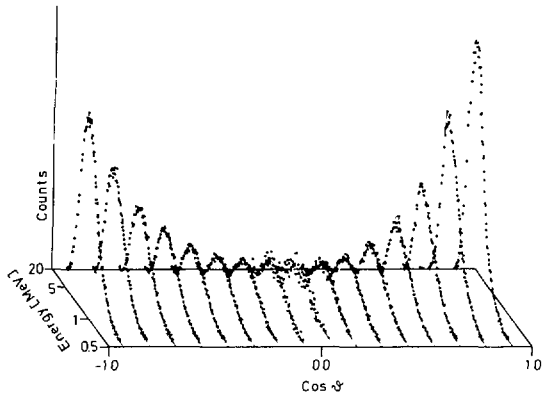

Fig. 28. Biparametric plot of the number of neutrons versus cos θ and versus the neutron time-of-flight. On the time-of-flight axis some equivalent neutron energies are indicated

neutron energies it can be seen that the neutrons are emitted mainly in the direction of either the light or the heavy fragment, confirming that most of the neutrons are emitted from the fully accelerated fragments. It is planned to continue the measurements with a ^{252}Cf source on a thin backing which will allow simultaneous detection of both fragments. This will allow to study the neutron spectra not only as function of the fission fragment emission angle, but also as function of the fission fragment mass and energy.

International fast neutron fluence intercomparison

H. Liskien, R. Widera

Under the auspices of CCEMRI/BIPM section III, four branches of intercomparison are presently going on. CBNM acts as coordinator for that branch which is based on $^{115}In(n,n')^{115m}In$. Results have recently been discussed by CCEMRI III.

Figure 29 shows the results from six laboratories at 2.5 and 5.0 MeV. One additional laboratory has withdrawn its results in an earlier stage. The numbers at each result indicate how many individual measurements have been executed.

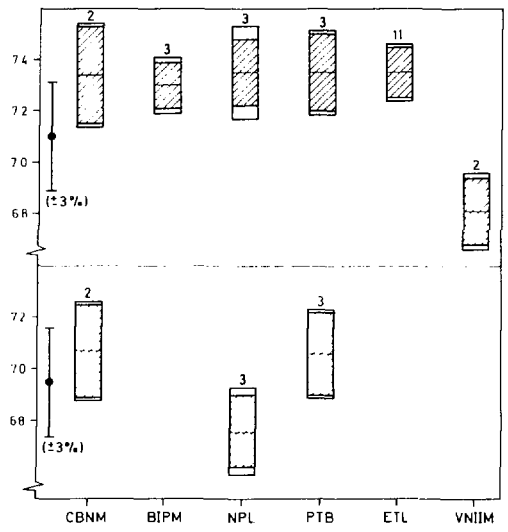

Fig. 29. Results of the fluence intercomparison by six laboratories at 2.5 MeV (above) and 5 MeV (below)

Averaging of these individual results has been performed by properly taking into account correlations. The smaller of the two given uncertainties refers to the fluence measurement alone. This demonstrates, that the uncertainty contribution from the transfer method is acceptable.

At 14.8 MeV partly inconsistencies show up. As most laboratories have also participated in another branch based on ^{93}Nb(n,2n), which did not reveal such inconsistencies, it is concluded that the problem is due to scattered neutrons. The different response of the detectors is explained in Fig. 30.

For Nb(n,2n) degraded neutrons see smaller activation cross sections than the primary neutrons. Below 9 MeV there is no response at all. For In(n,n') degradéd neutrons see much larger cross sections. There is response down to the 0.3 MeV region.

CCEMRI III came to the conclusion that the results at 2.5 and 5.0 MeV should be published in Metrologia. A manuscript entitled "International Fluence Rate Intercomparison for 2.5 and 5.0 MeV Neutrons" was prepared and accepted.

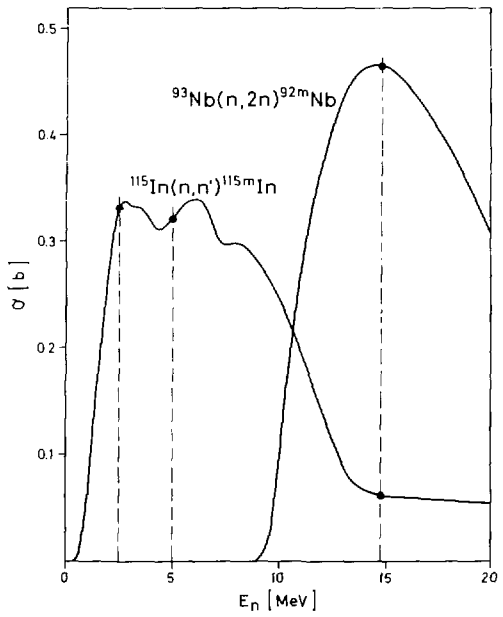

Fig. 30. Cross sections of $^{115}In(n,n')$ and $^{93}Nb(n,2n)$

The abstract reads as follows:

> "Fluence determinations for 2.5 MeV and 5 MeV neutrons as performed in standards laboratories have been compared. The intercomparison method is based on the determination of a γ-rate ratio between ^{115m}In as induced by fast neutrons in an indium sample on one hand, and ^{51}Cr from a calibrated source on the other hand. Results show that the uncertainty contribution from the transfer method does not essentially increase the overall uncertainty and that there is consistency with only one exception."

Concerning the 14.8 MeV results CCEMRI II demanded that the effect of scattered neutrons is studied more in detail and on equal basis for all participants.

1.7 UNDERLYING PHYSICS

Neutron resonance structure of light elements: ^{28}Si

I. Van Parijs*, L. Mewissen*, F. Poortmans*, H. Weigmann

A first series of high-resolution (0.01 ns/m) neutron total cross section measurements has been analysed up to the inelastic threshold at 1.78 MeV. The T = 3/2 isobaric analogue state in ^{29}Al has been found at 1200.8 keV neutron energy.
A second series of experiments between 1.5 MeV and 4 MeV has been started.

The $^{41}Ca(n,\alpha)^{38}Ar$ reaction in the resonance region

C. Wagemans*, H. Weigmann, R. Barthélémy, J. Van Gils*

The $^{41}Ca(n,\alpha)^{38}Ar$ reaction is of importance for astrophysics, since the observed abundance of the isotope ^{46}Ca is seriously lower than the value obtained in nucleosynthesis calculations. These calculations strongly depend on the reaction $^{41}Ca(n,\alpha)^{38}Ar$, for which no experimental data are available.
During a test experiment, a dozen (n,α)-resonances were observed in the neutron energy range from 4 to 140 keV. Meanwhile, the experimental conditions have been improved, which will result in a better energy resolution and which will allow an extension of the measurements towards higher neutron energies.

Fission fragment mass, kinetic energy and angular distributions for $^{235}U(n,f)$ in the neutron energy range from thermal to 6 MeV

Ch. Straede**, H.-H. Knitter, C. Budtz-Jørgensen

A double Frisch gridded ionization chamber has been used for the measurements of fission fragment mass, kinetic energy and emission angle of both fission fragments from neutron induced fission of ^{235}U. Data have been measured at different neutron energies, E_n, ranging from thermal to 6.0 MeV in steps of 0.5 MeV.

---

* SCK/CEN Mol, Belgium
** Bursary student

The evaluation of the acquired data is in progress. In the present figures only the results of the evaluation of a short (5 hours) thermal test run and the preliminary evaluations of the data acquired at 3.5 MeV, 4.5 MeV, 5.0 MeV and 5.5 MeV are shown.
In fig. 31 the pre-neutron emission mass distribution from the thermal test run is compared with data of Schmitt et al. (1).

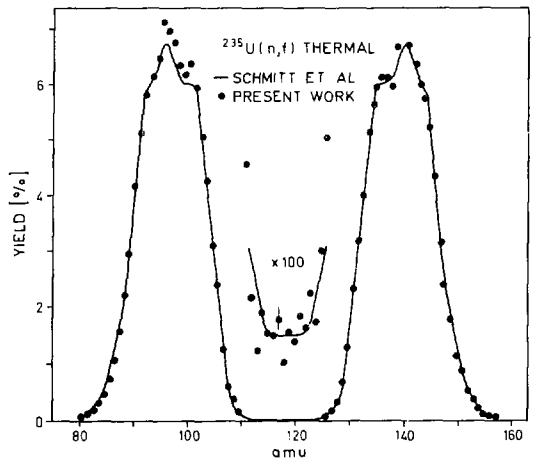

Fig. 31. Pre-neutron emission mass distribution from thermal neutron induced fission

In fig. 32 the so-called provisional mass distribution is shown for thermal neutrons and for E_n = 5.5 MeV. The typical changes of the yield for different mass splits are clearly seen.
Since both, kinetic energy and mass for each fission fragment is known from the measurement, it is possible to see how the mass distribution changes with KE, and thereby with excitation energy of the fission fragment. For thermal neutron induced fission the average pre-neutron emission KE of the light fission fragments is ≈ 102 MeV. When selecting increasingly higher KE, going towards cold fragmentation, the mass distribution shows more and more structure.

---

(1) H.W. Schmitt et al., Phys. Rev. 141, 1146 (1966)

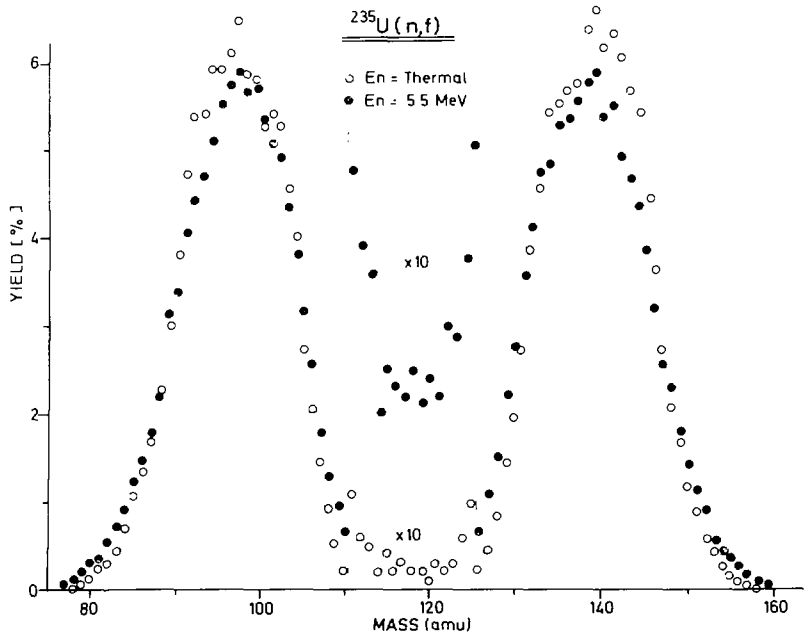

Fig. 32. Provisional mass distributions from neutron induced fission in ^{235}U

In fig. 33 the mass distribution from the short thermal run is plotted for a KE interval of (110 + 0.5) MeV. The distribution is compared to experimental data of Lang et al. [1], measured at the mass spectrometer LOHENGRIN. The mass resolution of LOHENGRIN is ≈ 0.2 amu and the comparison in fig. 33 shows that the mass resolution of the relatively simple ionization chamber is not worse than ≈ 2 amu.

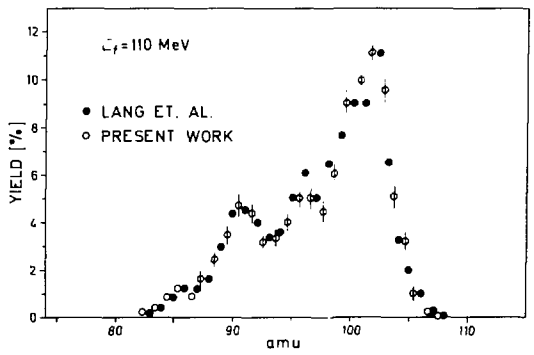

Fig. 33. Comparison of mass distributions from cold fragmentation

(1) W. Lang et al., Nucl. Phys. A345, 34 (1980)

In fig. 34 it is shown how the total kinetic energy, TKE, changes with neutron energy for different mass splits, and how the average total kinetic energy, $\overline{TKE}$, averaged over all mass splits, changes with E_n.

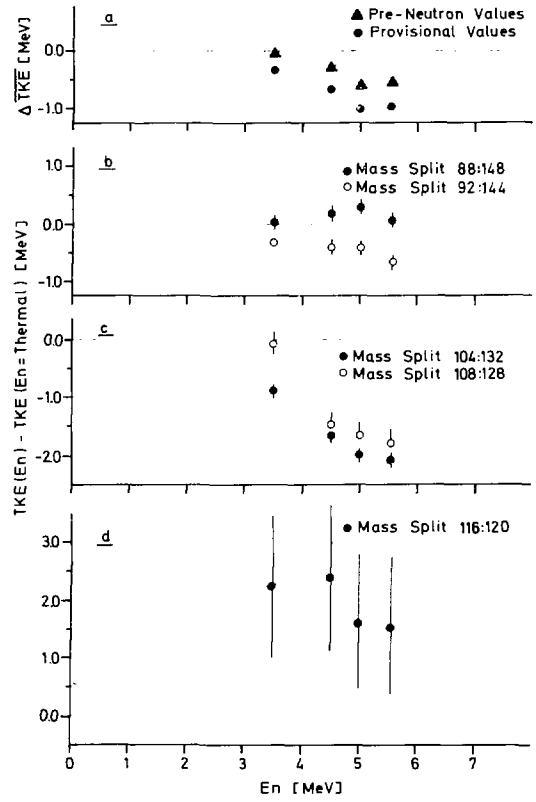

Fig. 34.

a : $\overline{TKE}(E_n) - \overline{TKE}(E_n = THERMAL)$ *for pre-neutron, Δ, and provisional, o, values;*

b,c,d : *changes in TKE with* E_n *for given mass splits averaged over 4 masses. Provisional values*

With the exception of $\overline{TKE}$ the present results are only the so-called provisional values, where no explicit correction for prompt neutron emission is made. Evaluations giving pre-neutron emission values are in progress. In the upper part of fig. 34 the shift in average total kinetic energy, $\overline{TKE}$, with E_n is shown. Pre-neutron and provisional values are shown for comparison. A decrease in $\overline{TKE}$ for $E_n \cong$ 4-5 MeV is found in agreement with earlier data [1]. A general decrease in $\overline{TKE}$ with increasing neutron energy is caused by changes in the fission fragment mass distribution, but it does not explain the structure at E_n = 4-5 MeV.

---

(1) J.W. Meadows and C. Budtz-Jørgensen, Proc. Int. Conf. on Nuclear Data for Science and Technology, Antwerp, 1982, p. 740, Ed. K.H. Böckhoff

An explanation of this structure might be found in the framework of a static scission point model [1]. According to this model a sudden decrease in TKE would be expected for mass splits close to the 104/132 split. The model also predicts a smooth increase in TKE for symmetric fissions with increasing E_n. Indeed a sudden drop in TKE is seen in fig. 34 for the 104/132 and 108/128 splits for $E_n \cong 4.5$ MeV. It is also seen that TKE for the symmetric splits, fig. 34d, in the presently evaluated data is higher than the thermal values. The nature of this shift will be seen in the evaluation of the lower neutron energy data. Furthermore fig. 34 shows that TKE is still close to the thermal value for the 88/148 and 92/144 splits for 3.5 MeV $\leq E_n \leq$ 5.5 MeV. Corrections for prompt neutron emission will shift the values upwards but probably not change the structure drastically. For mass-splits between the 84/152 and 76/160 split it is also found that TKE increases with increasing neutron energy. Finally angular distributions of the fission fragments have been measured. These data are in very good agreement with earlier data [2].

Determination of multipole strength in the reaction ^{207}Pb+n

R. Köhler, L. Mewissen*, F. Poortmans*, J. Theobald**, H. Weigmann

Prior to 1977 the overall claimed M1-strength in ^{208}Pb has been between 30.6 and 47.5 μ (45 % - 70 % of the energy weighted sum rule strength, EWSR). Re-examination of the experimental data and recent experiments show that most of the 1^+ assignments for these states is untenable. In fact, the total M1 strength in ^{208}Pb is highly uncertain, and the definite and probable strength measured now total only ~ 8.5 μ (12 % of EWSR).

Two experiments have been prepared to measure these transition strengths. The main measurement will use four BGO crystals to detect directly the capture γ-rays emitted from the sample at different angles.

To get better information about resonances where spin and parity cannot be determined by capture, or which cannot be seen in capture, a transmission experiment for the energy region up to 450 keV has been made and for the

---

(1) B.D. Wilkins, E.P. Steinberg and R.R. Chasman, Phys. Rev. C14, 1832 (1976)

(2) J.W. Meadows and C. Budtz-Jørgensen, Proc. Int. Conf. on Nuclear Data for Science and Technology, Antwerp, 1982, p. 740, Ed. K.H. Böckhoff

* SCK/CEN Mol, Belgium

** Technische Hochschule Darmstadt

high energy region a second transmission run is prepared. This experiment uses a transmission detector on flightpath 3/400 m and a 1 ns time-coder. To control the initial burst width of the Linac during a partial run, a monitor detector with a time-resolution of 200 ps has been installed at flightpath 18 in the annex. It could be shown that the Linac can achieve a burst width of better than 700 ps and even for longer runs resolutions of better than 1 ns are possible. The data from this monitor will be used to reject runs with worse time resolution so that the total time uncertainty will be 1 ns.

Systematics of the nuclear level densities

G. Rohr

This contribution has been presented as an invited paper at the IAEA Advisory Group Meeting on Basic and Applied Problems of Nuclear Level Densities (Brookhaven, 11-15 April 1983). The abstract reads as follows:

" Neutron resonance data are applied to study properties of highly excited states in nuclei. A level density systematics of compound resonances for a large number of nuclei of different even-odd character is discussed. The interpretation of the rather complicated structure in the systematics is that there is a step-shaped base line for the level density parameter formed by nuclei with minimal effects from residual interaction and no shell effects. This base line is used to answer questions relevant not only to level densities but also to nuclear physics in general. The step-like behaviour of the base line for light and medium-light nuclei is interpreted as changes in the level density due to changes of the average number of particles and holes participating in the compound excitation. The proof that the "compound states" in light and neutron closed shell nuclei are doorway (2p1h) states and therefore do not fulfil the Bohr assumption for a compound state may explain non-statistical effects observed in the capture process. Deviations of the level density parameter from the base line are interpreted as the effect of short range forces. A few examples are given and discussed for different mass regions. In the neighbourhood A ~ 75 the reduction of the pairing energy is assumed to be due to the blocking effect. In the mass range of the actinides the pairing energy has been readjusted at high excitation energy and at A ~ 105 it is shown that for neutron rich nuclei n-p interactions play the major role. Finally, the question is discussed whether or not there is a collective enhancement at higher excitation energy".

Indications of n-p interaction in the level density systematics at A = 100-115

G. Rohr

The following abstract has been published in the Proc. of the Int. Conf. on Nucl. Physics held at Florence 1983:

"Neutron resonance data are utilized to study properties of highly excited states in nuclei. A level density systematics of compound resonances for a large number of nuclei of different even-odd character is used. The interpretation of the rather complicated structure in the systematics is that there is a step-shaped base line for the level density parameter formed by nuclei with minimal effects from residual interaction and no shell effects (Fig. 35).

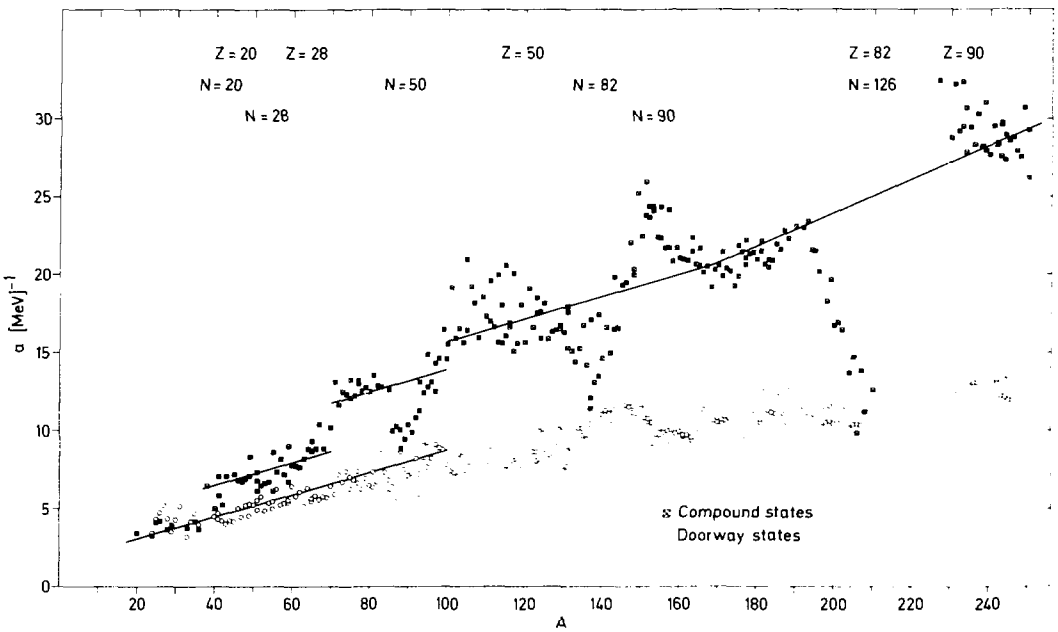

Fig. 35. The level density parameter for compound resonances and doorway states in dependence from the atomic mass

Deviations of the level density parameter from the base line are interpreted as the effect of short range forces. The assumption that the ground state pairing energy is changed at high excitation energy failed for nuclei in the neighbourhood of A ~ 105, where the deviation of the observed level density parameter from the base line increases with the atomic number, i.e. the residual interaction decreases with increasing odd number of neutrons. This is

seen in the upper part of Fig. 36 for two isotope series (Ru,Pd). In the lower part of the figure the energy of the lowest 2^+ state is plotted in dependence of A and shows an anticorrelation to the level density parameter indicated by arrows. The change in the energy of the 2^+ state is stronger for Mo and Zr isotopes and has been interpreted as a change of nuclei from spherical to deformed shape.

The level density parameter of the neutron rich nuclei with the strongest deviation from the base line are presented in Fig. 37. The deviation of the level density parameter corresponds, on average, to an increase of the level density by a factor six. The a values approach the base line if we assume that there is no effective residual interaction in these nuclei (Δ=0), indicated with the arrow-heads, and there is in addition a change in the moment of inertia from 0.7 I_{rig} to I_{rig}, indicated by the dots on the arrows.

We conclude that these nuclei seem to behave like normal matter and that the spherical-to-deformed transition with increasing number of odd neutrons may be explained by a phase transition from superfluid to normal state.

What is the mechanism for this transition? The explanation for the abrupt change to deformed nuclei (N > 60) is still a challenge in nuclear physics.

A shape transition due to a second deformed minimum has been excluded by calculations of the potential energy surface using the Strutinsky method [2]. More recently, Federman and Pittel have shown, using explicit shell-model calculations, that the n-p interaction may be responsible for this fact [3]. This interaction is largest for particles in spin orbit-partner orbits of large spatial overlap and counteracts the n-n and p-p pairing correlations which try

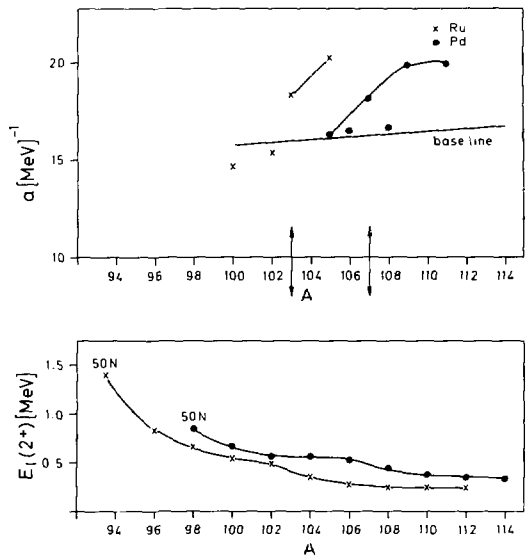

Fig. 36. The level density parameter of compound resonances and the energy of the first excited state in dependence of the mass in the interval 94 < A < 118

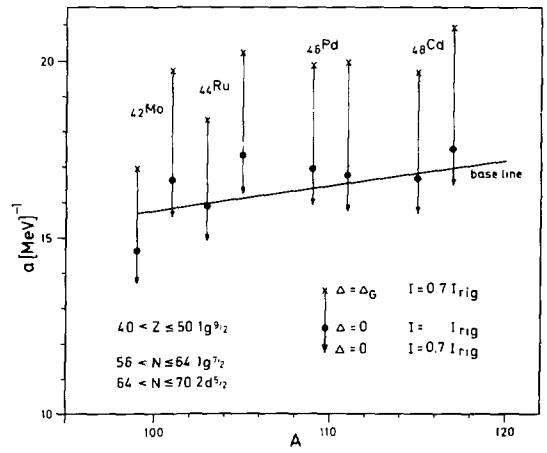

Fig. 37. The change of the level density parameter (x) assuming no pairing correlation (|) for a few nuclei in the mass range 98 < A < 118 and a change of the moment of inertia from 0.7 I_{rig} to I_{rig} (o)

to stabilize the spherical shape of nuclei. In the mass region A ~ 100, according to the authors, the strong attraction between 1g9/2 proton and 1g7/2 neutron can break the pairing correlation by a polarization mechanism which causes mutual promotion of neutrons and protons from lower single particle states into 1g7/2 and 1g9/2 respectively. The mutual polarization mechanism will stop if the gain in the n-p interaction is compensated for by the loss of single particle energy plus pairing energy.

The nuclei represented in Fig. 37 fulfil the assumption for neutron-proton interactions because the valence neutrons and protons are in the same shell and have almost the same angular momentum."

1.8 MAJOR RESEARCH EQUIPMENT

Electron linear accelerator

J.M. Salomé, R. Cools, R. Forni, F. Massardier, F. Menu, K. Meynants, P. Siméone, F. Van Reeth, J. Waelbers, C. Waller

During the covered period the accelerator was operated with the new compressing magnet as shown in Table 6. On the average, 4 neutron beams were used simultaneously for neutron measurements. A low energy electron beam was produced three times for activation analysis.

Table 6. Operational parameters of the linear accelerator

Pulse length ns	Rep. rate Hz	Peak current A	Mean current μA	Mean energy MeV	Time h	Time %
< 2	400	> 50	36	100	381	14
< 1	800	≈ 100	70	100	930	35
14	50-400	8	6-45	100	596	23
2000	25-100	0.2	10-40	50-80	444	17
1800	300	0.14	50	44	50	2
Miscellaneous					242	9

A new pulse compression system for intense relativistic electron beams

D. Tronc*, J.M. Salomé, K.H. Böckhoff

The pulsed beam of the 150 MeV Geel Electron Linear Accelerator (GELINA) [1] produces short bursts of neutrons in a mercury cooled uranium target [2], which are used in neutron time-of-flight experiments to study nuclear reactions in function of neutron energy. Neutron energy resolution requirements in the keV and MeV range call for very short neutron and therefore also electron bursts. The shortest electron pulse widths obtained with S- or L-band linacs before the pulse compression system described below became operational were about 4 ns (FWHM) at maximum possible peak current, which in the case of GELINA amounted to 12 A. Shorter pulses were possible, however with sacrifice in peak intensity.

Since the intrinsic potential of GELINA with respect to a further improvement of both parameters - intensity and pulse width - was fully exploited, possibilities of external pulse compression were studied. Pre-acceleration bunching with resonant systems turned out to be impracticable and costly. The use of a corresponding non-resonant system looked theoretically promising [3], the difficulties encountered however with its practical realization led to the study and finally the construction of the post-acceleration pulse compression system which is subject of this contribution.

---

(1) A. Bensussan and J.M. Salomé, GELINA: A Modern Accelerator for High Resolution Neutron Time-of-flight Experiments, NIM 155 (1978) 11-23

(2) J.M. Salomé and R. Cools, Neutron Producing Targets at Gelina, NIM 179 (1981) 13-19

(3) R.G. Alsmiller, Jr., F.S. Alsmiller, J. Barish and T.A. Lewis, Calculations Pertaining to the Design of a Prebuncher for an Electron Linear Accelerator, Particle Accelerators, 1979, Vol. 9, pp. 187-200

* CGR-MeV, Buc, France

The pulse compression method [1][2][3]

The electron pulses leaving the S-band accelerator consist each of a sequence of micropulses (in the following called bunches) which are assumed to have a width of the order of 10 picoseconds and have, corresponding to the S-band frequency of 3 GHz, a time distance of 333 picoseconds. For pulse widths considerably smaller than the filling time of the accelerator sections (1.1 μs), the electromagnetic energy stored in the cavities of the sections is the only source from which the electrons draw their energy. This is our case since we deal with pulses of about 10 ns.
Each of the bunches of such a pulse (except the first one) finds on its way through the accelerator less stored electromagnetic energy available for acceleration than its forerunner because that one uses already part of it. Consequently the total electron energy contained in a bunch is stepwise decreasing with the sequence of bunches. For a rectangular pulse consisting of bunches of equal charge, the energy decrease should be monotonous with time and in the ideal case linear. It has to be noted here that each electron bunch has its own energy spectrum which may overlap with those of its neighbours. The electron energies in the spectrum of a bunch may also be time correlated as in the classical textbook case shown in fig. 38. The first electrons have there the lower, the last ones the higher energies. In practice this must not be strictly true. The energy-phase relationship of relativistic electrons leaving the accelerator is generally more complex and can only be determined with larger computer programmes.

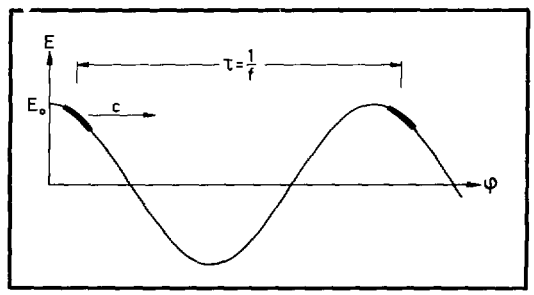

Fig. 38. Electron bunches in phase stable position on the travelling wave $E = E_0 \cos \varphi$

(1) D. Tronc, CGR-MeV, Internal Reports ST 7803 (1979), ST 8651 (1981)

(2) D. Tronc, Système magnétique de regroupement des particules chargées au sein d'un faisceau pulsé, french patent n° 7835 383 (15.12.1978); USA patent n° 4314 218 (2.02.1982)

(3) D. Tronc, Dispositif magnétique de regroupement, french patent n° 8316 797 (21.10.1983)

For the sake of transparency of the description of the pulse compression method we shall however assume that the energy decrease from bunch to bunch as well as the energy-phase relationship inside a bunch are both linear. These assumptions will yield the conditions for ideal pulse compression. If we now deflect such an ideal beam in a magnetic field (in our case over 360°) so that the electrons are allowed to leave the magnet in the same direction as they entered it, then the time-correlated decrease of electron energies along the sequence of bunches in a pulse transforms into a time correlated dispersion of trajectory lengths of the electrons at the exit of the magnet. The first bunch representing the leading edge of the pulse will have the longer trajectory and the last bunch the shorter one. Since all electrons have a speed very close to that of light, the arrival of the leading edge of the pulse at the exit of the magnet is delayed with respect to the arrival of the trailing edge: the pulse is compressed. With an appropriate design of the magnet and the vacuum chamber and with a sufficiently high vacuum in the chamber, the charge in the pulse will be conserved.

Transformation of the bunches by the magnetic field

- Widths of the bunches

Assuming that the beam is allowed to make a single-turn deflection in the magnetic field before it leaves this (fig. 39) and using the following denotations and dimensions:

t, t'	[s]	:	resp. arrival times of a reference electron at the entrance/exit of the magnet,
R(E)	[m]	:	radius of a trajectory,
E, E_o	[MeV]	:	resp. kinetic and rest energy,
B	[T]	:	magnetic induction,
c	[m/s]	:	speed of light,

one may write for the time t' which an electron needs to reach the magnet exit:

$$t' = t + \frac{2\pi R}{c} = t + \frac{2\pi}{300\ cB} E \qquad \text{since} \qquad (1)$$

$$R = \frac{[E(E + 2E_o)]^{1/2}}{300\ B} \approx \frac{E}{300\ B} \qquad \text{for } E \gg E_o.$$

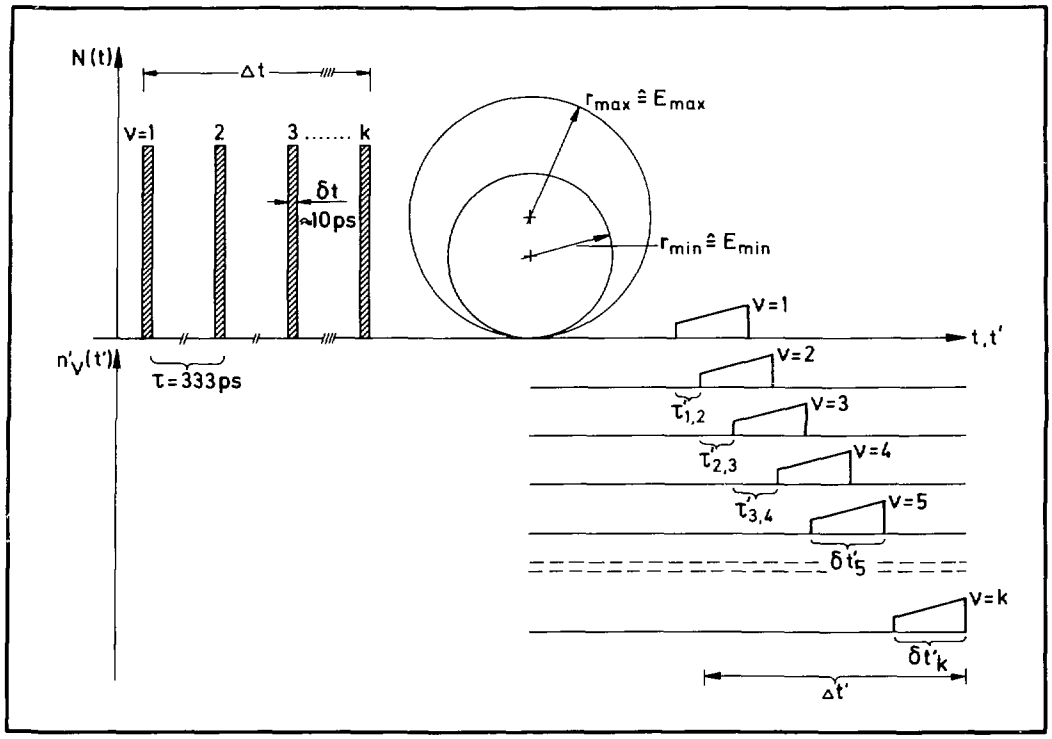

Fig. 39. Schematics of pulse compression. In the ideal case all bunches $n'_\nu(t')$ are stacked one on each other at the same place, forming a compressed pulse with a width $\Delta t'$ equal to $\delta t'$ and with an amplitude k-times that of $n'(t')$. In this case $\delta t'_\nu = \delta t'$ and $\tau'_{\nu,\nu+1} = \tau'$ for all ν.

From (1) we obtain for the finite width $\delta t'_\nu$ of a single bunch ν at the exit of the magnet:

$$\delta t'_\nu = \delta t + \kappa \delta E_\nu = \int [1 + \kappa (\frac{dE}{dt})_\nu] \, dt \qquad (2)$$

where δt stands for the width of the bunches (which are assumed to be equal) before they enter the magnet. δE_ν is the electron energy spread in the bunch ν and $\kappa = 2\pi/300$ cB.

δE_ν and hence $(dE/dt)_\nu$ will in general be negative as e.g. shown in the text-book case of fig. 38. By convention pulse and bunch widths are always counted positive.

In principle the widths $\delta t'_\nu$ of the transformed bunches can be made almost equal to the widths δt_ν by maximizing the induction B. Our goal is however to compress the pulses with a width Δt which comprise a sequence of bunches, and not to compress the individual bunches themselves. In fact the width $\delta t'$ is very much larger than that of the original bunch δt.
The bunches become "debunched" by a magnetic induction which is not adapted to their compression but to the compression of the pulses. The leading edges of the bunches, representing the lowest energies, are largely overpassed by the trailing edges, representing the highest energies.

- Shape of the transformed bunches

If $n'_\nu(t')dt'$ are the number of electrons in the time interval dt' within the bunch ν and $n_\nu(t)dt$ the corresponding number in the time interval dt, then

$$n'_\nu(t')dt' = n_\nu(t)dt$$

provided no electrons are lost on their way through the magnet.
From this and (1) and with $E = E_0 \cos\varphi$; $\varphi = \omega t$, we obtain for the shape of a bunch transformed by the magnetic field

$$n'_\nu(t') = \frac{n_\nu(t)}{1 + \kappa\left(\frac{dE}{dt}\right)_\nu} = \frac{n_\nu(t)}{1 - E_0\,\kappa\omega \sin\omega t} \qquad (3)$$

This relationship shows that the quantity $1 + \kappa\left(\frac{dE}{dt}\right)_\nu$ which stretches the width of the bunch ν, reduces its intensity and transforms a rectangular pulse $n_\nu(t)$ into an asymmetric one.
Maximum possible neutron output and at the same time smallest energy spread δE_ν in a bunch of given charge are obtained, when the bunches are kept in the highest possible position on the wave, centered about phase $\varphi = 0$. In this case half of the bunch has a negative phase. (This does not imply phase instability because the electrons are highly relativistic).
Expression (3) has a singularity at $\sin\omega t_0 = 1/E_0\kappa\omega$. It means that at the time t_0 the leading edge of the bunch is just being overpassed by the trailing edge (dt' = 0) and that then - theoretically - the intensity becomes infinite.

For the parameters of our facility

$$E_o = 120 \text{ MeV}; \kappa = \frac{2\pi}{300 \text{ cB}} = 1.75 \cdot 10^{-10} \text{ [s MeV}^{-1}\text{]}; \omega = 1.885 \cdot 10^{10} \text{ [s}^{-1}\text{]}$$

this situation occurs at $\varphi_s = 0.145°$ or $t_s = 0.134$ ps.
The shapes of the transformed bunches are shown in fig. 40 for two positions on the wave:

a) $\varphi_o = -13.671°$ $\varphi_1 = +13.671°$

corresponding to $\delta E = 2 \times 3.4$ MeV

b) $\varphi_1 = +13.671°$ $\varphi_2 = +41.015°$

corresponding to $\delta E = 26$ MeV.

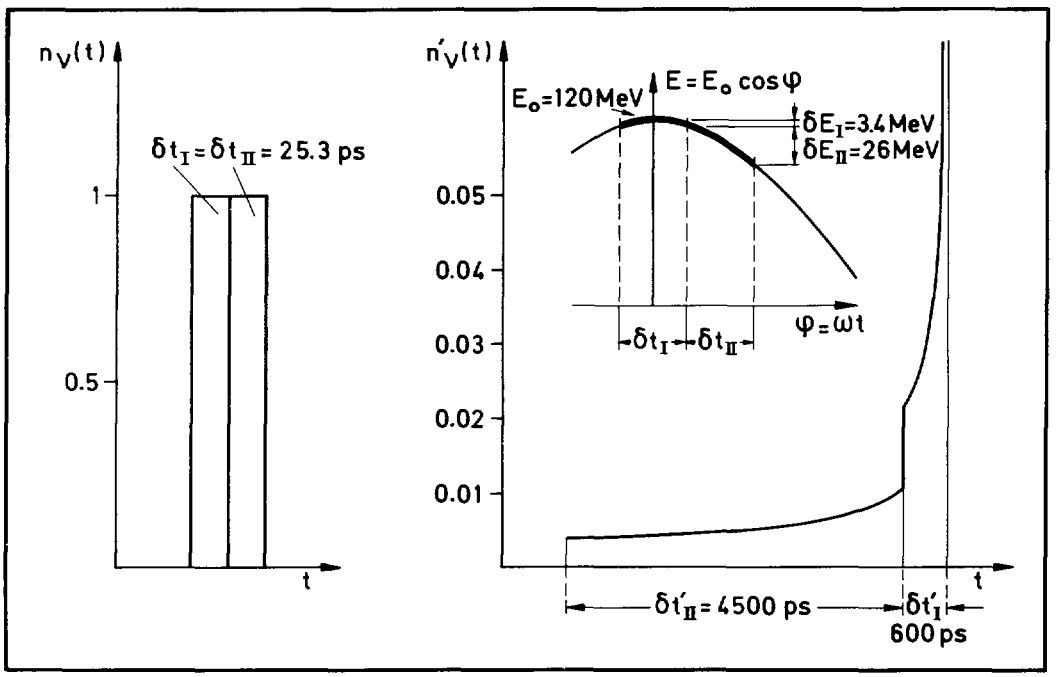

Fig. 40. Shape transformation of a rectangular bunch $n_\nu(t)$ into an asymmetric bunch $n'_\nu(t')$ by the compression magnet for two positions of the bunch on the travelling wave. It is assumed that for both cases the charge density and the total charges are the same ($\delta t_I = \delta t_{II}$) and that $\delta E_I = 3.4$ MeV which corresponds to the measured value $\delta t'_I \approx 600$ ps. The figure illustrates the advantages of placing the bunches over the crest of the wave

The first of these cases is believed to correspond typically to the actual case. It reveals a sharp spike at cross-over condition. This could not be seen with the available measurement equipment.

Compression of the pulse

The pulses N(t) having the width Δt consist of k bunches $n_\nu(t)$ with the widths δt_ν. Figure 39 shows schematically how the pulses look like before and after the compression magnet. The bunches $n_\nu(t)$ are well separated in time and have a period $\tau = 1/f$ with f = 3 GHz. The bunches $n'_\nu(t')$ are broadened, have a shape different from that of $n_\nu(t)$ and must not a priori have a constant period τ'_ν.
For any electron in the bunch $n_\nu(t)$ we may write according to (1)

$$t'_\nu = t_\nu + \kappa E_\nu$$

If we denote by t_ν and $t_{\nu+1}$ corresponding instants of two subsequent bunches, e.g. those of the first electrons or those where the bunches reach half of the maximum amplitude, we get

$$t'_{\nu+1} - t'_\nu = \tau'_{\nu,\nu+1} = \tau - \kappa(E_\nu - E_{\nu+1}).$$

A necessary condition for a reasonable pulse compression effect is that

$$\tau'_{\nu,\nu+1} = \tau' = \text{constant}$$

for all electrons in the subsequent bunches: the time-interval between the bunches should not depend on its position in the sequence. This means that

$$E_\nu - E_{\nu+1} = \Delta E_{\nu,\nu+1} = \Delta E = \text{constant}.$$

In other words: the energies of the bunches and of the electrons at corresponding places in the bunches must decrease linearly with time. In a specific experiment which was part of the feasibility study for the compression system an approximately linear relationship was demonstrated (1).
To achieve a constancy of $\tau'_{\nu,\nu+1}$ and with that the wanted linearity the following conditions have to be fulfilled:

---

(1) J.M. Salomé and R. Forni, Measurements of Microbunch Energy Spectra on a S-band Electron Linac 1981 Part. Acc. Conf., Washington DC, 11-13 March, 1981, IEEE Trans. on Nucl. Science June 1981, Vol. NS-28, p. 2234

- the pulse width Δt must be small against the filling time of the accelerator sections, so that only the electromagnetic energy W_{em} stored in the sections of the linac is used for the acceleration of the electrons.
- all bunches must contain the same number of electrons, which means that the pulses N(t) must be rectangular in shape. Real pulses have a finite rise- and fall-time. Linearity can therefore not be expected at the beginning and at the end of the pulses.
- the functions $(dE/dt)_\nu$ in (2) which together with B determine the shape transformation of $n_\nu(t)$ into $n'_\nu(t')$ must be the same for all bunches in a pulse: the bunches must have the same position on the wave (constant phase). This means that the widths $\delta t'_\nu$ must be all equal. Otherwise no common period τ' can be defined.

If these conditions are fulfilled, one obtains ideal pulse compression by choosing the magnetic induction B such that

$$\tau' = \tau - \frac{2\pi}{300\ cB_0}\ \Delta E = 0 \qquad \text{or}$$

$$B_0 = \frac{2\pi}{300\ c\tau}\ \Delta E = 0.212\ \Delta E\ \ [\text{Tesla}]. \qquad (4)$$

In such an ideal case all the transformed bunches $n'_\nu(t')$ are stacked one on each other on the same place, forming a compressed pulse N'(t') with a width $\Delta t'$ equal to the width $\delta t'$ of the individual bunch and with an amplitude k-times larger than that of the individual bunch $n'_\nu(t')$, where k is the number of bunches in the pulse.

Description of the magnetic deflection system and its auxiliary equipment

The electromagnet ★ (figs. 41-42) has a total weight of 40 tons and overall dimensions of 3.4 m x 2.4 m x 0.66 m. It is positioned horizontally with its vertical axis 8 m behind the exit of the accelerator and 4 m in front of the target. The horizontal dimensions are determined by the available space in the target bunker. It was very fortunate that this bunker, when constructed in 1963, was made exceptionally large in order to have in the future also

★ constructed by CGR-MeV, Buc, France

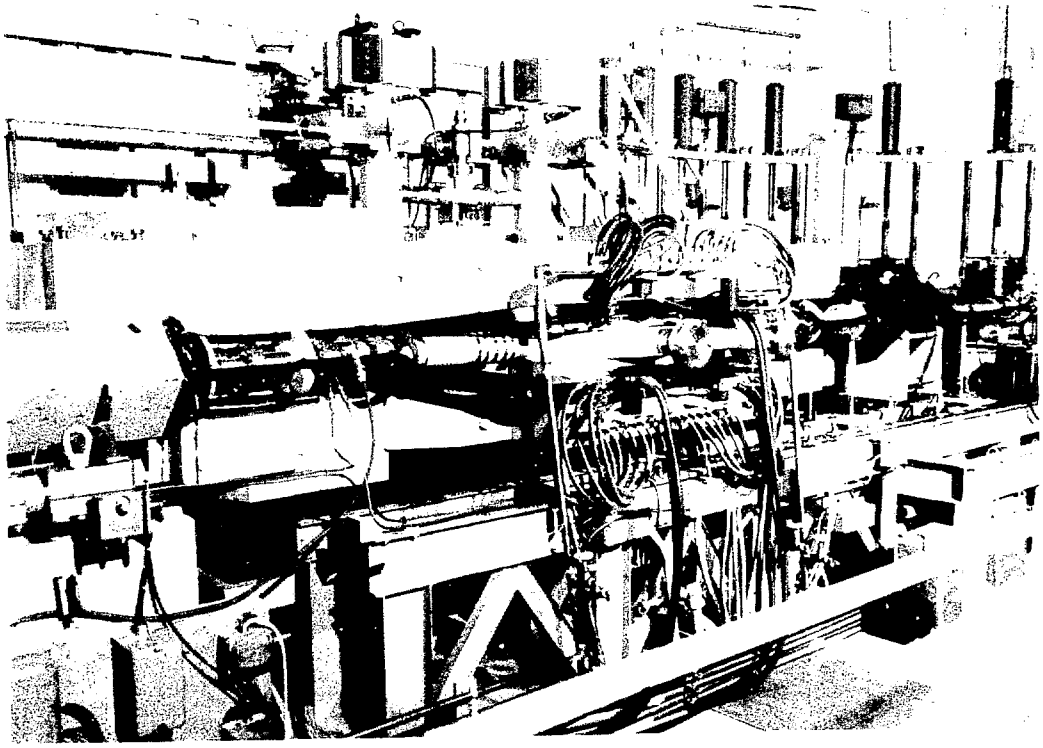

Fig. 41. The magnetic deflection system

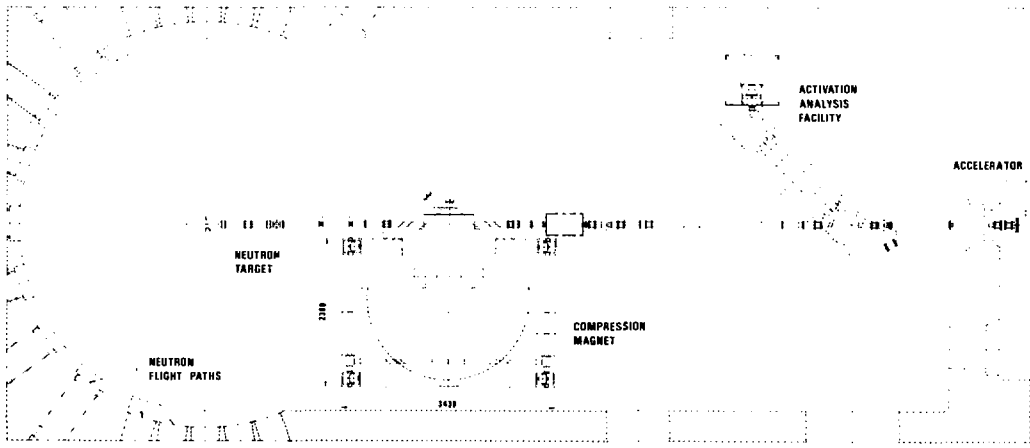

Fig. 42. Layout of the compression magnet and its location in the target room

space for a magnetic deflection system to compress a 10 ns pulse of 120 MeV electrons down to 1 ns. The ideas how to realize the beam optics were at that time not available and no effort for the realization of such a system was made.
The actual magnet allows a maximum equivalent trajectory radius of 1.2 m (the curvature of a trajectory is not constant). Under the realistic assumption that the leading/trailing edges of a short pulse represent the respective electron energies 146 and 86 MeV, the time difference between leading and trailing edge of the pulse is shortened by the compression system by about 10 ns.

Results

Measurements of the shape of the beam pulse are made with ferrite transformers placed in front and behind the magnet. Their rise time is about 1 ns, which is not sufficient to obtain appropriate shape information on the compressed pulse. To get a better information, in particular on the pulse width, a NE 110 plastic scintillator coupled to a RCA 8850 (2") photomultiplier has been installed at a backward flight path of the linac. The scintillator sees that part of the bremsstrahlung-flash produced by the electrons in the uranium target, which succeeded to pass a 3.70 m thick water filled opening in the target bunker. The intensity reduction of the flash by this absorber is such that pile-up of detected γ-quanta is avoided *.
On the average only about one out of hundred flashes yields a detector signal. The detector has a resolution of 300 ps. The shape of the compressed pulse is measured with a time-to-amplitude converter which has a resolution of 100 ps.
Typical results of measurements with ferrite transformers are given in fig. 43, those obtained with the plastic scintillator in fig. 44.
The following observations can be made regarding these results:

- The pulse compression system transforms a pulse with a width of Δt = 10 ns (FWHM) into a pulse with an observed width of $\Delta t'_{obs}$ = 0.67 ns (FWHM), which, taken the time resolution of the detector into account corresponds to a real pulse width of Δt = 0.6 ns (FWHM).

---

* Measurements made by F. Poortmans, SCK/CEN Mol, Belgium

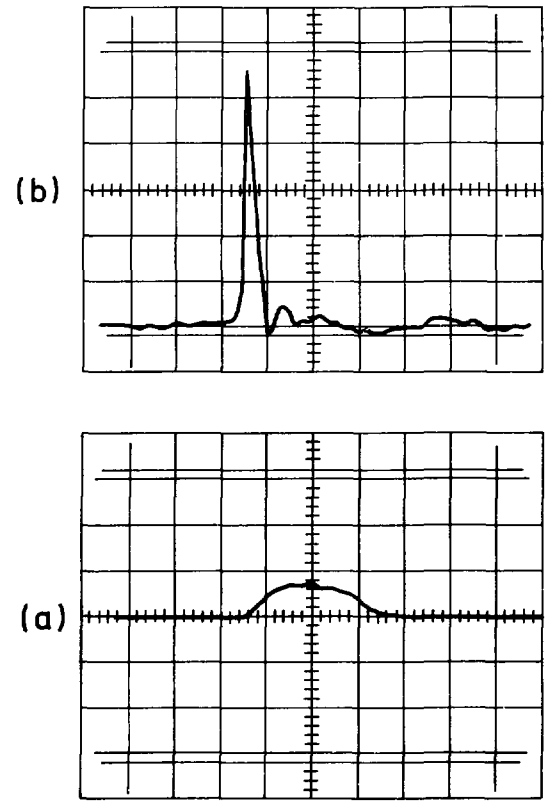

Fig. 43. Typical results of beam pulse measurements with ferrite transformers before (a) and after (b) compression.
Time scale: 5 ns/large division
Intensity scale: 12 A/large division

Since there are no observable beam losses, neither on the collimators nor within the vacuum chamber, the peak current rises from originally 10 A to a value of 100 A for the compressed pulse.

The value of the peak current was determined by fitting the measured shape to an analytical curve and normalizing the area under these curves to the measured charge in the pulse. A gaussian shape fit did not represent the wings of the pulse in a satisfactory way. An excellent fit was obtained with the analytical form

$$N(t) = \frac{k_1}{1 + (k_2 t)^2}$$

- The compressed pulse shows a high degree of symmetry, which is very useful for the calculation of the neutron time-of-flight resolution function.

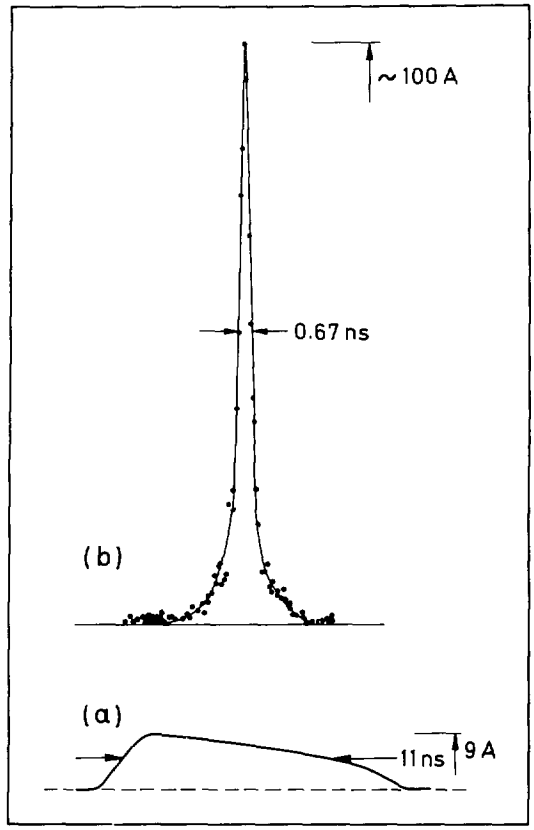

Fig. 44. Typical results obtained with a plastic scintillator, before (a) and after (b) compression

The original, not compressed pulse, measured with the plastic scintillator, does not show a flat top as does the measurement with the ferrite core transformer. This is due to the changes in the absorption of the bremsstrahlung spectrum, resulting from the time correlated electron energy spectrum. The compressed pulse is not influenced by this effect since here the energy-time relationship is lost due to the superposition of the bunches.
The compressed pulse measured with the ferrite shows some wiggles after the main pulse. These do not correspond directly to electrons in the pulse, as the comparison with the plastic scintillator measurement shows. They are probably due to waves excited in parts of the beam tube by the intense pulse.
Relating the observations with the formulas derived above the following conclusion can be drawn:

Assuming that the width $\Delta t'$ of the compressed pulse equals the width $\delta t'$ of the individual bunch and neglecting in (2) δt against $|\kappa \delta E_\nu|$, one obtains for the width δE of a bunch:

$$\delta E \approx \frac{\Delta t'}{\kappa} = 3.4 \text{ MeV}$$

The approximation is justified since δt is almost two orders of magnitude smaller than $|\kappa \delta E_\nu|$. The value $\kappa = 1.76 \cdot 10^{-10}$ [MeV^{-1} · s] was calculated for an average induction of 0.4 T.
From (4) we get for the energy difference ΔE between two subsequent bunches, that means for the reduction of stored energy by one bunch, the value:

$$E = \frac{B_o}{0.212} = 1.9 \text{ MeV}$$

The energy spectrum of an individual bunch therefore only overlaps with that of its next neighbours.

Operational experience

To arrive at the best possible pulse compression, that means the shortest pulse width and highest peak current, various sets of Linac parameters had to be tried. These investigations showed the importance of parameters such as the electrical field in the prebunching cavity of the accelerator and of the proper phasing of the different linac sections. They also showed the (expected) importance of the peak current stability for the pulse compression. To improve this stability the quality of the power supplies for the focussing coils of the linac sections has been improved, likewise the temperature control for the cooling water of the sections.
The profile of the compressed pulse was measured repeatedly over periods of 10 minutes with the plastic scintillator. The results always confirmed the observed pulse width of 0.67 ns. Extended measurements over periods of one day and more under normal running conditions - that means without specific care for peak intensity stability - yielded observed average pulse widths always shorter than 1 ns.
It has to be remarked that due to the intersection of the magnet, dark current electrons cannot reach the target, which is important for some neutron physics experiments.

The Linac and the compression magnet have now worked together over several months without any problem, supplying to a rotary uranium target [1] electron peak currents of about 100 A with widths shorter than 1 ns. The average electron energy was 110 MeV under these conditions and the repetition rate 800 Hz.

Cold neutron source

R. Cools, J.M. Salomé, K.H. Böckhoff

The design of a liquid methane moderator has been completed and an order for this moderator and the associated cryogenic equipment has been placed. The equipment is expected to be installed by the middle of 1984.

Moderator simulation study

C. Bastian

In view of the implementation of a cold moderator at the Linac, a comparative simulation of the neutron yield was performed on two rotation symmetric designs, one in polyethylene, the other in liquid methane. The APL workspace COLLGEEL [2] was therefore upgraded to accommodate a fission neutron generator. In the case of polyethylene, the results agree well with those obtained at Bologna [3] with a conventional Monte Carlo programme on the same geometry. The main purpose of the simulation was to determine the fraction of neutrons moderated and emitted in the thermal range i.e. ≤ 0.1 eV. It turns out that methane is better by a factor of 2 with respect to polyethylene. Details and graphs of the results are given in Ref. [4].

---

(1) J.M. Salomé and R. Cools, Neutron Producing Targets at Gelina, NIM 179 (1981) 13-19

(2) C. Bastian, APL Quote Quad, Vol. 13, N° 1 (1982) p. 23-30

(3) A. Bignami, C. Coceva and R. Simonini, EUR 157e (1974)

(4) Internal Report GE/R/LI/119/83

Van de Graaff accelerators

A. Crametz, P. Falque, J. Leonard, W. Schubert

During the 243 working days in 1983 - which corresponds to 1944 normal working hours - the total available machine time was 3337 hours. The breakdown of this number is given in Table 7.

Table 7. Exploitation of the Van de Graaff accelerators

	CN - 7 MV		KN - 3.7 MV	
Accelerator running	2351 = 70.5 %		450 = 13.5 %	
experiments		2023		435
adjustments		65		15
conditioning		263*		0
Maintenance	110 = 3 %			
Stopping hours for outside firms	207 = 6 %			
Pulse compression	219 = 6.5			

* not manned

- The stopping hours were needed for a better heat insulation of the target hall and a modification of the electrical circuitries.
- A report (1) which describes the calculations of field parameters of a double magnetic quadrupole lens has been written. The abstract is as follows:

"The properties of double magnetic quadrupole lenses are utilized in accelerators technology for guiding charged particle beams. The field parameters of such a doublet have been determined theoretically using first order Taylor expansion of relations deduced from the equation of motion of charged particles in the lens. A general program in BASIC has been written and results have been compared with current settings regularly used with a double magnetic quadrupole lens installed on an extension beam tube of the CN-7 MV Van de Graaff accelerator."

---

(1) Internal Report GE/R/VG/41/83

- An internal report concerning the optical study of a double magnetic quadrupole lens and the matrix formalism for beam transport optics is in preparation.

Pulse compression with a spiral resonator used as a post-acceleration buncher

A. Crametz, S. de Jonge, H. Ingwersen*, E. Jaeschke*, H. Liskien, F. Arnotte, W. Schubert, J. Leonard, P. Falque

Figure 45 represents the block diagram of the post-acceleration bunching system installed at the 7 MV CN Van de Graaff accelerator.

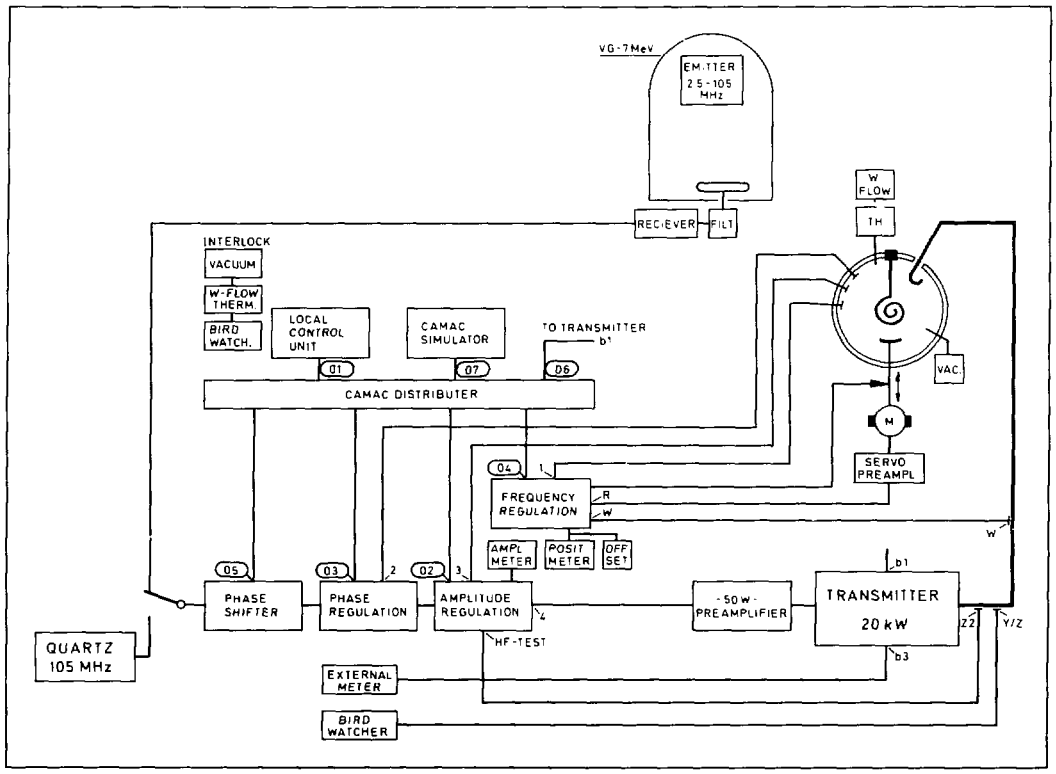

Fig. 45. Block diagram of the 7 MeV Van de Graaff post-bunching system

---

* Max Planck Institut für Kernphysik in Heidelberg

The picture (fig. 46) represents the spiral resonator installed between the analyzing and the switching magnets. The parallel resistance of the resonator has been determined to be 0.55 MΩ.

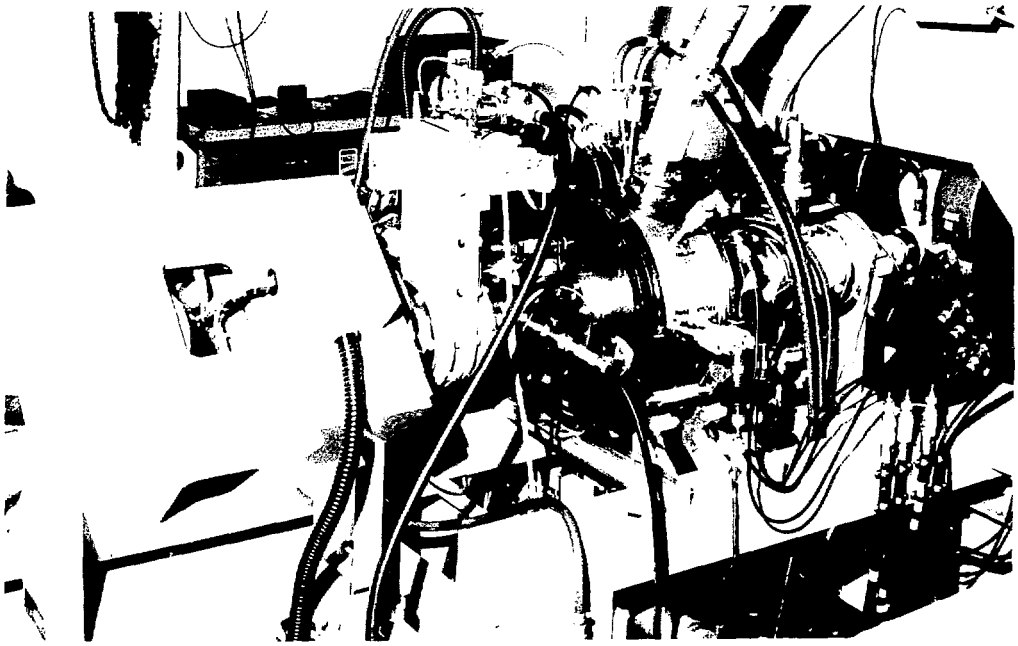

Fig. 46. Spiral resonator

To determine the obtainable pulse width measurements were performed with a 2 μA D.C. proton beam at 5.4 MeV energy. Coulomb scattered protons from a 0.67 mg/cm^2 gold foil are detected in the 45° direction with respect to the beam by a totally depleted ORTEC silicon surface detector of 400 μm thickness and 25 mm^2 sensitive area. An overbias of 150 Volts is applied. Best time resolution was found for a RF power of 1.6 kW corresponding to a peak voltage of 42 kV. The TOF spectrum represented in Fig. 47 shows that only the cross-over region of the buncher voltage is used, that the beam bunches are alternatively time-focussed and time-defocussed and that the integrals over these bunches are equal. One time-focussed beam bunch with a FWHM of 141 ps is represented in extended view in Fig. 48.

To synchronize the post-acceleration bunching system (105 MHz) with the pre-acceleration buncher (2.5 MHz), the 2.5 MHz signal is multiplied by a factor 42 in a phase-locked loop system, amplified by a 15 Watt VHF amplifier, and emitted by an antenna. This equipment is located in the H.V. terminal of the accelerator.

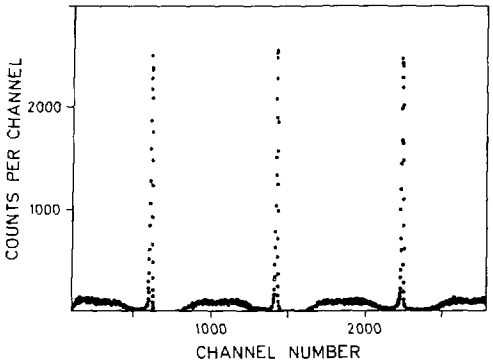

Fig. 47. Time-focussed and time-defocussed beam bunches

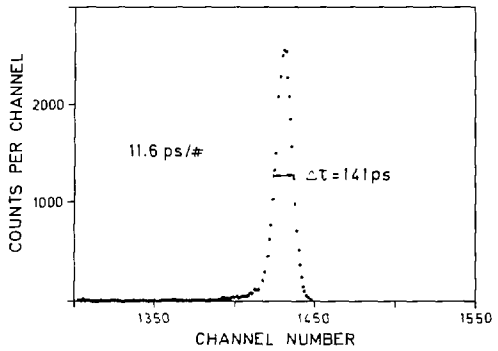

Fig. 48. One time-focussed beam bunch in extended view

The 105 MHz signal is received by a $\lambda/2$ dipole fixed on the grounded base plate and crosses the base plate with an attenuation factor of ≈ 5. It is amplified up to 1 V and sent with a 5/8" coaxial cable towards the control room.

The parasitic radiation of the 300 Watt, 136 MHz oscillator of the radio frequency ion source is filtered in the emitter and receiver by a resonance filter. Its strong second harmonic at 272 MHz and the 15 MHz signal emitted by the klystron buncher are filtered at the input of the receiver in a similar way.

Tests with the above described equipment under real working conditions (15 kg/cm^2 of insulation gas and high voltage on terminal) will follow.

2. NON-NEUTRON NUCLEAR DATA

2.1 DECAY STUDIES

Decay of $^{96}Sr/^{90}Y$

H.H. Hansen

The results of $^{90}Sr/^{90}Y$ β^--spectra measurements made at CBNM in the frame of an ICRM intercomparison have been reported at the ICRM Seminar on Applied Radionuclide Metrology [1]. The abstract of the paper is as follows:

" The β-ray spectra of ^{90}Sr and ^{90}Y have been remeasured with the CBNM magnetic β-ray spectrometer. From the measurements the endpoint energies ($W_0[m_oc^2]$ and $E_0[keV]$), the spectrum shapes (coefficient, a, of the shape-correction factor, 1+aW), and the ratio of the numbers of β particles emitted in the decays of respectively ^{90}Y and ^{90}Sr, (I_{β_1}/I_{β_2}), have been determined. The results are for:

^{90}Y, β_1 transition: $W_{0_1} = 5.4608 \pm 0.0058$
$E_{0_1} = (2279.5 \pm 2.9)keV$
$a_1 = -(0.0078 \pm 0.0024)$,

^{90}Sr, β_2 transition: $W_{0_2} = 2.0685 \pm 0.0032$
$E_{0_2} = (546.0 \pm 1.6)keV$
$a_2 = -(0.032 \pm 0.007)$.

The ratio of the numbers of emitted β particles is $I_{\beta_1}/I_{\beta_2} = 1.00 \pm 0.01$. Corrections to the measured data and the deduction of uncertainties are discussed."

Decay of $^{93}Nb^m$

R. Vaninbroukx, W. Zehner

The measurements for the determination of the half life of $^{93}Nb^m$ were finished. The results, together with the results of earlier determinations of the KX-ray-emission probability, have been presented at the ICRM Seminar on Applied Radionuclide Metrology, 16 to 17 May 1983, in Geel [2]. The abstract is as follows:

---

(1) H.H. Hansen, Measurements of the Beta-Ray Spectra of $^{90}Sr/^{90}Y$, Int. J. Appl. Radiat. Isot., 34, 1241 (1983)

(2) R. Vaninbroukx, Half life and KX-Ray-Emission Probability of $^{93}Nb^m$, Int. J. Appl. Radiat. Isot., 34, 1211 (1983)

" The half life and KX-ray-emission probability of $^{93}Nb^{m}$ were measured to be (16.13 ± 0.15) a and 0.115 ± 0.003, respectively. The half-life result is in excellent agreement with a recently published value, but the KX-ray-emission-probability value is about 7.5 % higher than the only other available experimental result, quoted with an uncertainty of ± 2.8 %."

K-shell conversion coefficient in the $^{121}Sn^{m}$ decay

H.H. Hansen, D. Mouchel

A paper has been published (1). It has the following abstract:

" The K-shell internal conversion coefficient α_K for the 37.2 keV transition ($7/2^+ \rightarrow 5/2^+$) occuring in ^{121}Sb after β^- decay of $^{121}Sn^{m}$ has been redetermined applying the X- to γ-peak method (XPG).
Measurements of photon spectra from thin sources have been performed at various source-detector distances with a high resolution, efficiency calibrated Si(Li) detector. Values of α_K have been deduced from the number of emitted KX rays compared to that of the emitted γ rays. The K-shell fluorescence yield for antimony has been taken from the literature.
From in total 14 experimental runs a mean result of α_K = 9.52 ± 0.27 has been obtained. The quoted uncertainty comprising statistical and systematic parts is discussed in detail. The present result is compared with the few existing earlier experimental values and with the theoretical value interpolated from the most recent tabulations."

Internal conversion ratios

H.H. Hansen, D. Mouchel

The work on the measurement of internal conversion ratios has been finalized by a report (2) presented at the ICRM Seminar on Applied Radionuclide Metrology. It has the following abstract:

" Measurements have been made with a magnetic β-ray spectrometer in order to determine the internal-conversion ratio R = K/LM+ for pure E2 transitions of 244.7 and 344.3 keV in the decay of ^{152}Eu and of 205.8 and 316.5 keV in the decay of ^{192}Ir. The results from several experimental runs for each transition are respectively, R = 2.92 ± 0.05, 3.43 ± 0.05, 1.05 ± 0.04 and 1.71 ± 0.05. A comparison has been made with previously published results as well as with theoretical values deduced for pure E2 multipolarity from the most recent tabulations of internal-conversion coefficients."

---

(1) H.H. Hansen and D. Mouchel, Determination of the K-Shell Internal Conversion Coefficient for the 37.2 keV Transition of $^{121}Sn^{m}$, Z. Phys. A 315, 239 (1984)

(2) H.H. Hansen and D. Mouchel, K/LM+ Internal Conversion Ratios for Pure E2 Transitions in the Decays of ^{152}Eu and ^{192}Ir. Int. J. Appl. Radiat. Isot., 34, 1233 (1983)

Half lives of excited nuclear levels

D. Mouchel, H.H. Hansen

The work on the determination of the half lives of the 482.2 keV and 615.3 keV levels in ^{181}Ta has been published (1). The abstract reads as follows:

" The half lives of the excited levels at 482.2 keV and 615.3 keV in ^{181}Ta have been measured by the delayed coincidence technique. In the nanosecond time range (482.2 keV level) the most serious sources of errors are jitter, walk and drift phenomena. To minimize those the time pick-off has been defined carefully by means of modern fast timing detectors and electronics. In the microsecond time range (615.3 keV level) the ratio of true delayed coincidences to chance coincidences influences considerably the final accuracy of the half-life measurements. It has been reduced as much as possible. From a series of independent measurements half lives of $T_{1/2}$ = (10.67 ± 0.05)ns and $T_{1/2}$ = (17.64 ± 0.14)μs have been deduced for the 482.2 keV and 615.3 keV levels, respectively. The results have been compared with other values published before."

The technique of half-life measurements of excited levels in the nanosecond and microsecond region has been described in a paper (2) presented at the ICRM Seminar on Applied Radionuclide Metrology. It has the following abstract:

" The application of the delayed-coincidence technique to accurate half-life measurements of excited levels in the nanosecond and microsecond region is described. In order to achieve an overall uncertainty of $\leq$ 1 % on the final value of the half lives a series of precautions depending on the time region have to be taken.
In the nanosecond time range the most serious sources of errors are jitter, walk and drift phenomena. To minimize those the time pick-off has to be defined carefully by means of modern fast timing detectors and electronics. In the microsecond time range the ratio of true delayed coincidences to chance coincidences influences considerably the final accuracy of the half-life measurements. It must be the aim to reduce the chance-coincidence rate as much as possible.
In both cases the analysis of the experimental data is of critical importance. The choice of the analysis region will be discussed. Time calibration and a careful consideration of system linearity, short- and long-term stability of the entire experimental system, are of great importance. Regular checks of these quantities performed during the measurements cycles allow proper quotation of the different systematic uncertainties.
The successful application of the experimental procedures mentioned above yielded the following half-life values for the 37.1-keV level in ^{121}Sb (3.46 ± 0.03)ns, the 81-keV level in ^{133}Cs (6.23 ± 0.03)ns, the 482.18-keV level in ^{181}Ta (10.67 ± 0.05)ns, the 23.87-keV level in ^{119}Sn (18.03±0.07)ns, the 6.21-keV level in ^{181}Ta (6.05 ± 0.12)μs and the 615.25-keV level in ^{181}Ta (17.64 ± 0.14)μs."

---

(1) D. Mouchel and H.H. Hansen, Half Lives of the 482.2 keV and 615.3 keV Levels in ^{181}Ta, Z. Phys. A 315, 113 (1984)

(2) D. Mouchel and H.H. Hansen, Half-Life Measurements of Excited Levels in the Nanosecond and Microsecond Region, Int. J. Appl. Radiat. Isot., 34, 1201 (1983)

Decay of ^{234}U

The decay data of ^{234}U have to be known for nuclear fuel assay. The required accuracies for the photon-emission probability and the α-particle emission probability are 2 % and 1 %, respectively, whereas the achieved accuracies are 10 % and 4 %, respectively [1].

Photon-emission probabilities in the decay of ^{234}U

R. Vaninbroukx, B. Denecke, W. Oldenhof

The emission probabilities for X- and γ-rays in the decay of ^{234}U were measured. Several sources have been prepared by different techniques. The disintegration rates, N_0, of the sources were measured by α-particle counting in well-defined solid angles. The photon-emission rates, N_{ph}, were measured with a calibrated high-purity-Ge detector. A photon spectrum is displayed in fig. 49. The photon-emission probabilities are obtained from the ratios N_{ph}/N_0. The measurements are finished. A few small corrections have to be calculated. The final results will be available in 1984.

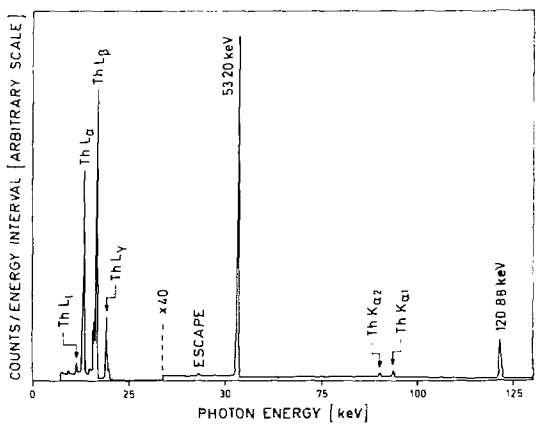

Fig. 49. ^{234}U photon spectrum

(1) A. Lorenz (ed.), Fifth Research Coordination Meeting on the Measurement and Evaluation of Transactinium Isotope Nuclear Data, Geel, Belgium, 1-3 September 1982; INDC(NDS)-138/GE (1982)

Alpha-particle emission probabilities

G. Bortels, W. Oldenhof

For the measurements of the α-particle emission probabilities, three sources have been used. They were prepared by evaporation in vacuum and have activities from about 400 to 2000 Bq. A passivated ion-implanted Si detector of 20 mm^2 active area with a resolution of typically 11.5 keV (FWHM) was used. The solid angle in these measurements ranged from 0.3 to 2 % of 4π sr. Over 240 measurement cycles of 2 hours duration each were recorded and these spectra were added together after correction of the peak drift. In part of the measurements a small permanent magnet of about 0.1 T was used which reduced by more than 90 % the number of conversion electrons reaching the detector. Consequently, the uncertainty on the tail correction of the major α peak due to α-particle and conversion-electron summing was clearly reduced. The measurements have been completed and the evaluation of the results is in progress.

Figure 50 shows the magnetic device and fig. 51 show the conversion-electron lines measured with the ion-implanted detector with and without the magnet.

Decay of ^{237}Np

The decay scheme of ^{237}Np is complex and not very well known. In particular the emission probability of the main α-particle transition is uncertain by 20 %. Requests for 1 % accuracy have been made and maintained [1], although it is questionable, if this accuracy can be obtained. In addition, the present knowledge of the γ-ray-emission probability in the decay of ^{237}Np and its daughter is unsatisfactory. The required accuracy is 0.5 % while the achieved accuracy is about 10 % for the γ rays of the ^{237}Np and 1 % for those of the ^{233}Pa [1] decay.

---

(1) A. Lorenz (ed.), Fifth Research Coordination Meeting on the Measurement and Evaluation of Transactinium Isotope Nuclear Data, Geel, Belgium, 1-3 September 1982; INDC(NDS)-138/GE (1982)

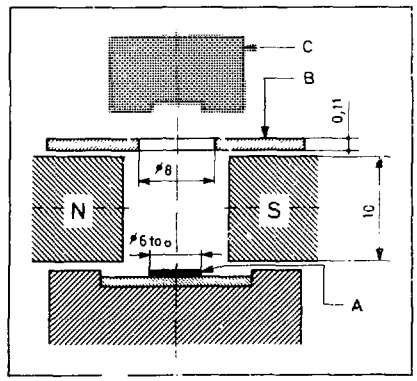

Fig. 50. Use of a small permanent magnet to eliminate conversion electrons in a spectrometry
(A) source, (B) tantalum diaphragm,
(C) detector of 20 mm^2 active area

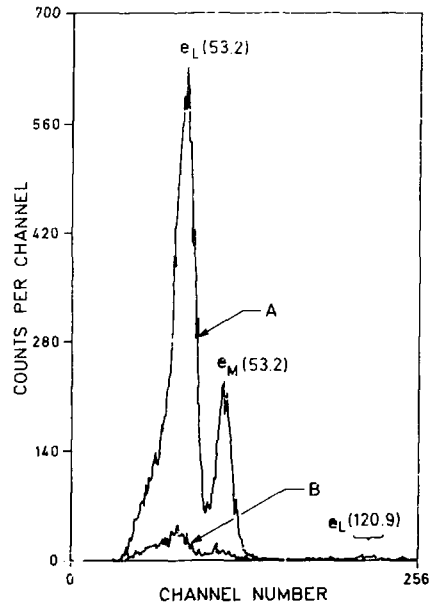

Fig. 51. Conversion-electron peaks from the ^{234}U-^{230}Th decay measured with a passivated ion-implanted detector
(A) without, and (B) with the use of a magnet. The energy of the corresponding γ transition is indicated in brackets

Gamma-ray-emission probabilities in the decay of ^{237}Np - ^{233}Pa

R. Vaninbroukx, B. Denecke

The emission probabilities for about 25 γ rays in the energy range from 29 keV to 416 keV are measured. Five sources are used with ^{237}Np amounts ranging from 16 μg to 660 μg, corresponding to activities between 440 Bq and 17200 Bq. The active area of these sources, which were prepared by CBNM's Sample Preparation Group, is 1.3 cm^2. The disintegration rates, N_0 of the sources are measured by α-particle counting under well-defined low solid angles. The γ-ray emission rates, N_γ, are measured with three calibrated photon detectors: a high-purity Ge detector with a thickness of 8 mm and an area of 1 cm^2, and two Si(Li) detectors each with an area of 3 cm^2, however with thicknesses of 3 mm and 5 mm, respectively. A typical γ-ray spectrum is shown in fig. 52.

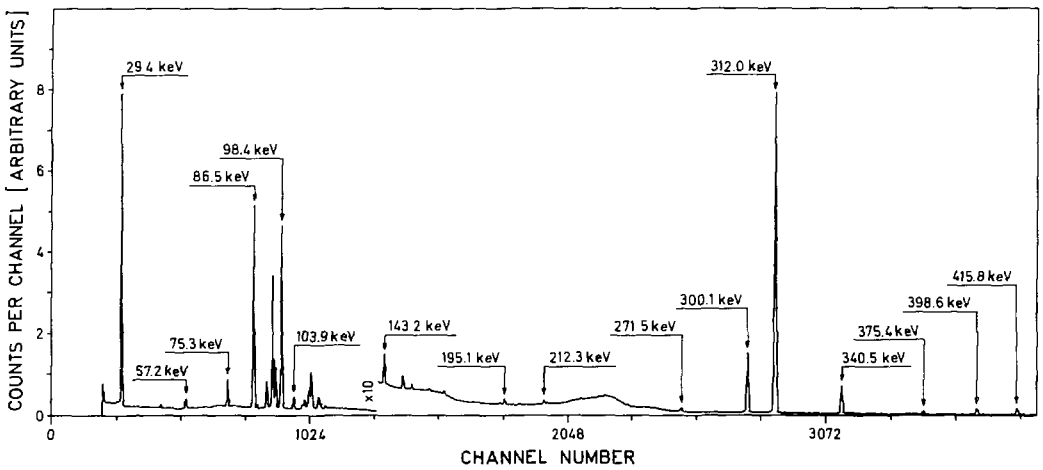

Fig. 52. Gamma-ray spectrum of ^{237}Np - ^{233}Pa

The solid angles of the detection systems vary between 0.1 sr and 0.3 sr. The γ-ray-emission probabilities are obtained from the ratio N_γ/N_0.
The measurement technique and the results are described in a paper that has been submitted for publication [1]. It has the following abstract:

---

(1) R. Vaninbroukx, G. Bortels and B. Denecke, Determination of Photon-Emission Probabilities in the Decay of ^{237}Np and its Daughter ^{233}Pa, Int. J. Appl. Radiat. Isot., in press

" Photon-emission probabilities of importance for the assay of ^{237}Np samples by gamma-ray spectrometry have been measured. The results were deduced from the photon-emission rates, measured with a calibrated high-purity-Ge detector, and the disintegration rates, measured with alpha-particle counting in a well defined solid angle."

Alpha-particle-emission probabilities in the decay of ^{237}Np

G. Bortels

A feasibility study [1] was made to investigate the parameters which influence the accuracy of the measurements of the α-particle-emission probabilities of the ^{237}Np decay. A typical α spectrum measured at CBNM, is shown in Fig. 53. The α peaks are indicated by the energy of the excited level in ^{233}Pa to which the decay proceeds.

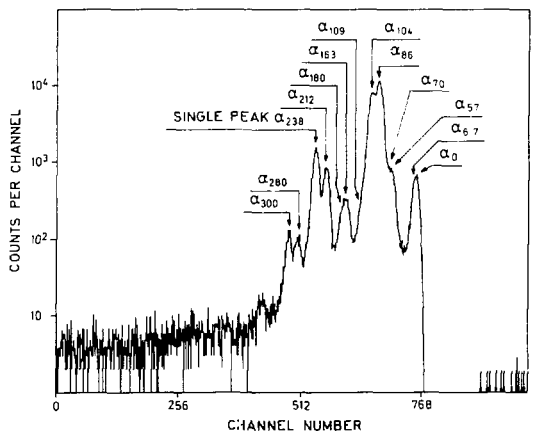

Fig. 53. Alpha-particle spectrum of ^{237}Np measured with a vacuum evaporated source of 14 $\mu g/cm^2$ thickness and a SB detector of resolution 12.5 keV FWHM. Measurement geometry was about 1.4 % of 4π sr

The most important α group in the spectrum contains five overlapping peaks from α_{57} to α_{109}, in the energy range between 4760 and 4820 keV.
The conclusions of the study are as follows:

---

(1) G. Bortels, Feasibility Study of Improving the Measurement of the Alpha-Particle-Emission Probabilities of ^{237}Np, CBNM Internal Report GE/R/RN/16/83

- Passivated ion-implanted detectors must be selected for a 10 keV full-width-half-maximum resolution or better.
- Peak broadening resulting from amplifier-gain instability should not exceed 0.1 keV.
- Measurement duration must be kept relatively short. Spectra can be added following a suitable linear adjustment of the energy scale.
- Sum pulses from coincident α particles and conversion electrons cause spectrum deformation. The conversion electrons should be eliminated by the use of a magnetic field.
- The analysis of the α spectra of ^{237}Np requires either the use of an internal reference peak or a suitable analytical model to fit the singlet α peaks. There are no other α-particle-emitting Np isotopes of suitable half life available. The preparation of very thin (5 μg/cm^2), homogeneously mixed sources of ^{237}Np and ^{238}Pu would be useful.

It will be necessary to improve the parameters mentioned above before starting new measurements of the ^{237}Np α-particle-emission probability.

Decay of ^{238}Pu

G. Bortels, B. Denecke, R. Vaninbroukx

A paper on the alpha-particle- and photon-emission probabilities in the ^{238}Pu-^{234}U decay has been presented at the ICRM Seminar on Alpha-Particle Spectrometry and Low-Level Measurements, Harwell, UK, 10-13 May 1983. The paper [1] has the following abstract:

" Emission probabilities for the alpha particles of 5358, 5456 and 5499 keV in the decay of ^{238}Pu have been measured using Si-surface-barrier detectors. Sources of ^{238}Pu, produced by evaporation in vacuum, were measured in various solid angles.
Similar sources were used for the measurement of emission probabilities for photons, LX and prominent γ rays, following the decay of ^{238}Pu. These measurements were performed with calibrated high-purity-Ge and Si(Li) detectors. The disintegration rates of the sources were measured by α counting in a well-defined small solid angle. The results also include values for the total internal-conversion coefficients. The results give a consistent set of data for the prominent α-particle and γ-ray transitions in the decay ^{238}Pu."

---

(1) G. Bortels, B. Denecke and R. Vaninbroukx, Alpha-Particle- and Photon-Emission Probabilities in the ^{238}Pu-^{234}U Decay, Nucl. Instr. and Meth., in press

Decay of ^{241}Am

B. Denecke

The measurements of the 60-keV γ-ray-emission probability were continued. The disintegration rates of seven sources with an activity ranging from 100 to 11000 Bq were measured with an accuracy of 0.1 % by counting the α-particles in a low-solid-angle arrangement.
The source material was evaporated under vacuum onto Mylar foils of 6.6 cm diameter and 450 $\mu g/cm^2$ superficial density. Stronger sources on polyimide foils of 100 $\mu g/cm^2$ superficial density are in preparation.
The γ-ray emission rates were measured with a CsI(Tl)-sandwich spectrometer realizing a solid angle of nearly 4π sr. Due to the large geometry the X rays are summed up with each other and with the 60-keV γ rays. Several peak-area-calculation programmes were tested for their ability to fit the complex experimental spectra.
The measurements indicated that the dead layers had to be removed from the CsI-crystal surfaces. Furthermore, the flatness of the crystals and the shape of the spherical cavity in the middle of them was not good enough to reach a solid angle as close as possible to 4π sr. Therefore, the window surfaces were abraded and polished to get flat contact planes between which the sources were mounted. A value of 0.66 was reached for the ratio of the scintillation efficiency between α particles and electrons. This shows that there are no significant dead layers left on the crystal surfaces.
Since only γ and X rays should be detected in the CsI-sandwich counter it is necessary to stop by specially designed absorbers all other radiation which is coincident with that to be investigated. The bowler-hat-shaped absorbers made from Makrolon foils were found to be too thin. Another type of absorbers formed from polysterene foils did not fit any more into the reshaped spherical cavities of the crystals. Therefore,a prototype of a mould was constructed for hot-pressing of new and better absorbers from pellets of high-density polyethylene, which is optimal as absorbing material. Transparent absorbers of various thicknesses were successfully fabricated.
The γ-ray resolution of the detector system as function of the energy was investigated. Sources of ^{47}Sc (E_γ = 159 keV) and ^{139}Ce (E_γ = 166 keV, E_{KX} = 33.4 keV) were measured. Measurements of $^{93}Nb^m$ (E_{KX} = 16.9 keV) and ^{109}Cd (E_γ = 88 keV, E_{KX} = 22.6 keV) sources are in progress.

2.2 COMPILATIONS AND EVALUATIONS

Internal conversion data

H.H. Hansen

The compilation of internal-conversion data for nuclides with $Z > 60$ has been finalized. The listings are sent to the publisher (FIZ, Karlsruhe) and the abstract of the report [1] reads as follows:

" A compilation of experimental values of internal-conversion coefficients and ratios is presented. Results quoted with an error and published prior to October 1982 have been retained. Separate tables have been prepared for results from studies on radioactive nuclides, from nuclear reactions experiments, from measurements on E0 transitions ($0^+ \rightarrow 0^+$), and from studies in different chemical environments. The tables include information on the origin of the isotope, transition energies, spin and parity of initial and final levels, experimental technique used, and literature references."

The work on the evaluation of experimental internal-conversion coefficients of some selected transitions useful for calibration purposes has been finished. A set of recommended values for K-shell and total internal-conversion coefficients, α_K and α, respectively, are shown in Table 8. An internal report on this subject is in preparation.

Directory of certified radioactive reference sources

G. Grosse, W. Bambynek

On request of the International Atomic Energy Agency, Vienna, an International Directory of Certified Radioactive Sources had been compiled and stored on magnetic tape. The compilation, which contains about 4500 entries, has been updated and has been published [2].

---

(1) H.H. Hansen, Compilation of Experimental Values of Internal Conversion Coefficients and Ratios for Nuclei with $Z > 60$, Phys. Data, in press

(2) G.Grosse and W. Bambynek, International Directory of Certified Radioactive Sources, Physics Data 27 - 1 (1983)

Table 8. Recommended values for some internal-conversion coefficients

Energy E_γ (keV)	Origin	Recommended values	
		a_K	a
14.413	^{57}Co	7.35 ± 0.19	8.18 ± 0.11
88.037	^{109}Cd	11.1 ± 0.2	26.0 ± 0.3
122.061	^{57}Co	$(2.14 \pm 0.12) \cdot 10^{-2}$	$(2.40 \pm 0.14) \cdot 10^{-2}$
136.474	^{57}Co	0.122 ± 0.013	0.137 ± 0.015
145.444	^{141}Ce	0.372 ± 0.006	0.435 ± 0.009
165.853	^{139}Ce	0.2146 ± 0.0010	0.2516 ± 0.0007
279.197	^{203}Hg	0.1640 ± 0.0010	0.2271 ± 0.0012
336.2	$^{115}In^m$	0.843 ± 0.011	1.072 ± 0.014
321.688	$^{113}In^m$	0.437 ± 0.004	0.540 ± 0.004
411.804	^{198}Au	$(3.01 \pm 0.02) \cdot 10^{-2}$	$(4.4 \pm 0.2) \cdot 10^{-2}$
661.661	^{137}Cs	$(8.99 \pm 0.09) \cdot 10^{-2}$	0.1103 ± 0.0007
834.843	^{54}Mn	$(2.24 \pm 0.10) \cdot 10^{-4}$	$(2.51 \pm 0.11) \cdot 10^{-4}$
1115.546	^{65}Zn	$(1.66 \pm 0.06) \cdot 10^{-4}$	$(1.85 \pm 0.07) \cdot 10^{-4}$
1173.238	^{60}Co	$(1.51 \pm 0.07) \cdot 10^{-4}$	$(1.68 \pm 0.04) \cdot 10^{-4}$
1274.545	^{22}Na	$(6.3 \pm 0.6) \cdot 10^{-6}$	$(6.8 \pm 0.4) \cdot 10^{-6}$
1332.513	^{60}Co	$(1.15 \pm 0.05) \cdot 10^{-4}$	$(1.28 \pm 0.05) \cdot 10^{-4}$

Fluorescence yields

W. Bambynek

A reevaluation of the K-shell fluorescence yield has been performed. There are about 100 new results since the last evaluation [1] in 1972. In addition to the various techniques to measure ω_K directly, there are methods which yield the product of the relative K-capture probability P_K and the fluorescence yield ω_K. About 90 of those measurements have been evaluated and included into the file.

For the calculation of the P_K values electron-wave functions have been used according to Mann and Waber and exchange and overlap corrections of Bahcall

(1) W. Bambynek, R.W. Fink, H.-U. Freund, Hans Mark, C.D. Swift, R.E. Price and P. Venugopala Rao, Rev. Mod. Phys. 44, 716 (1972)

and of Vatai, as recalculated by Chen, for $Z \leq 58$, and those of Suslov and of Martin and Bichert-Toft for $Z > 58$. The method of calculation is described elsewhere [1].

From the file of all published, experimentally determined K-shell fluorescence yields a set of recommended data has been selected and fitted to the relation

$$(\omega_K/(1 - \omega_K))^{1/4} = B_0 + \sum_{i=1}^{P} B_i Z^i .$$

The recommended and fitted ω_K values are compared to those of theoretical predictions [2][3].

Partial-α half life of ^{241}Pu and total half lives of ^{241}Pu and ^{241}Am

R. Vaninbroukx

As part of the CBNM contribution to the Coordinated Research Programme (CRP) on the Measurement and Evaluation of Transactinium Isotope Nuclear Data of the International Atomic Energy Agency (IAEA) the partial-α half life of ^{241}Pu has been evaluated. The measurements described in the literature have been reviewed and assessed and a weighted-mean value has been deduced [4].

The recommended value and its uncertainty on a 68 % confidence level is :

$$T_{1/2}(\alpha) = (6.00 \pm 0.05)10^5 \text{ a}.$$

There is a well recognized discrepancy between the results of the ^{241}Pu half-life determinations by the ^{241}Am-ingrowth method and those from recent direct measurements of the decay by mass spectrometry. The ratio of ^{241}Am and ^{241}Pu activities in a Pu sample is a function of the decay constants of both radionuclides and the time, t, elapsed since the Am/Pu separation. Consequently, if one of the decay constants, e.g. that of ^{241}Am, is assumed to be known, the other can be calculated from the activity ratio and the time t.

---

(1) W. Bambynek, H. Behrens, M.H. Chen, B. Crasemann, M.L. Fitzpatrick, K.W.D. Ledingham, H. Genz, M. Mutterer and R.L. Inteman, Rev. Mod. Phys. 49, 77 (1977)

(2) L. Walters and C.P. Bhalla, Phys. Rev. A3, 519 (1971), Phys. Rev. A3, 1919 (1971), At. Data 3, 301 (1971)

(3) M.H. Chen, B. Crasemann and Hans Mark, Phys. Rev. A21, 436 (1980)

(4) R. Vaninbroukx, Review of the Partial-Alpha Half Life of ^{241}Pu, CBNM Internal Report GE/R/RN/13/83

In order to contribute to a clarification of this discrepancy all measurements of the ^{241}Pu and ^{241}Am half lives described in the literature have been reviewed and assessed. In Table 9 the reviewed values are summarized. The value obtained for ^{241}Am confirms the recommended half-life value of (432.6 + 0.6)a [1]. The review, which is described in a CBNM Internal Report [2], shows that the recommended half life of ^{241}Am cannot be reconciled to the result of the recent decay measurements of the half life of ^{241}Pu.

Table 9. Review of the reported ^{241}Pu and ^{241}Am half lives

Nuclides	Methods applied	Half life in years Mean values and their standard deviations
^{241}Pu	Direct decay measurements, mainly by mass spectrometry, and ^{241}Am ingrowth by γ- and low-geometry α counting	14.56 ± 0.06
	Direct decay measurements (n=10)	14.60 ± 0.09
	Recent direct decay measurements (n=3)	14.36 ± 0.02
	^{241}Am ingrowth (n=3)	14.61 ± 0.04
^{241}Am	Specific-power measurements by calorimetry and specific-activity measurements by α counting (n=7)	433.0 ± 0.6

Probably systematic effects have been underestimated. Direct decay measurements by measuring the changes in the 148.6 keV and 208.0 keV γ-ray-emission rates of ^{241}Pu sources using high-purity-Ge detectors have been started. It is expected that the results from these measurements will help to solve the discrepancy. To our knowledge, this method has not yet been employed for the determination of the ^{241}Pu half life.

---

(1) A. Lorenz, Proposed Recommended List of Heavy Element Radionuclide Decay Data, INDC(NDS)-127/NE, IAEA, Vienna, 1981

(2) R. Vaninbroukx, Remarks on the Half Lives of ^{241}Pu and ^{241}Am, CBNM Internal Report GE/R/RN/02/83

Decay data of actinides

R. Vaninbroukx

A paper [1] on the IAEA coordinated research programme has been presented at the ICRM Seminar on Applied Radionuclide Metrology, Geel, 16-17 May 1983. It has the following abstract:

" In 1977 the Nuclear Data Section of the Atomic Energy Agency organized a Coordinated Research Programme on the Measurement and Evaluation of Transactinium-Isotope Nuclear Decay Data. The objectives of the Coordinated Research Programme, its organization, the achievements and the ongoing work are reported."

2.3 IMPROVEMENT OF MEASUREMENT AND SOURCE PREPARATION TECHNIQUES

Comparison of activity measurements of a ^{123}I solution

D. Reher, E. Celen, R. Vaninbroukx, W. Zehner

On request of the Institut National des Radioéléments (IRE) two solutions of ^{123}I were standardized. In this comparison of activity measurements SCK-CEN (Belgium), LMRI (France), NPL (UK), NIRH (Denmark) and CBNM were participating. The nuclide ^{123}I, which has a half life of (13.21 + 0.03)h, is used as radiopharmaceutical. It was produced via the reaction $^{127}I(p,5n)^{123}Xe$ at the cyclotron of Louvain-la-Neuve. The formed ^{123}Xe decays with a half life of 2.08 h to ^{123}I. Additionally to this reaction ^{125}Xe is generated by the reaction $^{127}I(p,3n)^{123}Xe$. This nuclide decays with a half life of 17 h to ^{125}I which builds up an appreciable impurity in the ^{123}I solution.
CBNM received two bottles containing each 5 ml of the ^{123}I solution. From each bottle 3.6 ml were filled into ampoules. The ampoules were flame-sealed and sent to the Bureau International des Poids et Mesures (BIPM) in Sèvres, France, for measurement in the International Reference System (SIR).
From the remaining solution quantitative sources were prepared and measured with the $4\pi(AX)$-γ-coincidence method and a calibrated planar high-purity-Ge detector. An investigation on further impurities was carried out by γ-ray spectrometry.

---

(1) R. Vaninbroukx, The IAEA Coordinated Research Programme on the Measurement and Evaluation of Transactinium-Isotope Nuclear Decay Data, Int. J. Appl. Radiat. Isot., 34, 1259 (1983)

The estimated overall uncertainties corresponding to the 68 % confidence level are ± 0.54 % for the coincidence method and ± 0.75 % for the calibrated-Ge-detector measurements. The agreement between the two individual results is 0.1 %. The activity concentration of the solution was found to be (500.8 ± 2.7)Bq/mg on the reference date 1 June 1983 0h UT. The ^{125}I impurity concentration at the same date was found to be (6.4 ± 0.4)Bq/mg. The measurements are described in an internal report (1).

Standardization and decay data measurements on ^{47}Sc

D. Reher, E. Celen, B.M. Coursey★, B. Denecke, H.H. Hansen, D. Mouchel, R. Vaninbroukx, W. Zehner

The nuclide ^{47}Sc is useful in two fields of application: (1) in radiotherapy and cancer research, and (2) in efficiency calibrations of solid state detectors at 160 keV. The Institut National des Radioéléments (IRE) requested CBNM to standardize a solution of ^{47}Sc. IRE supplied sufficient material, so that CBNM could organize a small international comparison for the determination of the activity concentration of the solution - similar to that on ^{123}I. NPL and LMRI accepted to participate and BIPM measured two ampoules in the International Reference System, SIR.

The measurements for the determination of the activity concentration were carried out using the $4\pi\beta$-γ coincidence technique and liquid scintillation counting. For the measurement of impurities a calibrated Ge detector was used. The results, which are still preliminary, agree within 0.2 %. This demonstrates that ^{47}Sc can be standardized rather accurately. At the occasion of this comparison we discovered that some of the decay-scheme parameters of ^{47}Sc are not very well known. Some additional measurements allowed us to determine more accurate values for the half life, the γ-ray emission probability, the branching ratio, and some K-conversion data. Preliminary results are available. The final results will be available in 1984.

---

(1) D. Reher, E. Celen, R. Vaninbroukx and W. Zehner, Standardization of a ^{123}I Solution, CBNM Internal Report GE/R/RN/21/83

★ Visiting Scientist from NBS, Washington

Low-energy X-ray and electron spectrometer

D. Reher, W. Bambynek

A paper [1] describing the low-energy X-ray and electron spectrometer (LEXES) has been presented at the ICRM Seminar on Applied Radionuclide Metrology, Geel, 16-17 May 1983. It has the following abstract:

" The Low Energy X-Ray and Electron Spectrometer (LEXES) has been designed for the simultaneous measurement of photons and electrons with windowless solid state detectors. Within this spectrometer two detectors can be moved independently of each other with respect to the source plane. The source is introduced through an interlock system in order to keep the detectors constantly cooled and under high vacuum. Special techniques and materials have been chosen to reach the low operating temperatures of the detectors and to keep the consumption of liquid nitrogen at an acceptable level. LEXES has been used for the measurement of various parameters, and recently, for the determination of conversion-electron ratios in the decay of $^{93}Nb^{m}$ (Reher, 1982). As a further example of such measurements the redetermination of the relative K-capture probability P_K in the decay of ^{139}Ce is described. A value of $P_K = 0.75 \pm 0.05$ has been found which is in good agreement with recent measurements (Hansen and Mouchel, 1975; Plch and co-workers, 1975)."

Satellite peaks in high-resolution alpha-particle spectra

A. Nylandsted Larsen*, G. Bortels, B. Denecke

A paper has been published [2]. The abstract reads as follows:

" The origin of satellite peaks accompanying some of the alpha peaks in spectra from decay-chain members measured with surface-barrier detectors is discussed. It is shown by the example of the ^{228}Th series that these satellite peaks stem from alpha-particle decay of nuclei which have been recoil implanted through the Au-surface-barrier layer of the detector and into the Si crystal. The energy separation between a given alpha-particle peak and its satellite peak corresponds to the fraction of energy lost by the recoiling atom to charge carriers in silicon. This fractional loss of energy for members of the ^{228}Th series has been measured. Results are consistently lower than values obtained from the theory of Lindhard et al."

---

(1) D. Reher and W. Bambynek, A Versatile Solid-State Detector Spectrometer, Int. J. Appl. Radiat. Isot., 34, 1301 (1983)

(2) A. Nylandsted Larsen, G. Bortels and B. Denecke, Satellite Peaks in High-Resolution Alpha-Particle Spectra of Decay-Chain Members measured with Silicon Surface-Barrier Detectors, Nucl. Instr. and Meth., 219, 339 (1984)

* Present address: Institute of Physics, University of Aarhus, DK-8000 Aarhus C., Denmark

Low-energy X-ray standards

G. Grosse, W. Bambynek

A press was designed and fabricated for the preparation of the fluorescence sources. It presses under vacuum the fluorescer foil and the glue against the backing. In this way we get flat sources. This is important for the reproducibility of the source position.

A new source holder was constructed. It allows one to rotate the source with respect to the counter axis between 0 and 45° in steps of 7.5°. Care has been taken that the radiating area remains in the rotation axis. Such a source holder is needed to determine the influence of the anisotropy with respect to the source rotation angle for the case of users performing calibrations at a non-normal angle to the source.

Improvements have been made to separate the Al-KX-ray peak at 1.5 keV from the low-energy tail of the 5.4 keV Mn-KX-ray peak. Fig. 54 shows the Al peak after subtraction of the tail and the background.

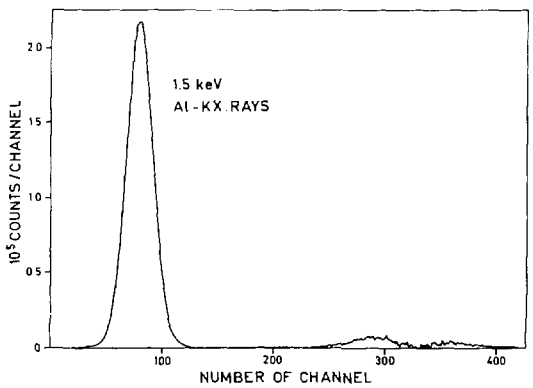

Fig. 54. Al-KX-ray fluorescence peak after separation from the low-energy tail of the excitation-radiation peak

Improvements of the $4\pi\beta$-γ-coincidence method

D. Reher, E. Celen, E. Funck*, A. Nylandsted Larsen**

A paper [1] on the influence from low-energy X rays and Auger electrons on $4\pi\beta$-γ-coincidence measurements of electron-capture-decaying nuclides has been published. It has the following abstract:

" The influence of low energy X-rays and Auger electrons emitted by electron capture nuclides on $4\pi\beta$-γ-coincidence measurements is investigated. Under the assumption that these radiations are not detected, correction terms are developed for a number of nuclides that are in common use."

A new β-counter was developed. With this counter the gas consumption could be reduced by more than a factor of three.
In addition, the homogeneity of the electric field was improved which resulted in a better resolution of the counter.
The mechanical construction of the counter and the materials used were kept as far as possible to the original properties in order to keep factors, such as the γ-ray efficiency of the β-ray counter $(\epsilon_\beta)_\gamma$, the same as before. This was checked by re-measuring $(\epsilon_\beta)_\gamma$ for ^{54}Mn and ^{7}Be.
An improved version of the $4\pi\beta$-γ coincidence-evaluation program BEGAC is implemented on the RNDAS computer. There remain some further improvements to be included, e.g. determination of the uncertainty on the single measurements, life-time data as input and input of data directly from a CAPRO-measurement disk.

Measurement of superficial densities in air pollution samples

B. Denecke

A paper [2] on electron-energy absorption used for the measurement of superficial densities of air pollution samples on thin membrane filters has been

---

(1) E. Funck and A. Nylandsted Larsen, The Influence from Low-Energy X Rays and Auger Electrons on the $4\pi\beta$-γ Coincidence Measurements of Electron-Capture Decaying Nuclides, Int. J. Appl. Radiat. Isot. 34, 565 (1983)

(2) B. Denecke, Electron-Energy Absorption Used for the Measurement of Superficial Densities of Air Pollution Samples on Thin Membrane Filters, Int. J. Appl. Radiat. Isot. 34, 1311 (1983)

* Physikalisch-Technische Bundesanstalt (PTB) Braunschweig, GFR

** Present address: Institute of Physics, University of Aarhus, DK-8000 Aarhus C., Denmark

presented at the ICRM Seminar of Applied Radionuclide Metrology, Geel, 16-17 May 1983. It has the following abstract:

" A sampling and analysis method to measure dust concentrations in air is described. The dust was deposited on membrane filters, the superficial density of which was measured by an electron-energy-absorption method. Internal-conversion electrons from the ^{109}Cd decay were used as the electron source. The electron detector was a gas-proportional counter operated at atmospheric pressure with a 90 % Ar + 10 % CH_4 gas flow. Detected superficial-density differences ranged from 0 to 400 $\mu g/cm^2$ with an estimated accuracy of 20 $\mu g/cm^2$. The measurement process was automated using a computer-controlled sample changer. About 8,000 samples were taken and analysed during 18 months. In addition to the total amount of dust the blackening index of the dust stains was also measured by an optical reflection method."

A CBNM Internal Report (1) on light-reflection measurements on dust stains of air-pollution samples has been written. It has the following abstract:

" A light reflection method for air quality measurements is described. The blackening index of dust stains on membrane filters is compared against shaded paper standards. Solid-state optoelectronic modules are used as light source and as light detector. A small compact probe has been developed and is used as a reflectometer in an automatic measuring system which is based on a computer-controlled sample changer. The analog output signal of the reflectometer is converted into digital form to be presented to the data acquisition system. The relation between the blackening index of the dust stains and the deposited dust amount on the filters is investigated."

Radionuclide Group Data Acquisition System

D. Reher, A.B. Idzerda

A paper (2) describing the Radionuclides Group Data Acquisition System, RNDAS, has been submitted for publication. It has the following abstract:

" A data acquisition system for the radionuclide-metrological laboratory of CBNM is described. It is implemented in three phases and its final configuration will be that of a small local area network. A comparison of the properties of the earlier centralized system with those of the new system shows that the latter is more flexible, faster in response and less affected by breakdowns."

---

(1) B. Denecke, Light-Reflection Measurement on Dust Stains of Air-Pollution Samples, CBNM Internal Report GE/R/RN/12/83

(2) D. Reher and A.B. Idzerda, A Data Acquisition System for a Radionuclide Laboratory, Nucl. Instr. and Meth., in press

The automatic gamma spectrometer, to be controlled by one of the four CAPRO-stations, was installed and tested. The software was adapted to the required source positions, which were determined by means of a test programme. The 8 floppy-disk drives were equipped with an automatic on/off control in order to avoid unnecessary wear during repeated measurements over a long period. Both the hard- and software of a CAPRO-station were adapted in order to implement a new multi-channel analyser of the type Nuclear Data ND-65.

SHIFT, a program to shift spectra by fractions of a channel

D. Reher, H. Frieauff *

An algorithm to shift spectra by fractions of a channel was developed and coded as a FORTRAN program, running on the RNDAS main computer. To describe the shape of a spectrum within a channel, this algorithm uses polynomial approximation with integral boundary conditions. This guarantees the conservation of some important parameters of a spectrum after shifting, as e.g. total integral, partial integrals, and resolution of the peaks. The program was tested with complex Ge-detector spectra. Peak positions, full-width at half-maximum, and peak area were determined using the peak fitting program RETEOH before and after the spectrum shift. The program was successfully used in the evaluation of ^{47}Sc conversion-electron-data measurements. An internal report will be available in the first half of 1984.

GEELEE, an electron-peak evaluation program

D. Reher, W. Westmeier**, H. Verdingh ***

For the evaluation of conversion-electron spectra measured with the windowless Si(Li) detector of LEXES, a computer program was developed which distinguishes between electron and photon peaks present in such spectra. The first experiments with this interactive program on the RNDAS main computer were very promizing. However, when we improved the program by adding some very useful features, it became too large to be handled by the actually used operating system RT-11. This is not a problem of available memory but of

---

* Stagiaire from TH Aachen, GFR

** University of Marburg, GFR

*** Stagiaire from HIK, Geel, Belgium

memory management by the operating system. With the timesharing operating system TSX-plus, which emulates RT-11, such large programs run easily as was tested in collaboration with the firm POSITRONIKA, Eindhoven.

Calibration service

G. Bortels, B. Denecke, R. Vaninbroukx

Sources of ^{54}Mn, ^{60}Co, ^{65}Zn, ^{133}Ba and ^{137}Cs for calibration of detector and samples of ^{234}U, ^{238}Pu, ^{239}Pu and ^{241}Am were standardized for various services inside CBNM.
A ^{238}Pu sample for neutron measurements has been investigated for the possible contamination by ^{245}Cm, within the detection limit of about 300 ppm, no ^{245}Cm was detected. The relative specific activity of 10 samples of a V-^{237}Np alloy of 1 % ^{237}Np and 10 samples of an Al-^{237}Np alloy of 3 % ^{237}Np was determined. The ^{234}Th content after Th/U separation was measured for 14 ^{238}U samples.

Source preparation

W. Oldenhof, W. Zehner

Various techniques were used for the preparation of about 170 radioactive sources (^{3}H, ^{7}Be, ^{46}Sc, ^{47}Sc, ^{54}Mn, ^{55}Fe, ^{57}Co, ^{60}Co, ^{65}Zn, ^{88}Y, $^{93}Nb^{m}$, ^{94}Nb, ^{109}Cd, ^{123}I, ^{133}Ba, ^{139}Ce, ^{234}U, ^{238}Pu, ^{239}Pu, ^{243}Am) on VYNS, Formvar and carbon backings and for liquid scintillation counting. About 370 supporting foils (VYNS, Formvar, carbon) were made.

ICRM General Meeting

W. Bambynek

The International Committee for Radionuclide Metrology (ICRM) held its General Meeting this year from 16 to 20 May 1983 at CBNM. The meeting was attended by 60 persons coming from two international organizations and 20 different countries.
The first two days were devoted to a Seminar on Applied Radionuclide Metrology. There were 33 papers, presented in six sessions: Introduction, Gamma-Ray Spectrometry, Standardization, Decay-Data Measurements, Decay-Data Evaluations, and Miscellaneous Measurement Techniques and Applications.

Eight contributions were presented by CBNM staff. The proceedings of the seminar has been published as a special issue of the Int. J. Appl. Radiat. Isct. Vol. 34 (1983).
During the rest of the week there were meetings of the working groups: Alpha-, Beta-, Gamma-Ray Spectrometry, Life Sciences and Non-Neutron Nuclear Data and during the last day the General Meeting of ICRM members.

COLLABORATION WITH EXTERNAL ORGANIZATIONS

The requirements for non-neutron nuclear data and the status of the measurements are reviewed by international nuclear data committees. CBNM is represented in the following committees:

- IAEA Advisory Group on Nuclear Structure and Decay Data;
- IAEA Advisory Group on Fission Product Nuclear Data;
- IAEA Advisory Group on Transactinium Isotope Nuclear Data;
- IAEA Coordinated Research Programme on Measurements and Evaluations of Transactinium Isotope Nuclear Decay Data;
- International Committee for Radionuclide Metrology (ICRM). A CBNM member is chairman of ICRM. Another CBNM member serves as coordinator of the ICRM Sub Group on α Spectrometry.

In addition, the high accuracy aspect of some of the measurements is discussed by the BIPM Consultative Committee on Measuring Standards for Ionizing Radiations (CCEMRI), Section II, Measurements of Radionuclides, in which CBNM is represented as well.

LIST OF PUBLICATIONS

NUCLEAR MEASUREMENTS

TOPICAL REPORTS

BÖCKHOFF, K.H. - Nuclear Data for Science and Technology (Intern. Conf.) Antwerpen, 6-10 Sept. 1982 - EUR 8355, EN EP (1983)

AXTON, E.J. - Evaluation of the thermal constants of ^{233}U, ^{235}U, ^{239}Pu and ^{241}Pu and the Fission Neutron Yield of ^{252}Cf - EUR 8805 EN EP

LE DUIGOU, Y. - Certification of a uranium dioxide reference material for chemical analyses - EUR 8753 EN

MEYER, H. - CAMAC, Updated Specifications, Vol. 2 - EUR 8500 EN

PAULSEN, A., BERTHELOT, Ch., van den BERG, M., BABELIOWSKY, T. - The feasibility of electromagnetic actinide isotope separation in the European Community. In press

BUDTZ-JØRGENSEN, C., GÜNTHER, P., SMITH, A., WHALEN, J. - Low-MeV neutrons incident on Yttrium, ANL/NDM-79, Argonne, USA - ART 25287

CORVI, F. - The $^{197}Au(n,\gamma)$ cross section, in: Nuclear Data Standards for Nuclear Measurements, IAEA Technical Reports Series No. 227 (1983)

WATTECAMPS, E. - The $^{10}B(n,\alpha)$ cross section, in: Nuclear Data Standards for Nuclear Measurements, IAEA Technical Reports Series No. 227 (1983) p. 19

VANINBROUKX, R., LORENZ, A. - Actinide half lives, in: Nuclear Data Standards for Nuclear Measurements, IAEA Technical Reports Series No. 227 (1983) p. 69

GROSSE, G., BAMBYNEK, W. - International directory of certified radioactive sources, Physik Daten/Physics Data 27-1 (1983)

VANINBROUKX, R. - Review of the partial alpha half life of ^{241}Pu, Sixth Research Coordination Meeting on the Measurement and Evaluation of Transactinium Isotope Nuclear Data, Idaho Fall, 21-24 June 1983 (Editor A. Lorenz), INDC Report INDC(NDS)-147/GE (1983) p. 19

HANSEN, H.H. - Compilation of experimental values of internal conversion coefficients and ratios for nuclei with $Z > 60$, Physik Daten/Physics Data, in press.

de RAS, E. (co-author) - Operational quantities for use in external radiation protection measurements - Edited by the Working Group of the Commission of the European Communities, DG V/E, Luxembourg, EUR 8346 EN

CONTRIBUTIONS TO CONFERENCES

AVALDI, L. MILAZZO, M., TRIVIA, G.L., MITCHELL, I.V. - Recent results on K-shell Ionization by Ion Collision, Conf. on Application of Accelerators, North Texas State University, Denton, Texas, Nov. 8-10, 1982 - ORA 30704

BERTHELOT, Ch., ESCHBACH, H.L., VERDINGH, V., VERHEYEN, F. - The homogeneity control of reference materials by photon activation, 1983-European Conference on Environmental Pollution, London, 13-14 June 1983 - ORA 30768

DE BIEVRE, P., WOLTERS, W., MACHLAN, L.A., GRAMLICH, J.W., FASSETT, J.A. - The IDA-80 measurement evaluation programme on mass spectrometric isotope dilution analysis of U and Pu: some preliminary results, "Recent advances in Nuclear Material Safeguards", IAEA, 8-12 Nov. 1982 - IAEA-SM-260/33 pp. 261-278 - ORA 30560

HANSEN, H.H.- Pläne zur Herstellung von Referenz-Materialien in ZBKM, Radioaktive Standards und ihre Anwendung im Bereich der Kerntechnik und Umgebungsüberwachsung, (Editor K. Debertin), PTB Bericht Ra-13 (1983) p. 82

ALLAERT, E., WAGEMANS, C., DERUYTTER, A., BARTHELEMY, R., SCHILLEBEECKX, P. - Comparative study of the energy and mass characteristics of the $^{239}Pu(n_{th},f)$ and the $^{240}Pu(s.f.)$ fragments, Frühjahrstagung DPG - BNV - NNV, Münster (BRD), 21-25.3.1983 - ORA 30798

PEETERS, G., THYS, A., DE BIEVRE, P., VANSANT, E.F. - Pore size engineering by modifying the Zeolite pore system of Mordenite LP, International Zeolite Conference, Reno, USA, July 1983 - ORA 30806

BUDTZ-JØRGENSEN, C., KNITTER, H.-H. - Investigation of fission layers for precise fission cross-section measurements with a gridded ionization ch mber, IAEA Consultants' meeting, Smolenice, Bratislava, CSSR, 28.3 - 1.4.1983 - ORA 30958

BUDTZ-JØRGENSEN, C., KNITTER, H.-H. - A precise method for charged particle counting employing energy and angle information from gridded ion chambers, Seminar on Alpha Particle Spectrometry and Low Level Measurements, ICRM, Harwell, 10-13.5.1983, Nucl. Instr. Meth., in press - ORA 30959

ROHR, G. - Systematics of the nuclear level densities, IAEA Advisory Group meeting on Basic and Applied Problems of Nuclear Level Densities, IAEA, Brookhaven National Laboratory - ORA 30960

MITCHELL, I.V., ESCHBACH, H.L., AVALDI, L., DOBMA, W. - Characterization of a new batch of ion implanted Bi in Si specimens as primary reference surface standards, 6th International Conference on Ion Beam Analysis, Arizona State University, Tempe, AZ, USA, May 23-27, 1983, Nucl. Instr. and Meth. 218 (1983) 91 - ORA 31000

KNITTER, H.-H., BUDTZ-JØRGENSEN, C. - Barrier heights of plutonium isotopes from (n,n'f) and (n,f) thresholds, Verhandlungen der DPG Vol. 5 (1983) 1129 Frühjahrstagung D.P.G., Münster, 21-25.3.1983

STRAEDE, Ch., BUDTZ-JØRGENSEN, C., KNITTER, H.-H., Total kinetic energy as function of mass-split and neutron energy for $^{235}U(n,f)$ measured with a double Frisch gridded ionization chamber, Verhandlungen der DPG, Vol. 5 (1983) 1130, Frühjahrstagung D.P.G., Münster, 21-25.3.1983 - ORA 30770

BAMBYNEK, W., DEBERTIN, K. - Introduction ICRM Seminar on RN Metrology, Geel, 16-17 May, 1983, Int. J. Appl. Radiat. Isot. 34, 1039 (1983)

MITCHELL, I.V., REHER, D. - Assay of radionuclide sources by energetic ion beams, ICRM Conference on Applied Radionuclide Metrology, Geel, 16-20 May, 1983, Int. J. Appl. Radiat. Isot. 34, 1301 (1983) - ORA 31001

AVALDI, L., MITCHELL, I.V., MILAZZO, M. - L-shell X-ray production cross-section of $_{48}Cd$, $_{50}Sn$, $_{52}Te$, $_{53}I$, and $_{56}Ba$, XIII International Conference on the Physics of Electronic and Atomic Collisions, Berlin, 27/7 - 3/8/1983 - ORA 31002

AVALDI, L., MITCHELL, I.V., ESCHBACH, H.L., Precise X-ray production cross-section measurements of medium Z elements by protons - 3rd. International Conference on PIXE and its analytical applications, Max-Planck-Institut für Kernphysik, Heidelberg, FRG., July 18-22 - ORA 31008

REHER, D., BAMBYNEK, W. - A versatile solid-state detector spectrometer, ICRM Seminar on Applied RN Metrology, Geel, 16-17 May, 1983, Int. J. Appl. Radiat. Isot. 34, 1301 (1983) - ORA 31009

VERDINGH, V., BEYRICH, W., ESCHBACH, H.L., LE DUIGOU, Y. - Characterization of a uranium dioxide reference material for in-plant use, 5th Annual Symposium on Safeguards and Nuclear Material Management, ESARDA, Versailles, 19-21 April 1983 - ORA 31007

VANINBROUKX, R. - Status Report 1983: JRC-CBNM participation in the IAEA Coordination Research Programme, Sixth Research Coordination Meeting on the Measurement and Evaluation of Transactinium Nuclear Decay Data of Transactinium Isotope Nuclear Data, Idaho Falls, 21-24.6.1983, INDC(NDS)-147/GE (1983) p. 6 - ORA 31121

ROHR, G. - Indication of n-p interaction for nuclear levels observed at high excitation energy, International Conference Nuclear Physics, OIC, Firenze, 29.8 - 3.9.1983 - ORA 31120

BEYRICH, W., GOLLY, W., SPANNAGEL, G., DE BIEVRE, P., WOLTERS, W. - The IDA-80 measurement evaluation programme on mass spectrometric isotope dilution analysis of uranium and plutonium: statistics on generation and transfer of data, ESARDA Symposium, Versailles, 19-21/4/1983, Proceedings p. 225 - ORA 31138

DE BIEVRE, P., WOLTERS, W.H., G. MUSCHENBORN, W. DE BOLLE, W., BEYRICH, W. GOLLY, W. - The 1982 state of the practice in low enrichment UF_6 isotopic measurements in Western Europe, 5th ESARDA Symposium, Versailles, 1983, Proceedings pp. 177-181

VANINBROUKX, R. - Half life and KX-ray-emission probability of $^{93}Nb^{m}$, ICRM Seminar on Applied RN Metrology, Geel, 16-17 May, 1983, Int. J. Appl. Radiat. Isot., 34, 1211 (1983) - ORA 31061

DENECKE, B. - Electron-energy absorption used for the measurement of superficial densities of air pollution samples on thin membrane filters, ICRM Seminar on Applied RN Metrology, Geel, 16-17 May, 1983, Int. J. Appl. Radiat. Isot., 34, 1311 (1983) - ORA 31062

MOUCHEL, D., HANSEN, H.H. - Half-life measurements of excited levels in the nanosecond and microsecond region, ICRM Seminar on Applied RN Metrology, Geel, 16-17 May, 1983, Int. J. Appl. Radiat. Isot., 34, 1201 (1983) - ORA 31063

HANSEN, H.H., MOUCHEL, D. - K/LM+ internal-conversion ratios for pure E2 transitions on the decays of ^{152}Eu and ^{192}Ir, ICRM Seminar on Applied RN Metrology, Geel, 16-17 May, 1983, Int. J. Appl. Radiat. Isot., 34, 1233 (1983) - ORA 31064

HANSEN, H.H. - Measurement of the beta-spectra of ^{90}Sr-^{90}Y, ICRM Seminar on Applied RN Metrology, Geel, 16-17 May, 1983, Int. J. Appl. Radiat. Isot., 34, 1241 (1983) - ORA 31065

VANINBROUKX, R. - The IAEA coordinated research programme on the measurement and evaluation of the transactinium-isotope nuclear decay data, ICRM Seminar on Applied RN Metrology, Geel, 16-17 May, 1983, Int. J. Appl. Radiat. Isot., 34, 1259 (1983) - ORA 31066

BORTELS, G., DENECKE, B., VANINBROUKX, R. - Alpha-particle and photon-emission probabilities in the ^{238}Pu-^{234}U decay, ICRM Seminar on Alpha Particle Spectrometry and Low Level Measurement, Harwell, 10-13 May 1983, Nucl. Inst. and Meth., in press - ORA 31067

ESCHBACH, H.L. - Preparation and characterization of reference layers at the CBNM, Geel, Invited Seminar Lecture, Sandia National Laboratory, Albuquerque, NM, USA, 20.5.1983 - ORA 31068

WAGEMANS, C., DERUYTTER, A.J. - Fission Cross-Section Normalization Problems, IAEA Consultants' Meeting on "The Uranium-235 Fast-Neutron Fission Cross Section", Smolenice, Czechoslovakia - ORA 31082

CORVI, F., BRUSEGAN, A., BUYL, R., ROHR, G. - The neutron capture cross section of ^{56}Fe from 1 to 350 keV, Consultants'Meeting on Nuclear Data for Structural Materials, Vienna, 2-4 November 1983 - ORA 31277

WINKLER, G., PAVLIK, A., UHL, M., PAULSEN, A., LISKIEN, H. - Neutronen-induzierte Reaktionen an ^{58}Ni, Verhandlungen der DPG Vol. 3 (1984), 923 Frühjahrstagung D.P.G., Innsbruck, 26-30.3.1984 -

STRAEDE, Ch., BUDTZ-JØRGENSEN, C., KNITTER, H.-H. - Fission fragment mass, kinetic energy and angular distributions for $^{235}U(n,f)$ in the neutron energy range from thermal to 6 MeV, Verhandlungen der DPG Vol. 3 (1984), 957 Frühjahrstagung D.P.G., Innsbruck, 26-30.3.1984 - ORA 31342

de RAS, E. - Comments on the CBNM results of the photon dosemeter intercomparison (1980/1982) organized by the Health and Safety Directorate V/E/3 of the Commission of the European Communities, Fourth Information Seminar on the European Radiation Protection Dosemeter Intercomparison Programme (1980-1982), 25-27 October 1982, Bilthoven, EUR document in press

SCIENTIFIC OR TECHNICAL ARTICLES

AVALDI, L., MILAZZO, M., TRIVIA, G., MITCHELL, I.V. - Ionization cross-sections of Cd, Sn, Te, I and Ba for protons and alpha particles, Jour. Phys. - B, At. and Molec. Phys. 16 (1983) 1957 - ART 24982

DE BIEVRE, P., GALLET, M., HOLDEN, N.E., BARNES, I.L. - Isotope abundance and atomic weights of the elements - An evaluated compilation, submitted to Journal of Physical and Physico-Chemical Reference Data - ART 25150

PEISER, H.S., BARNES, I.L., DE BIEVRE, P. et al. - Element by element review of the atomic weights, submitted to Pure and Applied Chemistry - ART 25151

DE BIEVRE, P., DE CORTE, F., MOENS, L., SIMONITS, A., HOSTE, J. - The need for accurate minor isotope abundance values in reactor neutron activation analysis, Int. Journ. of Mass Spectrom. Ion Phys., 51 (1983) 31

MICHIELS, E., DE BIEVRE, P. - Absolute isotopic composition and the atomic weight of a natural sample of lithium, Int. Journ. of Mass Spectrom. Ion Phys. 49 (1983) 265

VERLINDEN, J., GIJBELS, R., SILVESTER, H., DE BIEVRE, P. - SIMS investigation on the diffusion of chromium, iron and molybdenum in polycrystalline rhenium, J. Microsc. Spectrosc. Electron., Vol. 7, 1982, 291

VANSANT, E.F., DE BIEVRE, P., PEETERS, G., THIJS, A., VERHAERT, I. - Occlusion and storage of krypton in solids, European Appl. Res. Rept.-Nucl. Sci. Technol. Vol. 4, No. 4, 1982, p. 893

VANINBROUKX, R., HANSEN, H.H. - Determination of γ-ray emission probabilities in the decay of ^{288}Th and its daughters, Int. J. Appl. Radiat. Isot., 34, 1395 (1983)

BORTELS, G., REHER, D., VANINBROUKX, R. - Emission probabilities for the 5.449 MeV α particles and 241 keV γ rays in the ^{224}Ra - ^{220}Rn decay, Int. J. Appl. Radiat. Isot., in press - ART 24851

DONNELLY, S.E., BARFOOT, K.M., WEBB, R.P., BODART, F., WERZ, R. - Helium ion bombardment of thin aluminium films, thin solid films. - ART 24890

COPPIETERS, L., TRIFFAUX, J., VAN AUDENHOVE, J., VAN CAMPENHOUT, J. - Work performed under Contract N° CBNM/ST/80-45, Nucl. Instr. and Meth. - ART 25110

JACOBS, G.J.H., LISKIEN, H. - Energy spectra of neutrons produced by α-particles in thick targets of light elements, Annals of Nucl. Energy, Vol. 10 (1983) 541 - ART 25132

VANSANT, E.F., THIJS, A., PEETERS, G., DE BIEVRE, P., PENZHORN, R.D., DOREA, A., SCHUSTER, P. - Microprobe analysis on noble gas encapsulated in zeolites, Berichte der Bursengesellschaft für Physik. Chemie - (submitted) - ART 25152

DE BIEVRE, P., GALLET, M., WERZ, R. - Determination of the ^{241}Pu half-life by isotope mass spectrometry, Intern. Journ. of Mass Spectrom. Ion Phys., 51 (1983) 111 - ART 25153

DUCHATEAU, N., DE BIEVRE, P. - Thermal ionization mass spectrometry using negative materials ions: a new method for trace boron assay, Intern. Journ. of Mass Spectrom. Ion Phys., 54 (1983) 289

BUDTZ-JØRGENSEN, C., KNITTER, H.-H. - Investigation of fission layers for precise fission cross section measurements with a gridded ionization chamber, Nucl. Sc. Eng. 86, 10 (1984)

THIJS, A., PEETERS, G., VANSANT, E.F., VERHAERT, I., DE BIEVRE, P. - Zeolite modification, Part I: purification of gases by pore sized engineered zeolites, Journ. Chem. Soc. (submitted) - ART 25310

THIJS, A., PEETERS, G., VANSANT, E.F., VERHAERT, I., DE BIEVRE, P. - Zeolite modification, Part 2: the encapsulation of gases in modified zeolites, Journ. Chem. Soc. (submitted) - ART 25311

BORTELS, G. - Preface and introduction for proceedings of ICRM Seminar on alpha-particle spectrometry techniques and applications, Geel, 14 October 1981, Int. J. Appl. Radiat. Isot., in press - ART 25367

NYLANDSTED LARSEN, A., BORTELS, G., - DENECKE, B. - Satellite peaks in high-resolution alpha-particle spectra of decay-chain members measured with silicon surface-barrier detectors, Nucl. Instr. and Meth., 219, 339 (1984) - ART 25441

TJOONK, J. - Improvement of adherence of electro-sprayed deposits for nuclear measurements, Newsletter of the INTDS, 10 (2), 23 (1983) - ART 25482

LISKIEN, H.- International fluence rate intercomparison for 2.5 and 5.0 MeV neutrons, Metrologia - ART 25483

DE BIEVRE, P., BAUMANN, GÖRGENYI, T., KUHN, E., DERON, S., DE REGGE, P. - 1983 target values for uncertainty components in element and isotope assay, ESARDA Bulletin (submitted) - ART 25449

HANSEN, H.H., MOUCHEL, D. - Determination of the K-shell internal conversion coefficient for the 37.2 keV transition in the decay of ^{121m}Sn, Z. Phys. A, 315, 239 (1984) - ART 25450

REHER, D., IDZERDA, A.B. - A data acquisition system for a radionuclide laboratory, Nucl. Instr. and Meth., in press - ART 25473

AVALDI, L., MITCHELL, I.V., MILAZZO, M. - L-shell X-ray production cross-sections of $_{48}Cd$, $_{50}Sn$, $_{52}Te$, $_{53}I$ and $_{56}Be$ for alpha particles, Journ. Phys. B Mol. & Atomic Physics - ART 25362

BASTIAN, C., CERVINI, C. - Polygon shading with a pen plotter, APL Quote Quad, Lynne C. Shaw Arcadia Parkway 19, Rochester, New York - ART 25472

MOUCHEL, D., HANSEN, H.H. - Half lives of the 482.2 keV and 615.3 keV levels in ^{181}Ta, Z. Phys. A 315, 113 (1984) - ART 25471

KLOPF, P., STÜBER, W. - A dedicated CAMAC crate controller for Z 80-micro-computers, Nucl. Instr. and Meth. - ART 25486

PAUWELS, J., VAN GESTEL, J. - UDEL polysulfone P-1700 thin foils: An interesting substrate material for nuclear targets ?, Newsletter of the INTDS, 10 (2), 33 (1983) - ART 25597

KNITTER, H.-H., BUDTZ-JØRGENSEN, C., SMITH, D., MARLETTA, D. - Angular distribution measurements for the reaction $^{6}Li(n,t)^{4}He$, Nucl. Sc. and Eng. 83, 229 (1983)

BORTELS, G., HUTCHINSON, J.M.R. - Concluding ICRM session of the Seminar on alpha particles spectrometry and low-level measurements, Harwell, 10-11 May, 1983, Nucl. Instr. and Meth., in press - ART 25636

BLONS, J., MAZUR, C., PAYA, D., RIBRAG, M., WEIGMANN, H. - On the existence of triple-humped fission barriers in $^{271,233}Th$, Nucl. Phys. 414 (84) 1

FUNCK, E., NYLANSTED LARSEN, A. - The influence from low-energy radiation on $4\pi\beta-\gamma$ coincidence measurements of electron-capture-decaying nuclides, Int. J. Appl. Radiat. Isot. 34, 565 (1983)

MOORE, M.S., WARTENA, J.A., WEIGMANN, H., BUDTZ-JØRGENSEN, C., KNITTER, H.-H., OLSEN, C.E. - Neutron-induced fission cross section of ^{244}Pu, Nucl. Phys. A393 (1983) 1-14

BASTIN, J., BOMANS, M., DUGAIN, F., MICHAUT, C., PUJADE-RENAUD, J.-M., VAN AUDENHOVE, J. - Utilisation de matériaux de référence pour analyse commerciale de grande précision - Exemple de minerais concentrés de zinc - III. - Sélection de trois méthodes de référence pour le dosage du zinc, Analusis, 1983, v. 11, n° 1, p. 2

TECHNICAL NOTES

DE KEYSER, A. - Real time clock for APPLE II computer - GE/TN/DE/90/83

DE ROOST, E. - Instruction manual - goniometer automation - GE/TN/DE/93/83

TEULING, C. - Catalog of APPLE Software - GE/TN/DE/94/83

de JONGE, S. - Multiplexed 16 bit multiple hit read-out for Le Croy 4208 TDC - GE/TN/DE/95/83

CERVINI, C., WERZ, R. - APL programme to print all functions and variables of an APL workspace - GE/TN/DE/96/83

BASTIAN, C., CERVINI, C. - Multiparameter event list processing in APL - GE/TN/DE/97/84

CRAMETZ, A., LISKIEN, H. - Determination of the pulse width as obtainable with the new Van de Graaff rebunching system - GE/R/VG/40/83

CRAMETZ, A. - Calculations of fields parameters of a double magnetic quadrupole lens - GE/R/VG/41/83

VANINBROUKX, R. - Remarks on the half lives ^{241}Pu and ^{241}Am - GE/R/RN/02/83

DENECKE, B. - Light-reflection measurement on dust stains of air pollution samples - GE/R/RN/12/83

CUYPERS, W. - Het onderzoek van dode tijdseffecten in nucleaire meetsystemen - GE/R/RN/23/83

CELEN, E. - A new proportional counter for $4\pi\beta$-γ coincidence measurements - GE/R/RN/24/83

REHER, D., FRIAUFF, W. - A program of shift spectra by fractions of channels - GE/R/RN/25/83

REHER, D., CELEN, E., COURSEY, B.M., VANINBROUKX, R., ZEHNER, W. - Standardization of a ^{47}Sc solution - GE/R/RN/26/83

VANINBROUKX, R., BORTELS, G., DENECKE, B. - Determination of photon-emission probabilities in the decay of ^{237}Np and its daughter ^{233}Pa - GE/R/RN/27/83

BORTELS, G. - Feasibility of improving the measurements of the α-emission probabilities of ^{237}Np - GE/R/RN/16/83

REHER, D., CELEN, E., VANINBROUKX, R., ZEHNER, W. - Standardization of a ^{123}I solution - GE/R/RN/21/83

MUSCHENBORN, G., DE BOLLE, W. - $^{235}U/^{238}U$ isotope ratio measurements on double collector UF_6 mass spectrometers

TRAAS, L.J. - Interfacing a MAT TH5 mass spectrometer to a personal computer using the IEEE-488 interface bus system

DE BOLLE, W. - Preparation of $^{235}U_3O_8$ and $^{235}UF_6$ as IRM batches

DE BOLLE, W. - The cleaning and re-assembling of UF_6 containers

DE BOLLE, W. - Conversion of UF_6 in uranyl nitrate for isotopic measurements by thermionic mass spectrometry

DE BOLLE, W., LYCKE, W. - Measuring small differences in $^{235}U/^{238}U$ ratios in natural uranium

QUIK, F., MEYER, H. - Comparison of gamma-counting and mass spectrometric measurements for the determination of isotope abundance ratios of plutonium - ST/04/83

COMMUNICATIONS

BATCHELOR, R. - 1982 Annual Status Report Nuclear Measurements, Proc./EUR - EUR 8529

BATCHELOR, R. - 1983 Annual Status Report Nuclear Measurements, in press

DEBUS, G.H. (Editor) - PPR Nuclear Measurements - January - June 1983, EUR-Report - COM 4108

DEBUS, G.H. (Editor) - PPR Nuclear Measurements - July - December 1983, EUR-Report - in press

VAN AUDENHOVE, J. (Editor) - Newsletter of the INTDS, 10(1) August 1983

VAN AUDENHOVE, J. (Editor) - Newsletter of the INTDS, 10(2) December 1983

CINDA ENTRIES LIST

ELEMENT Z	A	QUANTITY	TYPE	ENERGY MIN	ENERGY MAX	DOCUMENTATION REF VOL PAGE	DATE	LAB	COMMENTS
NI	62	TOTAL	EXPT-PROG	+3	15+6	INDC(EUR)18 49	484	GEL	JAN PAPERS+
U		ABSORPTION	EVAL-PROG	MAXW	25-2	INDC(EUR)18 3	484	GEL	AXTON.ERROR COVAR MATRIX
CA	041	N,ALPHA	EXPT-PROG	47+3	14+6	INDC(EUR)18 44	484	GEL	WAGEMANS+
CR	052	RESON PARAMS	EXPT-PROG	16+3		INDC(EUR)18 16	484	GEL	BRUSEGAN+SCATT WIDTH
CR	052	RESON PARAMS	EXPT-PROG	16+3		INDC(EUR)18 19	484	GEL	POHR+CAPTURE AREA
CR	053	RESON PARAMS	EXPT-PROG	20+3	11+4	INDC(EUR)18 20	484	GEL	BRUSEGAN+REL TO 1.5KEV P2CR RES
CR	053	N,GAMMA	EXPT-PROG	20+3	11+4	INDC(EUR)18 20	484	GEL	BRUSEGAN+REL TO 1.5KEV P2CR RES
FE	054	RESON PARAMS	EXPT-PROG	+3	30+5	INDC(EUR)18 21	484	GEL	BRUSEGAN+
FE	056	RESON PARAMS	EXPT-PROG	+3	3e+5	INDC(EUR)18 22	484	GEL	CORVI+RE-ANALYSIS
FE	056	RESON PARAMS	EXPT-PROG	1.+3		INDC(EUR)18 25	484	GEL	POHR+RE-ANALYSIS
FE	056	RESON PARAMS	EXPT-PROG	24+5	85+6	INDC(EUR)18 25	484	GEL	CORNELIS+HIGH RESOL TRANSM
FE	057	RESON PARAMS	EXPT-PROG	+3	60+3	INDC(EUR)18 26	484	GEL	POHR+HIGH RESOL TRANSM+CAPT
SM	149	N,GAMMA	EXPT-PROG	+3	30+5	INDC(EUR)18 28	484	GEL	CORVI+TBL
PB	207	TOTAL	EXPT-PROG	+3	45+5	INDC(EUR)18 33	484	GEL	KOEHLER+
U	233	NUBAR (NU)	EVAL-PROG	MAXW	25-2	INDC(EUR)18 3	484	GEL	AXTON.ERROR COVAR MATRIX
U	233	ABSORPTION	EVAL-PROG	MAXW	25-2	INDC(EUR)18 3	484	GEL	AXTON.ERROR COVAR MATRIX
U	233	N,FISSION	EXPT-PROG	25-2	30+4	INDC(EUR)18 4	484	GEL	WAGEMANS+TBC
U	233	N,FISSION	EVAL-PROG	MAXW	25-2	INDC(EUR)18 3	484	GEL	AXTON.ERROR COVAR MATRIX
U	233	N,GAMMA	EVAL-PROG	MAXW	25-2	INDC(EUR)18 3	484	GEL	AXTON.ERROR COVAR MATRIX
U	233	ETA	EVAL-PROG	MAXW	25-2	INDC(EUR)18 3	484	GEL	AXTON.ERROR COVAR MATRIX
U	233	ALPHA	EVAL-PROG	MAXW	25-2	INDC(EUR)18 3	484	GEL	AXTON.ERROR COVAR MATRIX
U	235	NUBAR (NU)	EVAL-PROG	MAXW	25-2	INDC(EUR)18 3	484	GEL	AXTON.ERROR COVAR MATRIX
U	235	ABSORPTION	EVAL-PROG	MAXW	25-2	INDC(EUR)18 3	484	GEL	AXTON.ERROR COVAR MATRIX
U	235	N,FISSION	EXPT-PROG	25-2	30+4	INDC(EUR)18 4	484	GEL	WAGEMANS+TBC
U	235	N,FISSION	EXPT-PROG	50-3	15-1	INDC(EUR)18 14	484	GEL	WAGEMANS+
U	235	N,FISSION	EXPT-PROG	60+3	33+4	INDC(EUR)18 5	484	GEL	CORVI+ANALYSIS OF INTERM STRUCTURE
U	235	N,FISSION	EVAL-PROG	MAXW	25-2	INDC(EUR)18 3	484	GEL	AXTON.ERROR COVAR MATRIX
U	236	FISS YIELD	EXPT-PROG	25-2	60+6	INDC(EUR)18 49	484	GEL	STRALDE+
U	238	FRAG SPECTRA	EXPT-PROG	25-2	60+6	INDC(EUR)18 49	484	GEL	STRALDE+ENERGY SPECTRA+ANGDIST
U	238	N,GAMMA	EVAL-PROG	MAXW	25-2	INDC(EUR)18 3	484	GEL	AXTON.ERROR COVAR MATRIX
U	238	ETA	EVAL-PROG	MAXW	25-2	INDC(EUR)18 3	484	GEL	AXTON.ERROR COVAR MATRIX
U	238	ALPHA	EVAL-PROG	MAXW	25-2	INDC(EUR)18 3	484	GEL	AXTON.ERROR COVAR MATRIX
U	238	N,GAMMA	EXPT-PROG	NDG		INDC(EUR)18 15	484	GEL	CORVI+TBD
U	238	RESON PARAMS	EVAL-PROG	15+3		INDC(EUR)18 16	484	GEL	POORTMANS+
PU	238	FISS YIELD	EXPT-PROG	SPON		INDC(EUR)18 6	484	GEL	WAGEMANS+TBC
PU	238	FRAG SPECTRA	EXPT-PROG	SPON		INDC(EUR)18 6	484	GEL	WAGEMANS+TBC
PU	239	NUBAR (NU)	EVAL-PROG	MAXW	25-2	INDC(EUR)18 3	484	GEL	AXTON.ERROR COVAR MATRIX
PU	239	ABSORPTION	EVAL-PROG	MAXW	25-2	INDC(EUR)18 3	484	GEL	AXTON.ERROR COVAR MATRIX
PU	239	N,FISSION	EVAL-PROG	MAXW	25-2	INDC(EUR)18 3	484	GEL	AXTON.ERROR COVAR MATRIX
PU	239	FISS YIELD	EXPT-PROG	25-2		INDC(EUR)18 6	484	GEL	ALLAERT+TBP
PU	239	FRAG SPECTRA	EXPT-PROG	25-2		INDC(EUR)18 6	484	GEL	ALLAERT+TBP
PU	239	N,GAMMA	EVAL-PROG	MAXW	25-2	INDC(EUR)18 3	484	GEL	AXTON.ERROR COVAR MATRIX
PU	239	ETA	EVAL-PROG	MAXW	25-2	INDC(EUR)18 3	484	GEL	AXTON.ERROR COVAR MATRIX
PU	239	ALPHA	EVAL-PROG	MAXW	25-2	INDC(EUR)18 3	484	GEL	AXTON.ERROR COVAR MATRIX
PU	240	FISS YIELD	EXPT-PROG	SPON		INDC(EUR)18 6	484	GEL	ALLAERT+TBP
PU	240	FRAG SPECTRA	EXPT-PROG	SPON		INDC(EUR)18 6	484	GEL	ALLAERT+TBP
PU	241	NUBAR (NU)	EVAL-PROG	MAXW	25-2	INDC(EUR)18 3	484	GEL	AXTON.ERROR COVAR MATRIX
PU	241	ABSORPTION	EVAL-PROG	MAXW	25-2	INDC(EUR)18 3	484	GEL	AXTON.ERROR COVAR MATRIX
PU	241	N,FISSION	EVAL-PROG	MAXW	25-2	INDC(EUR)18 3	484	GEL	AXTON.ERROR COVAR MATRIX
PU	241	N,GAMMA	EVAL-PROG	MAXW	25-2	INDC(EUR)18 3	484	GEL	AXTON.ERROR COVAR MATRIX
PU	241	ETA	EVAL-PROG	MAXW	25-2	INDC(EUR)18 3	484	GEL	AXTON.ERROR COVAR MATRIX
PU	241	ALPHA	EVAL-PROG	MAXW	25-2	INDC(EUR)18 3	484	GEL	AXTON.ERROR COVAR MATRIX
PU	242	N,FISSION	EXPT-PROG	20+5	13+6	INDC(EUR)18 7	484	GEL	WARTENA+STATIST ANAL TBC
AM	241	N,GAMMA	EXPT-PROG	50+2	30+5	INDC(EUR)18 11	484	GEL	CORNELIS+LINAC MEAS C6D6 DET
AM	243	N,FISSION	EXPT-PROG	80-1	40+6	INDC(EUR)18 13	484	GEL	KNITTER+LINAC+VDG MEAS
CF	252	NUBAR (NU)	EVAL-PROG	MAXW	25-2	INDC(EUR)18 3	484	GEL	AXTON.ERRDR COVAR MATRIX